

# **CNWRA** A center of excellence in earth sciences and engineering

A Division of Southwest Research Institute™  
6220 Culebra Road • San Antonio, Texas, U.S.A. 78228-5166  
(210) 522-5160 • Fax (210) 522-5155

September 24, 2001  
Contract No. NRC-02-97-009  
Account No. 20.01402.571

U.S. Nuclear Regulatory Commission  
ATTN: Dr. Tae Ahn  
Two White Flint North  
11545 Rockville Pike  
Mail Stop T7 C6  
Washington, DC 20555

Subject: Submittal of report, "Effect of Environment on the Corrosion of Waste Package and Drip Shield Materials" (CNWRA 2001-03), Intermediate Milestone 01402.571.170

Reference: Letter from T. Ahn to V. Jain dated August 23, 2001—Acceptance of Intermediate Milestone 01402.571.170, "Effect of Environment on the Corrosion of Waste Package and Drip Shield Materials"

Dear Dr. Ahn:

Enclosed is the subject report that was revised based on NRC staff comments. This report documents the possible environments that may be encountered at Yucca Mountain and the effects that these environments may have on waste package and drip shield corrosion. Also enclosed with the report is CNWRA staff responses to the NRC comments.

If you have any questions regarding this report, please feel free to contact Sean Brossia at (210) 522-5797 or Gustavo Cragolino at (210) 522-5538.

Sincerely yours,



Vijay Jain  
Element Manager  
Corrosion Science & Process Engineering

VJ:jg

Enclosure

cc:	J. Linehan	J. Piccone	T. McCartin	T. Essig	L. Browning	G. Cragolino
	D. DeMarco	K. Stablein	J. Thomas	W. Patrick	D. Dunn	Y-M. Pan
	B. Meehan	B. Leslie	C. Greene	CNWRA Dirs.	O. Moghissi	T. Nagy (contracts)
	E. Whitt	S. Wastler	T. Bloomer	CNWRA EMs	O. Pensado	P. Maldonado
	J. Greeves	D. Brooks	J. Andersen	S. Brossia	L. Yang	



Washington Office • Twinbrook Metro Plaza #210  
12300 Twinbrook Parkway • Rockville, Maryland 20852-1606

## RESPONSES TO NRC COMMENTS ON IM 01402.571.170

### **“EFFECT OF ENVIRONMENT ON THE CORROSION OF WASTE PACKAGE AND DRIP SHIELD MATERIALS”**

#### **Reviewer 1**

- 1. In p. v, last sentence “perhaps years are needed,” what is the common sense basis for such a long time?**

Testing was only conducted for seven weeks and it is uncertain if at longer times, perhaps even much longer times, may be needed for crevice corrosion to initiate. Thus, the statement that a longer period of testing may be needed to address this. No change made.

- 2. In p. xix, the second line of the second paragraph, the range (of) environments: add**

Accept, change made.

- 3. In 1-1, the first paragraph, use “the average member of the critical group.”**

Accept, change made.

- 4. Address how the analysis of the deliquescence humidity will be modified in the low temperature operation.**

For the LTOM case, the deliquescence humidity analysis already conducted is still valid and will not change substantially. No change made.

- 5. In p. 3-4, regarding the uncertainties associated with the activation energy, how is this related to the CLST agreements?**

CLST agreements 1.4 and 1.10 are applicable. The issue of the effect of temperature on the passive corrosion rate will be addressed in the SSPA Technical Exchange September 13-14, 2001. It is anticipated that the DOE will continue tests in order to fully assess the effect of temperature on passive corrosion rate. No change made.

- 6. In p. 3-7, the first sentence in the second paragraph, two “simulated diluted water.”**

Text corrected to read simulated dilute water and simulated concentrated water.

- 7. In p. 3-8, gamma radiolysis was assumed to increase the potential by 200 mV in previous document and SSPS.**

Reference added to text.

8. **In p. 3-18, Section 3.2, state why we chose these test solutions.**

Additional text added. Solutions were chosen to determine the effect of chloride concentration on the passive dissolution rate.

9. **In p. 3-26, Section 3.2.1.3, address “misfit dislocation” raised by R. Rapp in the last NWTRB WP meeting.**

A series of references have been added supporting the notion of vacancy injection as a consequence of the oxidation/dissolution process. The injection and accumulation of vacancies is readily observed in Ni-Cr alloys oxidized in air at high temperatures (>1000°C). It is also acknowledged that not only dislocations in the metal, but also high angle grain boundaries, pre-existing voids, and suitable regions at the metal-scale interface could perform as vacancy sinks. The computations presented correspond to the bound case where the existence of sinks is disregarded. Incorporation of vacancy sinks into the model will yield extended times to failure. This is proposed as work to be performed in the future provided we develop a testing scheme to verify the existence of vacancies in the alloy.

10. **In p. Section 4.2, address States’ test results.**

Accept. Some discussion of the State of Nevada’s test results have been included.

11. **In p. 6-2, last three sentences of the first paragraph, add a potential mitigation process (e.g. strict QA procedures)**

We have modified the text to reflect that DOE will be providing additional information on thermal aging after they have tested waste package mock-ups.

## Reviewer 2

1. **Page xvii. Last paragraph. Fifth line. Clarify the types of water. From reading the sentence, there could be three water types.**

There are only 2, as saturated zone water and perched unsaturated zone water are considered similar.

2. **Page xix. Last paragraph. Third line, “The possibility of SCC.” Which report are they referring to?**

This refers to a report to be issued in FY2002. We are conducting tests to be reported therein.

3. **Page 2-3. Table 2-1. Where are the trace elements like Pb? Same for Table 2-2 on Page 2-4.**

Analytical data on minor and trace element concentrations in YM UZ groundwaters were not reported in the referenced papers, and are not currently available from a QA source. There are NRC/DOE agreements under the ENFE KTI, however, that address the lack of minor and trace element data that could be important to performance. No change made.

4. **Page 3-3. Section 3.1.2. The corrosion rate decreases with time because of passive film growth. The film is only a couple of nm thick so how do they account for the large changes in corrosion rates? At 6 mo → 50 nm/yr, 1 yr → 30 nm/yr, 2 yr → 10 nm/yr. The changes are 20 nm/yr. Is this right?**

DOE is quoted correctly. The subject of decreasing corrosion rate that is not supported by increased passive film growth is the basis for several CLST Technical exchange agreements. No. change made.

5. **Page 3-4. Section 3.1.3. 2<sup>nd</sup> paragraph define three phenotypic bacteria groups involved in MIC Then, in the next paragraph, 6 line, they test four bacteria types. Do the slime-forming bacteria participate MIC?**

Paragraph describing DOE tests where slime formers are included are correct. Slime-formers do not generally contribute directly to MIC however they can produce biofilms that allow other bacteria such as sulfate-reducing bacteria to thrive and contribute to MIC. This processes is described in the Geesey, 1993. No change made.

6. **Page 3-9. First paragraph, four and third to last sentence. Sections 3.1.7.4 and 3.1.7.5 do not exist. Might be Sections 3.1.6.3 and 3.1.6.4.**

Document corrected.

7. **Page 3-10. Section 3.1.6.3 MIC. Should the  $G_{MIC}$  is 2, but results of the tests are 2 to 6 times greater. Why just 2? Also, a reference is needed for the second sentence for the SS  $G_{MIC}$ .**

MIC of alloy 22 is the subject of a CLST technical exchange agreement. Reference added.

8. **Page 3-12. 2<sup>nd</sup> paragraph. Last sentence. “and the maximum dose rate at 100, 000 yr is  $2 \times 10^{-2}$  mrem/yr (figure 3-5).” That is 0.02 mrem/yr, not 200 mrem/yr as indicated in the figure. Should be  $2 \times 10^2$ , not  $10^{-2}$ .**

Accept, change made.

9. **Page 3-13. Last paragraph. Which figure are these numbers referring to?**

The TSPA SR Section 5.3.3.2 on p. 5-36. The appropriate figures are 5.3-5 and 5.3-6 in the TSPA SR. No. change made.

10. **Page 3-22. Figure 3-11. Graph label typo on X-axis.**

Corrected.

11. **Page 3-25. First sentence. Typo, 4.0 m should be 4.0 M (molar)**

Corrected.

12. **Page 3-35. Section 3.2.2.1. First sentence. Should be Table 3-1 instead of Table 3-2.**

Corrected.

13. **Page 3-35. Section 3.2.2.1 2<sup>nd</sup> paragraph. The paragraph discusses thermal aging tests but the last sentence states, “The effect of thermal aging for times less than 30 minutes was not studied.”**

Last sentence deleted.

14. **Page 4-4. 1<sup>st</sup> paragraph. 4<sup>th</sup> line. Is this statement about a filled d orbital protecting from MIC true?**

This is unknown. As stated in the text, this has been proposed as the explanation and reason for the resistance of Ti alloys to MIC. This has been clarified further.

15. **Page 4-8. Figure 4-5. The graph cannot stand alone. The legend needs addition information. Suggest adding Degraded case to 95<sup>th</sup> percentile and Enhanced Case to 5<sup>th</sup> percentile. The chart is explained in the text, but the chart alone is insufficient.**

Accept. These are, however, DOE figures and we should be careful about altering them. Consequently, no change to the figure was made but the figure caption was modified to help clarify.

16. **Page 4-12. 1<sup>st</sup> paragraph, 2<sup>nd</sup> line. The plateau is at  $10^{-2}$  or  $10^{-1}$ ? It looks like  $10^{-1}$  from the graph (figure 4-9), but I am not certain.**

The difference between  $10^{-2}$  and  $10^{-1}$  is relatively small and the rate of change is decreasing sharply between these concentrations. Thus, even though a slight increase in the passive current density was observed when the fluoride concentration was increased from  $10^{-1}$  to  $10^{-2}$  it seems more likely that the start of the plateau is at or very near  $10^{-1}$ .

### Reviewer 3

This paper brings together significant and in-depth technical analyses of the environmental factors likely to affect the WP and DS in a format that will assist the US NRC staff in evaluating the DOE safety case for the proposed repository at Yucca Mountain. The possible effect of a lower deliquescence point due to mixed salts, the effect of fluoride on the uniform corrosion of the DS, and the susceptibility of Alloy 22 to intergranular corrosion following high temperature exposure are among some of the significant issues that are discussed in this paper.

#### **1 Introduction:**

1. **1<sup>st</sup> paragraph: Arched mailbox-shaped drip shield may be confusing -- “Inverted U-shape” may better describe the currently selected shape of the drip shield.**

“Arched” is generally understood to mean “inverted U-shape.” The word “arched” was added to help clarify the shape of the drip shield for those who may be unfamiliar with the current drip shield design.

2. **Undisturbed repository conditions, corrosion is expected—should be general or uniform corrosion and expected by whom?**

We cannot classify specifically which form of corrosion may occur as they are all possible depending on environmental conditions including the range of corrosion potentials. References are provided.

3. **Corrosion requires water—in lieu of noxious gases. Are gases considered?**

Yes, gases are considered because they are an important part of the repository environment for a number of reasons. Gases can be dissolved in or released from groundwater, and it is therefore important to understand how they contribute to water compositions in the EBS. No redox pairs result from the aqueous speciation of analytical pore water compositions described in Table 2-1, so  $pO_2(g)$  was simply fixed as expected to atmospheric values. Measured  $pCO_2(g)$  values from Yucca Mountain were used to recalculate pHs following the approach of Browning et al. (2000), and some of the revised pore water compositions are presented in Table 2-1.

4. **Aqueous flow pathways in the saturated zone -- confusing, the DS and WP are not planned to be emplaced in the saturated zone. Also, please qualify by excluding IA air pathways.**

The text was revised for clarity, so that it does not give the reader the false impression that the DOE's application will request that waste be stored in the saturated zone. Because the claim is not made that radionuclide transport only occurs via groundwater, inclusion of IA air pathways is not mentioned and is outside the scope of this report.

5. **It does not follow that ambient groundwater compositions adequately characterize seepage compositions if temperatures at the drift crown will remain above boiling for several hundred years.**

This is the point of the discussion. Temperature at the drift crown are only expected to remain above boiling for a few hundred years. It is agreed that ambient groundwater compositions will not adequately characterize seepage compositions, despite the fact that temperatures around the drift are expected to be below boiling for the vast majority of the 10,000 year compliance period. The text is based on the observation that thermodynamic and kinetic data for ambient temperatures may be more relevant to in-drift conditions than the above-boiling values over the entire course of the compliance period. This observation demonstrates the importance of our efforts to calibrate our coupled THC models against large amounts of available ambient system site characterization data, for example, but does not justify excluding up temperature influences. To examine this further, there are several activities under the Quantity and Chemistry of Water Contacting Waste Packages and Waste Forms ISI, such as coupled THC models and evaporation/salt formation experiments, that are designed to evaluate the full range of environmental conditions that may impact seepage water compositions in a complex natural/engineered environment. The text has been modified to clarify this.

6. **It also is not clear why the author states pore water drips from the drift crown would be unimportant even though corrosion is enhanced in higher temperature, more saline solutions.**

No DOE or CNWRA models predict that any seepage will occur during the thermal period, unless that seepage is artificially and unrealistically forced. There is also agreement among the hydrologists that seepage waters will originate from fractures, rather than from pores in the rock. Both types of models

would have to be wrong in order to have high temperature, saline seepage waters that originated from matrix pores. If for some reason seepage water does originate from matrix pores, then it is likely that this will occur after the thermal period when temperatures are lower. The text was modified to clarify these points.

- 7. Table 2-1 does not list fluoride which seems to be a very significant factor in DS corrosion and expected life time.**

It is true that there is a strong relationship between fluoride and DS corrosion and consequently there are efforts aimed at obtaining information about fluoride concentrations from the DOE. Table 2-1 does not list fluoride, because analytical fluoride concentrations are not available for the UZ pore waters. No change made.

- 8. Trace elements promote localized corrosion and SCC if concentrated above levels possible at YM and in extremely acidified solution.**

Additional text added.

- 9. Discussion of Deliquescence Behavior is lacking fundamental explanation since solid sodium nitrate must be precipitating for the solution to become enriched in sodium chloride for the liquid to go from 15% sodium chloride at B to 38% sodium chloride at B1 in Figure 2-3. A solidus curve should be added to the figure to define the solid + liquid phase region.**

There were errors in the text. The NaCl in the 1<sup>st</sup> paragraph of page 2-9 should be replaced by NaNO<sub>3</sub>. Corrections have been made to the text.

- 10. Table 2-4 title needs correcting.**

Accept. Title was changed in the text.

- 11. Page 2-10, top, are aqueous salt films likely at RH of 20 percent? Also magnesium-chloride not Ma chloride.**

According to the one available deliquescence point from the handbook for the mixture of NaNO<sub>3</sub>-KNO<sub>3</sub>-NaCl, 30 percent at 16 °C, it is likely that the deliquescence point of the salt mixture from the Yucca Mountain waters is 20 percent at elevated temperatures.

- 12. Page 2-11, 2<sup>nd</sup> paragraph, 850 times the original [Cl<sup>-</sup>] of 7.2 mg/L or 681 times the original Cl-concentration of 76.6 mg/L? Apparent inconsistency.**

Accept. The synthetic J-13 water had an original Cl<sup>-</sup> concentration of 7.2 mg/L, and the synthetic pore water had an original Cl<sup>-</sup> concentration of 76.6 mg/L.

- 13. Page 2-14, undefined PCO<sub>2</sub> and fCO<sub>2</sub>.**

There is not much difference between PCO<sub>2</sub> and fCO<sub>2</sub> under ambient atmospheric conditions. PCO<sub>2</sub> was defined and fCO<sub>2</sub> was changed to PCO<sub>2</sub>, however, for clarity.

**14. Page 2-15, low nitrate content.**

Accept, nitrate has been added to the text.

**15. Page 2-18, nitrate level when chloride reaches 3.5 M is not mentioned.**

Nitrate was not and cannot be measured by the sensor systems used and thus it was not reported. No change made.

**16. Bottom of page 3-2 and top of page 3-3, corrosion rate independent of time in model - but 6 mo, 1 yr and 2 yr experimental data is different.**

Addressed in comment from Reviewer 2.

**17. Page 3-3 simulated dilute water, simulated dilute water - document QC problem (see also page 3-7, or page 3-9 was assumed was assumed).**

Corrected.

**18. Page 3-5 topologically close-packed not a topologically-closed, packed-phase. The author is clearly confused.**

Corrected.

**19. Page 3-11, 2<sup>nd</sup> paragraph under Predicted Performance - the first waste package failure number has been revised by DOE, should be first waste package failure other than failures from manufacturing defects.**

This paragraph specifically refers to the TSPA SR.

**20. Page 3-18, define acronym SCE.**

Defined on first appearance on page 3-5.

**21. Table 3-3, last column, no units.**

Corrected.

**22. Page 3-28, definition of  $V_m$  - metal vacancies in the bulk of alloy, however this appears to be a surface phenomenon occurring at the oxide/metal interface not in the bulk material.**

Vacancies should be defined as existing in the alloy. In experiments with oxidation of Ni-Cr alloys in air at high temperatures, vacancies condense and form voids not only at the metal-scale interface, but also at inclusions and grain boundaries in the bulk of the alloy. This is why it is preferred to define vacancies as existing in the alloy. The word "bulk" has been deleted to make the definition less stringent. This was clarified further in the text.

23. **Page 3-29, footnote 10, in this example the material is in a stress field and does not correlate well with the author's model.**

The reference is intended to provide additional examples where 50 percent is selected as an arbitrary threshold value. It is not intended to mean that the two models are similar. The footnote has been clarified.

24. **Look at well documented chemical composition variation in oxide/deposit layers of high temperature steam superheater chromium alloy tubing.**

We checked the literature and found that for nickel-chromium alloys of high chromium content (chromium alloys for superheater tubing are generally ferritic chromium steels), the most likely oxide controlling the dissolution/oxidation process is  $\text{Cr}_2\text{O}_3$ . Boudin et al. (1994) is listed as pertinent reference, but there are others supporting the formation of chromium oxide. Secondary layers are frequently found on top of the chromium oxide film, which are likely deposits and not the result of solid state reactions as is chromium oxide.  $\text{Cr}_2\text{O}_3$  is the film responsible for the phenomenon of passivity; thus, in the model we assumed that chromium oxide controls the dissolution process and disregarded the possible existence of deposit layers. Deposit layers may perform as diffusion layers, limiting the supply of oxygen, but given that their stability is questionable, no credit should be taken by their existence.

25. **Look at copper-nickel diffusion couple. Vacancies do not accumulate, this would be a high-energy, low probability configuration.**

Accumulation of vacancies is readily observed in Ni-Cr alloys oxidized in air at high temperatures, and also in Ni oxidized at high T. This fact has been added to the text with pertinent references. It is true, however, that vacancies do not necessarily form voids but can annihilate at sinks (e.g., dislocations in the metal, high angle grain boundaries, pre-existing voids, and suitable regions at the metal-scale interface). The injection of vacancies has been proposed as a mechanism responsible for intergranular oxidation in Ni-Cr alloys (Shida et al., 1981).

We believe that our model is consistent with the observations at high temperatures. For example, it has been observed for some systems that the void density decreases with increasing distance from the metal-scale interface (Evans, 1988; Shida et al., 1981). Thus, voids could form by the accumulation of vacancies diffusing away from the interface. The size of the voids increases with increasing oxidation time, which suggests that vacancy condensation occurs only at preferred sites (inclusions, grain boundaries, or the metal-scale interface). Condensation of vacancies underneath the scale has been proposed as a mechanism for film decohesion in iron (Dunnington et al., 1952; Tylecote and Mitchell, 1960).

At low temperatures, vacancies do not have enough thermal energy to diffuse away from the interface. It is likely that these vacancies can annihilate at sinks, but even if they annihilate, we are uncertain on their influence to the quality of the attachment of the oxide to the metal. We analyze an extreme case, where we assumed that accumulation of vacancies can cause film detachment. We introduced some caveats in the text explaining that our model corresponded to an extreme case, and that introduction of sinks into the model would yield extended times to failure.

26. **Page 3-35, 1<sup>st</sup> paragraph, should read (Table 3-1).**

Corrected.

27. **Page 3-35, 1<sup>st</sup> paragraph - does this mean specimens that say 5 min at 870C were really only held at 870C for 2 min due to the 3 min heat up time? Clarify.**

Specimens were placed in the oven for 5 min. Oven temperature was maintained at 870 °C. The specimens were removed and rapidly quenched. Separate measurements were performed to determine the time necessary to heat the specimen which was approximately 12 mm thick. The temperature for the center of the specimen was measured to be 450 °C after 1 min, 650 °C after 2 min, and 810 °C after 3 min. Obviously the time-temperature at the surface of the specimen would be different.

28. **Page 3-36, 1<sup>st</sup> paragraph, does the WP need to be continuously wet for failure in the stated 10,000 to 34,000 year time frame? Perhaps qualify this statement in terms of risk significance (short term corrosion rate extrapolated 4 orders of magnitude and neglecting 5 cm of 316 NG SS).**

Yes. The surface of the WP would have to be continuously wet. However, if DOE does not take credit for the 316NG shell, there is no reason for qualifying the statement in this report.

29. **Page 4-9, Why deaerated conditions? Seems as though solutions in the repository will be aerated.**

To accurately measure anodic (corrosion) currents using potentiostatic and potentiodynamic methods and applying Faraday's law, one needs to minimize other possible cathodic reactants in the environment, the most prominent being oxygen, which artificially decrease the experimentally measured current. Other tests that were mentioned in the report were conducted in air-saturated solutions to examine the effects of oxygen on the corrosion potential.

30. **Page 4-11 top of page, should refer to Chapter 2 and realistic water chemistries.**

Accept. A reference back to chapter 2 with respect to water chemistry has been added.

31. **Page 4-19 Numbering problem -- Figures 4-19 and 4-20, not 4-18 and 4-19 (also page 4-20, Figure 4-19, not 4-18).**

Accept.

32. **Page 5-1, the temperature -- around 250C seems repository relevant, clarify if author means aqueous + 250C is not relevant.**

Yes, it has been clarified. Though these high temperatures will occur at the repository, they will also be at ambient pressure meaning that aqueous solutions will not be present. One would need high pressures (e.g., autoclaves, pipelines, pressure vessels, etc.) to achieve these high temperatures and still maintain an aqueous solution.

33. **Alloy 22 in more relevant conditions is warranted -- does the author mean more realistic? Please clarify.**

Yes, relevant means realistic. This was clarified.

34. **1<sup>st</sup> paragraph, “these components” -- should be more specific, these engineered components significant to HLW isolation or DS and WP.**

Accept.

35. **2<sup>nd</sup> paragraph, trace elements are talked about in two places, are these the same trace elements or different trace elements? The way it is worded it seems to be different trace elements.**

These are not different trace elements.

36. **3<sup>rd</sup> paragraph, last sentence seems to be very risk significant and should be emphasized.**

Agree.

37. **1<sup>st</sup> paragraph, as-received material susceptible to LC under anticipated repository conditions. Perhaps this should be qualified further as in possible, but unlikely. This statement needs to be more consistent with the statement in the last paragraph on page 6-3 -- Alloy 22 has been found to be highly resistant to LC in the wrought condition,.**

This has been clarified. In the wrought condition, Alloy 22 is resistant to localized corrosion but is still susceptible to it (i.e., not immune to it). When thermally treated, the resistance decreases significantly.

38. **2<sup>nd</sup> paragraph, Where is HIC of Ti DS addressed or going to be addressed?**

See response to Reviewer 2, comment 2.

#### **Reviewer 4**

1. **Page 2-2 Just an interesting point. In the second paragraph, it states that pore water compositions vary significantly both laterally and vertically. In the TSPA I TE Bo mentioned how consistent the pore waters were across the site. I don't recall whether that observation was challenged.**

Perhaps Bo was referring to pore water analyses collected from the Tsw unit. Variations in pore water composition are most closely associated with units containing high zeolite and clay abundances, such as the Paintbrush (above the Tsw) and the Calico Hills (below the Tsw).

2. **Page 2-3 I didn't see an explanation for the constant value for K concentration.**

The K values shown on page 2-3 are assumed, because potassium was not measured in the vast majority of pore water analyses from Yucca Mountain. The referenced Browning et al. paper describes additional assumptions and calculations that were necessary to revise the incomplete and internally inconsistent analytical pore water data. Since issuance of that MRS paper, the assumed K concentration was reduced from 14mg/L to 8 mg/L. This is now noted in the table.

3. **Page 2-4 First paragraph says J-13 well water is more dilute than pore water compositions. Then it goes on to say that the J-13 has higher concentrations of Na. It looks like 7 out of 12 pore water entries of Table 2-1 have higher concentrations of Na. This part was confusing.**

Sodium is only one component of these groundwaters that contribute to their ionic strength. When considering the contributions made by all species present in J13 and pore waters, pore waters are more concentrated overall. In the big scheme of things, however, both types of water are fairly dilute. This was clarified.

4. **Page 2-5 The discussion about Cl in the perched water and pore water is interesting. Has anybody taken the concentration gradient and the porosity and permeability info and assuming matrix diffusion, constrained the time for the persistence of this gradient? How does the time compare with the age of the perched water?**

We are not aware of anyone having done this before, but have thought in the past of doing it ourselves. It was decided against, because the problem is influenced by advective, as well as diffusive, transport and becomes difficult to handle analytically. We may revisit this.

5. **Page 2-8 and Page 2-9 I agree with the other reviewer who noted that the text describing the phase diagram was in error. On drying sodium nitrate precipitates enriching the liquid in NaCl. The path in which RH increases is also reversed.**

See response to Reviewer 3, comment 9.

6. **Page 2-10  $\text{MaCl}_2$  should be  $\text{MgCl}_2$ .**

Accept.

7. **Page 2-11 Last paragraph says F concentrations as high as 185 mg/L but chloride concentrations of 76.6 mg/L. This seems to be apples and oranges.**

Accept. This was corrected as it was an error as the concentrations were referring to chloride.

# **EFFECT OF ENVIRONMENT ON THE CORROSION OF WASTE PACKAGE AND DRIP SHIELD MATERIALS**

*Prepared for*

**U.S. Nuclear Regulatory Commission  
Contract NRC-02-97-009**

*Prepared by*

**Center for Nuclear Waste Regulatory Analyses  
San Antonio, Texas**

**September 2001**



# **EFFECT OF ENVIRONMENT ON THE CORROSION OF WASTE PACKAGE AND DRIP SHIELD MATERIALS**

*Prepared for*

**U.S. Nuclear Regulatory Commission  
Contract NRC-02-97-009**

*Prepared by*

**C.S. Brossia  
L. Browning  
D.S. Dunn  
O.C. Moghissi  
O. Pensado  
L. Yang**

**Center for Nuclear Waste Regulatory Analyses  
San Antonio, Texas**

**September 2001**

## PREVIOUS REPORTS IN SERIES

Number	Name	Date Issued
CNWRA 91-004	A Review of Localized Corrosion of High-Level Nuclear Waste Container Materials—I	April 1991
CNWRA 91-008	Hydrogen Embrittlement of Candidate Container Materials	June 1991
CNWRA 92-021	A Review of Stress Corrosion Cracking of High-Level Nuclear Waste Container Materials—I	August 1992
CNWRA 93-003	Long-Term Stability of High-Level Nuclear Waste Container Materials: I—Thermal Stability of Alloy 825	February 1993
CNWRA 93-004	Experimental Investigations of Localized Corrosion of High-Level Nuclear Waste Container Materials	February 1993
CNWRA 93-014	A Review of the Potential for Microbially Influenced Corrosion of High-Level Nuclear Waste Containers	June 1993
CNWRA 94-010	A Review of Degradation Modes of Alternate Container Designs and Materials	April 1994
CNWRA 94-028	Environmental Effects on Stress Corrosion Cracking of Type 316L Stainless Steel and Alloy 825 as High-Level Nuclear Waste Container Materials	October 1994
CNWRA 95-010	Experimental Investigations of Failure Processes of High-Level Radioactive Waste Container Materials	May 1995
CNWRA 95-020	Expert-Panel Review of the Integrated Waste Package Experiments Research Project	September 1995
CNWRA 96-004	Thermal Stability and Mechanical Properties of High-Level Radioactive Waste Container Materials: Assessment of Carbon and Low-Alloy Steels	May 1996
CNWRA 97-010	An Analysis of Galvanic Coupling Effects on the Performance of High-Level Nuclear Waste Container Materials	August 1997
CNWRA 98-004	Effect of Galvanic Coupling Between Overpack Materials of High-Level Nuclear Waste Containers—Experimental and Modeling Results	March 1998

## PREVIOUS REPORTS IN SERIES (cont'd)

<u>Number</u>	<u>Name</u>	<u>Date Issued</u>
CNWRA 98-008	Effects of Environmental Factors on Container Life	July 1998
CNWRA 99-003	Assessment of Performance Issues Related to Alternate Engineered Barrier System Materials and Design Options	September 1999
CNWRA 99-004	Effects of Environmental Factors on the Aqueous Corrosion of High-Level Radioactive Waste Containers— Experimental Results and Models	September 1999
CNWRA 2000-06	Assessment of Methodologies to Confirm Container Performance Model Predictions	January 2001 Revision 01

## ABSTRACT

To aid in evaluating the DOE safety case for the proposed Yucca Mountain repository, as well as to help elucidate the uncertainties in the safety case, the CNWRA has been engaged in a limited scope experimental effort to examine some of these concerns. Additionally, the results generated from the CNWRA experimental efforts are utilized in the NRC/CNWRA Total-system Performance Assessment code (TPA) to predict the performance of the proposed repository. This experimental program has assisted in identifying concerns and deficiencies in the DOE approach regarding the effects of thermal aging on corrosion of Alloy 22 and the effects of fluoride on corrosion of Ti Grade 7. These experimental efforts have also demonstrated that enhanced concentration of various deleterious species can occur through evaporative processes, and thus a wide range of possible environments may be encountered in the repository over time. Alloy 22 has been found to be resistant to localized corrosion in the wrought condition; however thermal aging and welding tend to make the material more susceptible to localized corrosion. It has also been shown that the passive corrosion rate of Alloy 22 is relatively insensitive to environmental conditions. Using the NRC/CNWRA TPA code, Alloy 22 is predicted to fail only by general corrosion using the appropriate parameters for the wrought material. Efforts to modify the code to allow a fraction of the waste package surface to have modified properties to reflect the effect of weldments is being considered. Ti Grade 7 has been observed to be essentially immune to pitting corrosion except at extremely high potentials (well above those that would reasonably be expected in the repository). Long-term polarization at lower potentials has also revealed that Ti Grade 7 is highly resistant to crevice corrosion, though it is uncertain if crevice corrosion might initiate at longer times (perhaps years are needed). Ti Grade 7 owes this high resistance to localized corrosion to the addition of Pd. Pd additions, however, did not mitigate the effects of fluoride that was shown to dramatically increase the passive corrosion rate by several orders of magnitude at low concentrations.

# CONTENTS

Section	Page
FIGURES .....	ix
TABLES .....	xiii
ACKNOWLEDGMENTS .....	xv
EXECUTIVE SUMMARY .....	xvii
1 INTRODUCTION .....	1-1
2 POSSIBLE REPOSITORY ENVIRONMENTS .....	2-1
2.1 AMBIENT AND THERMALLY PERTURBED GROUNDWATER COMPOSITIONS FROM THE VICINITY OF YUCCA MOUNTAIN .....	2-1
2.1.1 Ambient Unsaturated and Saturated Zone Groundwater Compositions ....	2-2
2.2 DELIQUESCENT BEHAVIOR OF SALT MIXTURES AND FORMATION OF AQUEOUS FILM AT LOW RELATIVE HUMIDITIES .....	2-7
2.3 EVAPORATIVE/BOILING CONCENTRATING OF YUCCA MOUNTAIN WATERS .....	2-10
2.4 AQUEOUS SOLUTIONS FOR CORROSION TESTING .....	2-15
2.5 EFFECT OF MICROBIAL ACTIVITY ON THE ENVIRONMENT .....	2-15
2.6 EVOLUTION OF CHEMISTRY IN LABORATORY-SCALE HEATER TEST .....	2-18
3 CORROSION OF CANDIDATE CONTAINER MATERIALS .....	3-1
3.1 U.S. DEPARTMENT OF ENERGY INVESTIGATIONS .....	3-2
3.1.1 Humid-Air Corrosion .....	3-2
3.1.2 Uniform Corrosion .....	3-3
3.1.3 Microbially Influenced Corrosion .....	3-4
3.1.4 Effect of Thermal Aging on Corrosion .....	3-5
3.1.5 Localized Corrosion .....	3-6
3.1.6 U.S. Department of Energy Model Abstraction and Predicted Performance .....	3-8
3.1.6.1 Humid-Air Corrosion .....	3-8
3.1.6.2 Uniform Corrosion .....	3-8
3.1.6.3 Microbially Influenced Corrosion .....	3-10
3.1.6.4 Thermal Aging .....	3-10
3.1.6.5 Localized Corrosion .....	3-10
3.1.6.6 Predicted Performance .....	3-11
3.1.7 Assessment of the U.S. Department of Energy Approach .....	3-14
3.2 CENTER FOR NUCLEAR WASTE REGULATORY ANALYSES INVESTIGATIONS .....	3-18
3.2.1 Passive Corrosion of Alloy 22 .....	3-18
3.2.1.1 As-Received Material .....	3-18
3.2.1.2 Passive Corrosion of Welded Material .....	3-25

# CONTENTS (cont'd)

Section	Page
3.2.1.3 Modeling of Alloy 22 Passive Dissolution .....	3-25
3.2.2 Localized Corrosion .....	3-32
3.2.2.1 Effect of Thermal Aging on Localized Corrosion .....	3-34
3.2.3 Center for Nuclear Waste Regulatory Analyses Approach to Performance Prediction .....	3-35
4 GENERAL AND LOCALIZED CORROSION OF THE DRIP SHIELD .....	4-1
4.1 U.S. DEPARTMENT OF ENERGY INVESTIGATIONS .....	4-2
4.1.1 Humid-Air Corrosion .....	4-2
4.1.2 Aqueous General/Passive Corrosion .....	4-2
4.1.3 Microbially Influenced Corrosion .....	4-3
4.1.4 Localized Corrosion .....	4-5
4.1.5 Evaluation of U.S. Department of Energy Model Abstraction and Predicted Performance .....	4-6
4.2 CENTER FOR NUCLEAR WASTE REGULATORY ANALYSES INVESTIGATIONS .....	4-9
4.2.1 Passive and General Corrosion .....	4-9
4.2.2 Localized Corrosion .....	4-12
4.2.3 Center for Nuclear Waste Regulatory Analyses Model Abstraction and Predicted Performance .....	4-21
5 FUTURE WORK .....	5-1
6 SUMMARY AND CONCLUSIONS .....	6-1
7 REFERENCES .....	7-1
APPENDIX A—TABULATED CORROSION DATA .....	A-1

## FIGURES

Figure	Page
2-1	Comparison between revised pore and perched water compositions from borehole USW UZ-14 and saturated zone water compositions from Yucca Mountain (Yang et al., 1996; Kerrisk, 1987) . . . . . 2-5
2-2	Deliquescent points (Civilian Radioactive Waste Management System Management and Operating Contractor, 2000c) . . . . . 2-8
2-3	Relative humidity (RH) at saturation of an aqueous solution of NaNO <sub>3</sub> and NaCl at 25 °C (Ge et al., 1998) . . . . . 2-8
2-4	Previous predictions of relative humidity and temperature on the waste package over time after closure (Civilian Radioactive Waste Management System Management and Operating Contractor, 2001) . . . . . 2-10
2-5	Chemical divide diagram . . . . . 2-13
2-6	Response of pH and chloride concentration in evaporation and dryout . . . . . 2-19
3-1	Example of Type 1 polarization behavior for Alloy 22 (Civilian Radioactive Waste Management System Management and Operating Contractor, 2000f) . . . . . 3-6
3-2	Example of Type 2 polarization behavior for Alloy 22 (Civilian Radioactive Waste Management System Management and Operating Contractor 2000f) . . . . . 3-7
3-3	Cumulative distribution function for the corrosion rate of Alloy 22, 2-yr data from the long-term corrosion test facility . . . . . 3-9
3-4	Thick line: fraction of penetrated waste package surface versus time (Center for Nuclear Waste Regulatory Analyses computations based on corrosion rates in figure 3-3) . . . . . 3-12
3-5	U.S. Department of Energy predicted mean dose rate as a function of time for the basecase corrosion rate, and the 5 <sup>th</sup> and 9 <sup>th</sup> percentile median corrosion rates are fixed at the 5 <sup>th</sup> and 95 <sup>th</sup> percentile values of the uncertainty variance . . . . . 3-13
3-6	Fraction of penetrated waste package surface by general corrosion versus time . . . . . 3-16
3-7	Steady-state anodic current densities for Alloy 22 in Cl <sup>-</sup> solutions at 95 °C . . . . . 3-20
3-8	Effect of temperature on steady-state anodic current densities for Alloy 22 . . . . . 3-20
3-9	Anodic current density and total charge as a function of time measured on Alloy 22 at 100 mV <sub>SCE</sub> in 0.028 M chloride solution at 95 °C . . . . . 3-21
3-10	Anodic current density and total charge as a function of time measured on Alloy 22 at 500 mV <sub>SCE</sub> in 0.028 M chloride solution at 95 °C . . . . . 3-22
3-11	Metal ion concentrations measured using capillary electrophoresis from the anodic dissolution of Alloy 22 at 500 mV <sub>SCE</sub> in 0.028 M chloride at 95 °C . . . . . 3-22
3-12	Charge in coulombs for metal ions calculated from the measured solution concentrations. Total charge is the sum of the charge based on solution concentrations . . . . . 3-23
3-13	Steady-state passive dissolution rate for welded and as-received Alloy 22 . . . . . 3-25
3-14	After the fraction of vacancies between $x_0$ and $x_1$ exceeds a maximum threshold value, $P_{max}$ , the new metal/film interface is defined to be located at $x_1$ . . . . . 3-30

## FIGURES (cont'd)

Figure	Page
3-15	Lifetime of an Alloy 22 plate (with an initial thickness of 2 cm) versus the critical vacancy concentration fraction, $P_{\max}$ ..... 3-31
3-16	Repassivation potentials as a function of chloride at 95 °C for Alloys 825, 625, and 22 as well as Type 316L stainless steel ..... 3-33
3-17	Effect of temperature on the repassivation potential for crevice corrosion of Alloy 22 in $\text{Cl}^-$ solutions ..... 3-33
3-18	Repassivation potential for crevice corrosion of Alloy 22 as a function of $\text{Cl}^-$ concentration at various temperatures ..... 3-34
3-19	Repassivation potential for crevice corrosion of base metal and welded Alloy 22 in $\text{Cl}^-$ solutions ..... 3-35
3-20	Effect of thermal aging at 870 °C on the repassivation potential of Alloy 22 ..... 3-36
4-1	Distribution of corrosion rates calculated by U.S. Department of Energy from weight-loss data generated for Ti Grade 16 after 1-yr exposure ..... 4-3
4-2	Composite distribution of general corrosion rates for Ti Grade 16 after 1-yr exposure at the long-term corrosion test facility ..... 4-4
4-3	Polarization behavior of Ti Grade 7 in simulated concentrated water at 120 °C conducted by the U.S. Department of Energy ..... 4-5
4-4	Distribution of drip shield corrosion rates illustrating range of values when uncertainties and variability have been included ..... 4-6
4-5	Predicted drip shield failure times using WAPDEG for the basecase (mean), and enhanced (95 <sup>th</sup> percentile) and degraded (95 <sup>th</sup> percentile) drip shield cases ..... 4-8
4-6	Effect of drip shield case on the predicted dose rate demonstrating little effect of drip shield performance on dose rate consequence ..... 4-8
4-7	Long-term passive current measurement for Ti Grade 7 in deaerated, 1M NaCl solution at 95 °C ..... 4-10
4-8	Effect of fluoride on the anodic polarization behavior of Ti Grade 7 as compared to the polarization behavior in chloride-only solutions ..... 4-10
4-9	Effect of fluoride on the passive current density for Ti Grade 7 over time in a deaerated, 1 M NaCl solution at 95 °C and an applied potential of 0 $V_{\text{SCE}}$ ..... 4-11
4-10	Effect of fluoride on the steady-state passive current density for Ti Grade 7 in deaerated, 1 M NaCl solution at 95 °C and an applied potential of 0 $V_{\text{SCE}}$ ..... 4-12
4-11	Effect of fluoride on the passive current density of Ti Grade 7 in various deaerated solutions containing chloride, nitrate, and sulfate at 95 °C ..... 4-13
4-12	Polarization behavior of Ti Grade 7 in deaerated, 5 M NaCl at 95 °C with a scan rate of 0.167 mV/s ..... 4-13
4-13	Effect of chloride concentration on the breakdown ( $E_{bd}$ ) and repassivation ( $E_{rp}$ ) potential for wrought and welded Ti Grade 7 in deaerated solutions at 95 °C ..... 4-14
4-14	Postpolarization scanning electron micrograph showing corrosion attack ..... 4-15
4-15	Effect of temperature on the repassivation potential ( $E_{rp}$ ) of wrought and welded Ti Grade 7 in deaerated, 1 M NaCl solutions ..... 4-16

## FIGURES (cont'd)

Figure		Page
4-16	Backsc showin arly uniform atomic mass distribution	4-17
4-17	Optica micro: graph at 100x showing base metal, heat affected zone, and weldment res for Ti Grade 7	4-17
4-18	Potent. deaerat polarization of creviced Ti Grades 2 and 7 specimens in M NaCl at 95 °C and an applied potential of 0 V <sub>SCE</sub>	4-18
4-19	Cathodi 5 M NaC rization of Ti Grades 2 and 7 in a simulated crevice solution of M HCl, at 95 °C	4-19
4-20	Anodic 5 M NaC zation of Ti Grades 2 and 7 in a simulated crevice solution of M HCl, at 95 °C	4-20

## TABLES

Table		Page
2-1	Revised pore water compositions from Yucca Mountain vicinity .....	2-3
2-2	Composition of J-13 Well water .....	2-4
2-3	Lead concentration in groundwater near Yucca Mountain .....	2-6
2-4	Deliquescence point single salt and salt mixtures at 16.5 °C .....	2-9
2-5	Evaporation concentrating of synthetic 100X J-13 Well water .....	2-12
2-6	Evaporation concentrating of synthetic pore water .....	2-13
2-7	The composition of several aqueous solutions used for corrosion testing .....	2-16
2-8	Recipe for basic saturated water .....	2-17
3-1	Chemical composition (in weight percent) of the heats of Alloys 22 and 622 filler metal .....	3-18
3-2	Chemical analyses of test solutions and corrosion products .....	3-23

## ACKNOWLEDGMENTS

This report was prepared to document work performed by the Center for Nuclear Waste Regulatory Analyses (CNWRA) for the U.S. Nuclear Regulatory Commission (NRC) under Contract No. NRC-02-97-009. The activities reported here were performed on behalf of the NRC Office of Nuclear Material Safety and Safeguards, Division of Waste Management. The report is an independent product of the CNWRA and does not necessarily reflect the views or regulatory position of the NRC.

The authors gratefully acknowledge G. Cragnolino for technical review, the programmatic review of B. Sagar, and the editorial reviews of C. Cudd, B. Long, J. Pryor, and A. Woods. Appreciation is due J. Gonzalez for assistance in preparing of this report.

**QUALITY OF DATA:** Sources of data are referenced in each chapter. CNWRA-generated laboratory data contained in this report meet quality assurance (QA) requirements described in the CNWRA QA Manual. Data from other sources, however, are freely used. The respective sources of non-CNWRA data should be consulted for determining levels of QA.

**ANALYSES AND CODES:** The NRC/CNWRA Total-system Performance Assessment code Versions 3.2 and 4.1 were used for some analyses presented in this report. Additionally, a procedure in Mathematica Version 4.0, a commercial scientific software program was constructed to perform some of the calculations associated with Alloy 22 passive film modeling. Details concerning this procedure can be found in CNWRA scientific notebook number 304. Other analyses from the DOE total system Performance Assessment code are also presented.

## EXECUTIVE SUMMARY

The current U.S. Department of Energy (DOE) safety strategy for the proposed high-level waste repository at Yucca Mountain, Nevada, relies on several key attributes, including long-lived waste packages and drip shield. The reference waste package design is composed of two concentric containers of different metallic materials emplaced horizontally in a drift. The outer container or barrier will be made of a highly corrosion-resistant Ni-Cr-Mo alloy, Alloy 22, that will be at least 2 cm thick surrounding an inner container made of Type 316 nuclear grade stainless steel. Extending the length of the emplacement drifts, enclosing the top and sides of the waste package will be an arched mailbox-shaped drip shield, fabricated with a Ti-Pd alloy (Ti Grade 7). In undisturbed repository conditions, corrosion is expected to be the primary degradation process limiting the lives of the waste package and drip shield. Through-wall penetration of the drip shield by corrosion will allow the water entering into the emplacement drifts to contact the waste package outer surface. The quantity and chemistry of the water contacting the waste package, as well as the relative humidity (RH) and the waste package temperature, will determine the mode and rate of corrosion of the waste package outer container. Loss of containment as a result of corrosion will allow release of radionuclides to the environment surrounding the waste package and eventual radiation exposure (measured as dose) to the public. As part of the precicensing consultations between the U.S. Nuclear Regulatory Commission (NRC) and DOE, effort has been made to resolve key technical issues that are important to repository performance. Under this issue resolution process, the issue of waste package and drip shield degradation are considered "closed-pending," that is it is anticipated that the DOE will be able to supply to the NRC sufficient information to review any license application that DOE may issue.

To aid in this review process, the Center for Nuclear Waste Regulatory Analyses (CNWRA) performed limited scope experimental studies to examine the effects of environmental variables on the general and localized corrosion of the waste package and drip shield. In addition to aiding in issue resolution, these studies also assist NRC staff in responding to public comments and comments generated by the Advisory Committee on Nuclear Waste. This report examines the effects of environmental variables on general and localized corrosion of the waste package and drip shield and provides a review of recent work conducted at the CNWRA considering the possible environments predicted for the repository and the DOE experimental program.

The report is organized into five chapters (i) background and introductory information, (ii) possible environments predicted to occur in Yucca Mountain, (iii) the influence of the various components of the predicted environments on the general and localized corrosion of the waste package, (iv) the influence of the various components of the predicted environments on the general and localized corrosion of the drip shield, and (v) areas that warrant further investigation.

The environment in the emplacement drifts may have a significant effect on the long-term performance of the engineered barriers. Environmental characteristics identified as important to long-term engineered barrier performance include temperature, chemistry of deliquescent salts, groundwater composition, concentration of trace elements in the host rock and groundwater, and evaporative concentration of dissolved salts. Groundwater at Yucca Mountain has been classified into two types: unsaturated zone pore water, and saturated zone water and perched water in the unsaturated zone. The compositions of the saturated zone and perched waters are dominated by rock/mineral interactions and are sodium bicarbonate based waters. Unsaturated zone water samples have been extracted from boreholes. Because of uncertainties associated

with the extraction of pore waters from relatively dry rocks at Yucca Mountain, the characteristics of pore waters are not yet fully understood. Groundwater and the host rock in the Yucca Mountain region have measurable concentrations of trace elements such as lead and mercury. These trace elements may promote localized corrosion and stress corrosion cracking of engineered barrier subsystem components.

Hygroscopic salts may be deposited onto the surfaces of engineered barrier subsystem components by evaporation of groundwaters or from dust or aerosols entrained in the drift air. Analysis has shown that the mutual deliquescence RH of a salt mixture is lower than the deliquescence point of any of its pure components. Based on the deliquescence point of the NaCl-NaNO<sub>3</sub>-KNO<sub>3</sub> system, and the presence of the highly hygroscopic salts such as CaCl<sub>2</sub> and MgCl<sub>2</sub>, the minimum deliquescence point may be close to 20 percent. With such a low deliquescence point, the engineered barrier system components, if in contact with salt deposits, would be subject to aqueous corrosion during the entire emplacement period.

Evidence exists that the effect of bacteria on the average bulk environment is small, and this conclusion cannot be extrapolated to local environmental effects. Arguments based on low microbial activity, because of limited nutrients, water, energy, or other components of the metabolic process, do not explain how localized impacts can be distributed in the repository, in the drift, or over a waste package surface. To characterize adequately the effects of microbial activity on the environment, the distribution of components or effects, including development of biofilms, needs to be considered. DOE has not investigated the effects of localized impacts such as biofilm development, colloid formation, and the production of inorganic acids, methane, organic byproducts, carbon dioxide, and other chemical species that could change the longevity of materials and the transport of radionuclides from the near field. In addition, use of repository construction and structural materials should be considered as possible nutrient and energy sources.

The DOE prediction of waste package lifetimes is based on uniform corrosion rates in the absence of localized corrosion. Data used by the DOE for the uniform corrosion rates are confounded by the deposition of silica on the test specimens and limited by the relatively poor sensitivity of weight-loss measurements. Susceptibility of Alloy 22 to localized corrosion was determined to be negligible based on a comparison of corrosion potentials to a critical potential for the initiation of localized corrosion. The comparison did not include the critical potential for crevice corrosion, even though it is the most likely localized corrosion mode for the waste packages. Phase instability as a result of thermal aging and microbially influenced corrosion was assumed to accelerate the uniform corrosion rate rather than increase susceptibility of the alloy to localized corrosion. CNWRA studies showed the performance of the Alloy 22 waste package outer barrier to be dependent on the composition of the environment and fabrication processes. Passive uniform corrosion rates measured for potentiostatic conditions are less than 10<sup>-3</sup> mm/yr, suggesting that in the absence of conditions necessary for pit initiation and propagation of localized corrosion, lifetimes of the proposed 20-mm-thick waste packages will be greater than the 10,000-yr regulatory compliance period. It should be noted, however, that the base alloy in the as-received condition is susceptible to localized corrosion in the chloride solutions at concentrations possible during anticipated repository conditions. Fabrication processes, such as welding and local thermal aging as a result of the proposed induction annealing stress mitigation process, can significantly alter the long-term performance of the alloy. Thermal aging tests have shown a significant decrease in the localized corrosion resistance compared to as-received material.

DOE currently is predicting drip shield lifetimes to be greater than the 10,000-yr compliance period. This prediction is based on the observation that localized corrosion of Ti Grade 7 is difficult to initiate and thus the primary mode of corrosion failure for the drip shield is uniform general corrosion (excluding hydrogen-induced

cracking). The corrosion rates used by DOE in predicting performance are derived from weight loss measurements. Unfortunately, weight loss measurements on highly corrosion-resistant materials exposed to relatively benign solutions typically are not sensitive measures of the corrosion rate (i.e., the amount of weight lost is too small to measure effectively and accurately). CNWRA studies showed that pitting corrosion of Ti Grade 7 is an unlikely failure mode for the drip shield because pitting was only observed at potentials well outside the thermodynamic stability region for aqueous solutions. The possibility of crevice corrosion occurring on Ti Grade 7 at lower potentials has been investigated, but no corrosion has been observed. In contrast to DOE, CNWRA used long-term potentiostatic polarization testing to monitor passive current density of the possible effects of environment on dissolution rates. It is clear the presence of fluoride, even at relatively low concentrations, led to a considerable increase in the dissolution rate of Ti Grade 7. The effects of this increase on the predicted performance of the drip shield should be evaluated further by the DOE (as agreed to in DOE/NRC technical exchanges).

It is clear a number of uncertainties exist in the current information provided by DOE in the areas of waste package and drip shield performance. These uncertainties include the range of environments to which the waste package and drip shield may be exposed, the effects and concentrations of trace impurities that may be present, the effects of microbial activity and thermal aging on the materials, and the general corrosion rates that have been calculated. Because of these uncertainties, various agreements between DOE and NRC have been arranged that commit DOE to provide technical justifications, additional measurements, or both using the same or alternative methods. CNWRA examinations of some of the concerns have assisted in resolving these issues. The results generated are also used in the NRC/CNWRA Total-system Performance Assessment code to predict performance of the proposed Yucca Mountain repository. The CNWRA experiments demonstrated that enhanced concentration of various deleterious species can occur through evaporative processes, and a wide range of possible environments may be encountered in the repository. Alloy 22 has been found to be resistant to localized corrosion in the wrought condition; however, thermal aging and welding tend to make the material more susceptible to localized corrosion. Also, the passive corrosion rate of Alloy 22 has proven to be relatively insensitive to possible variations in the environmental conditions. Ti Grade 7 has been observed to be essentially immune to pitting corrosion except at extremely high potentials (well above those reasonably expected in the repository). Long-term polarization at lower potentials revealed that Ti Grade 7 is highly resistant to crevice corrosion, though it is uncertain if crevice corrosion might begin at longer times (perhaps years are needed). Ti Grade 7 owes this high resistance to localized corrosion to the addition of Pd. Pd additions, however, did not mitigate the effects of fluoride, which was shown to dramatically increase the passive corrosion rate by several orders of magnitude even at relatively low concentrations.

Additional efforts are needed to evaluate the potential DOE safety case. These efforts include examining the effects of minor impurities and fabrication on corrosion and understanding the effects of fluoride on corrosion of Ti. The possibility of stress corrosion cracking of Alloy 22 and hydrogen induced cracking of Ti will be addressed in a subsequent report. These activities not only improve the technical credibility of the NRC and CNWRA but also help identify high risk issues DOE should focus on prior to the license application.

# 1 INTRODUCTION

The current U.S. Department of Energy (DOE) safety strategy for the proposed high-level waste (HLW) repository at Yucca Mountain, Nevada, relies on several key attributes, including long-lived waste packages and drip shield (Civilian Radioactive Waste Management System Management and Operating Contractor, 2000a). In the proposed DOE site recommendation, the reference waste package design is composed of two concentric containers of different metallic materials emplaced horizontally in a drift. The outer container or barrier will be made of a highly corrosion-resistant Ni-Cr-Mo alloy, Alloy 22, that will be at least 2-cm thick surrounding an inner container made of Type 316 nuclear grade stainless steel. Extending over the length of the emplacement drifts enclosing the top and sides of the waste package will be an arched mailbox-shaped drip shield, fabricated using a Ti-Pd alloy (Ti Grade 7). Under undisturbed repository conditions, corrosion is expected to be the primary degradation process limiting the life of the waste package and the drip shield (Civilian Radioactive Waste Management System Management and Operating Contractor, 2000a; U.S. Nuclear Regulatory Commission, 2001). Through-wall penetration of the drip shield by corrosion will allow the water entering into the emplacement drifts to contact the waste package outer surface. The quantity and chemistry of the water contacting the waste package, as well as the relative humidity (RH) and the waste package temperature, will determine the mode and rate of corrosion of the waste package outer container. Loss of containment as a result of corrosion will allow the release of radionuclides to the environment surrounding the waste package and an eventual dose to the average member of the critical group.

The corrosion-related processes that are considered important in the degradation of the waste package and drip shield include humid-air and uniform aqueous (general) corrosion, localized (pitting, crevice, and intergranular) corrosion, microbially influenced corrosion, stress corrosion cracking, and hydrogen embrittlement, in addition to dry-air oxidation that occurs during the initial period following waste emplacement when the radioactive decay heat keeps moisture away from the gaseous environment surrounding the waste package. Degradation of the waste package and drip shield are considered under the U.S. Nuclear Regulatory Commission (NRC) Container Life and Source Term (CLST) Key Technical Issue as subissues 1 and 6 and as ENG 1 (Degradation of Engineered Barriers) under the integrated subissue structure. As part of the prelicensing consultations between the DOE and the NRC, effort has been made to resolve key technical issues that are important to repository performance. Under this issue resolution process, the issue of waste package and drip shield degradation are considered "closed-pending," that is it is anticipated DOE will be able to supply to the NRC sufficient information to review any license application that DOE may issue.

To aid in this review process, the Center for Nuclear Waste Regulatory Analyses (CNWRA) engaged in a series of limited scope experimental studies to examine the effects of environmental variables on the general and localized corrosion of waste package and drip shield materials. These studies also assist NRC staff in responding to public comments and comments generated by the Advisory Committee on Nuclear Waste. This report examines the effects of environmental variables on the general and localized corrosion of waste package and drip shield materials and provides a review of recent work conducted at CNWRA regarding the possible environments that have been predicted for the repository and the DOE experimental program. How these results are utilized in making long-term predictions of material performance will also be given where applicable.

The various environments that are predicted to occur in the repository are discussed in chapter 2. These environments include waters based on J-13 Well water, pore waters, and seepage waters. Also included is

a discussion of the water chemistry that can develop when water is in contact with rock fracture surfaces. The deliquescence of various possible salts is also addressed. The possible changes to the environment resulting from microbial activity as well as some experimental work conducted at the CNWRA laboratory heater test facility to monitor water chemistry changes are also presented.

Chapter 3 highlights the issues related to general and localized corrosion of the waste package outer barrier of Alloy 22. The main environmental variables that influence corrosion of Alloy 22 are mentioned, and a discussion of the DOE program to evaluate and examine the corrosion behavior of Alloy 22 is provided. Work conducted at the CNWRA related to localized and passive corrosion of Alloy 22 is then summarized, and the way these results are used in the NRC/CNWRA Total-system Performance Assessment (TPA) code to predict waste package performance is described.

Similar to chapter 3, chapter 4 examines the general and localized corrosion of Ti alloys for use as a drip shield material. A brief discussion of the important environmental variables on the general and localized corrosion of Ti alloys is provided. An overview of the DOE approach to determine the corrosion rate for general corrosion, the conditions needed for initiation of localized corrosion, and the utilization of these results to perform long-term predictions of material performance is also given. Efforts at CNWRA to evaluate the effects of temperature, chloride, fluoride, and applied potential on the corrosion of Ti Grade 7 are then discussed.

Because of changes in the waste package design and materials chosen, as well as new findings of possible environmental variables not fully evaluated (e.g., trace impurities), a number of areas deserve additional examination as discussed in chapter 5, including examination of the effects of minor impurities on the corrosion of Alloy 22 and Ti Grade 7. Additional work in these areas will assist in issue resolution and aid in reviewing any license application.

## 2 POSSIBLE REPOSITORY ENVIRONMENTS

### 2.1 AMBIENT AND THERMALLY PERTURBED GROUNDWATER COMPOSITIONS FROM THE VICINITY OF YUCCA MOUNTAIN

Understanding groundwater chemistry at Yucca Mountain is necessary in predicting the long-term performance of the proposed high-level waste repository. Drip shield and waste package corrosion requires the presence of water, and water is also expected to facilitate the transport of radionuclides away from breached waste packages. The modes and rates of drip shield and waste package corrosion are strongly influenced by the concentrations of dissolved components in the water, but these concentrations will change with time as the groundwater interacts chemically with surrounding materials along a thermally perturbed flow path. To predict the range of water compositions that might seep into the waste emplacement drifts during the 10,000-yr compliance period, DOE and the NRC and CNWRA staffs are using a combination of analytical groundwater data and models. Analytical ambient groundwater compositions are generally used to characterize current geochemical conditions at Yucca Mountain, parameterize site specific mineral behavior, and initialize numerical reactive transport models. There are fewer available data on groundwater compositions under thermally perturbed conditions, and these data are generally used in numerical models to extrapolate from ambient to thermal conditions and across extended time intervals.

The chemical compositions of ambient groundwater from Yucca Mountain are expected to evolve significantly before contacting drip shields and waste packages. A number of different factors will control the composition of water as it percolates through the overlying rock toward the emplacement drifts, including temperature, the types of materials that interact chemically with the water along the flow pathway, and the flow velocity versus reaction rates. Thermal-hydrological models developed by the DOE indicate temperatures at the drift crown only will remain above the nominal boiling temperature (e.g., 97 °C) for several hundred years (Civilian Radioactive Waste Management System Management and Operating Contractor, 2000b). This may suggest that groundwater compositions may adequately characterize seepage compositions for the majority of the 10,000-yr compliance period. It is unlikely that pore waters at any temperature will ever drip from the drift crown at the Yucca Mountain repository in significant volumes because fractures are expected to be the predominant flow pathway to the drift. Even if pore water did drip from the drift crown after the thermal period, the effects would likely be unimportant to the lifetime of the drip shield/waste package because corrosion is enhanced in higher temperature, more saline solutions. Regardless of its origins, the chemical composition of seepage water is expected to evolve significantly in the drift environment through evaporation and salt formation processes and by interaction with engineered materials. Thus, ambient groundwaters that originated above the proposed repository would be subjected to a variety of environmental conditions that would change its chemical composition over time. Predictions of the quantity and chemistry of water contacting the drip shields and waste packages over the 10,000-yr compliance period for the proposed Yucca Mountain repository are difficult and must be accomplished by considering both analytical data and numerical models for a realistic set of conditions.

Section 2.1.1 discusses the range of analytical groundwater compositions from Yucca Mountain, measured under both ambient and thermally perturbed conditions. In addition, section 2.1.1 summarizes seepage water compositions and evaporating water compositions in the engineered barrier subsystem environment predicted by numerical models.

### 2.1.1 Ambient Unsaturated and Saturated Zone Groundwater Compositions

The unsaturated zone at Yucca Mountain contains pore water, fracture water, and isolated lens of perched water. There are no measured fracture water compositions from Yucca Mountain because of the difficulty of collecting fracture water samples. However, fracture water has been collected from Rainier Mesa (White et al., 1980), and it appears to be similar in composition to perched and saturated zone waters collected at Yucca Mountain.

Yang et al. (1996, 1998) squeezed pore waters from core samples from boreholes USW UZ-14 and UE-25 UZ#16, SD-7, SD-9, and SD-12 using high-pressure uniaxial compression techniques. Samples were collected from various depths in the boreholes and analyzed for their chemical compositions. Perched water compositions from boreholes USW UZ-14 and SD-7 and extracted pore water compositions were measured using inductively coupled plasma spectroscopy and ion chromatography. These data indicate that pore water compositions contain significantly larger concentrations of chloride and dissolved solids than the compositions of saturated zone waters, perched waters, and, by analogy with Rainier Mesa data, fracture waters. Pore water compositions vary significantly both laterally and vertically, and ionic strengths may increase substantially with depth.

Although the pore water chemistry data reported by Yang et al. (1996, 1998) provide a valuable characterization of groundwater chemistry at Yucca Mountain, there are indications that aspects of the reported data are unreliable. Yang et al. (1998) discuss uncertainties associated with the extraction process and report persistent large ionic charge imbalances with the data. Browning et al. (2000) further evaluated the data for reliability and identified unequilibrated aqueous speciation relationships and erratic variability with depth in some species concentrations. Unfortunately, Yang et al. (1996, 1998) do not report several minor and trace element concentrations that may be important to drip shield and waste package performance.

Uncertainties associated with the extraction of pore waters from relatively dry rocks at Yucca Mountain cannot be avoided and are not fully understood. Thus, modeling approaches have been developed to improve the reliability of available pore water data collected from Yucca Mountain. Apps (1997) used the geochemical code EQ3/6 (Wolery, 1992) to adjust the bicarbonate concentrations reported by Yang et al. (1996, 1998) to force calcite equilibria. This approach is reasonable because calcite reaction rates are expected to be rapid. This approach does not charge balance the data or reduce erratic variations in measured pH with depth, however, suggesting that these problems may be related to the extraction process rather than the more familiar types of analytical uncertainties. Browning et al. (2000) used EQ3/6 (Wolery, 1992) to restore thermodynamic consistency to the data by introducing measured CO<sub>2</sub> gas pressure as a constraint, imposing equilibrium aqueous speciation and adjusting the pH to achieve charge balance. This method eliminated charge imbalances, reduced erratic variations in pH with depth, and restored internal thermodynamic consistency to the data but resulted in some solutions being supersaturated in calcite. Reinterpreted water chemistry data were used to evaluate and interpret vertical and lateral variations in water chemistry and differences between unsaturated zone pore and perched water compositions and water-rock equilibria. Table 2-1 contains a range of revised pore water compositions from Browning et al. (2000). These particular analyses were selected from a larger database to represent different compositional categories in the chemical divide theory discussed in section 2.3.

Table 2-1. Revised pore water compositions from Yucca Mountain vicinity

Compositional Group*		III	III	III	IV	IV	IV	V	V	V	VI	VI	VI
Species	Units	SD-12/ 1558 <sup>†</sup>	UZ-14/ 1542	UZ-14/ 1734	UZ-14/ 100.4	UZ-14/ 85.2-ε	SD9/ 251.8-2	UZ-14/ 1277	SD-9/ 94.2	NRG-6/ 158.2	UZ-14/ 1409	NRG-6/ 244.ε	UZ-14/ 240.8
Mg <sup>++</sup>	mg/L	0.1	0.5	0.3	13.8	13.2	8	5.1	24	23.3	0.7	4.9	1
SiO <sub>2(aq)</sub>	mg/L	76.1	143	50.7	91.8	89.8	55	3.8	74	97.4	57	51	61
K <sup>+</sup>	mg/L	8	8	8	8	8	8	8	8	8	8	8	8
Al <sup>+++</sup>	mg/L	2.60E-05	3.35E-06	9.21E-05	1.86E-05	1.86E-05	7.46E-05	5.59E-04	0.105	2.05E-05	9.22E-05	6.95E-05	2.83E-05
SO <sub>4</sub> <sup>2-</sup>	mg/L	54	28	17.5	83	66	73	38	260	159	106	115	100
Ca <sup>++</sup>	mg/L	4.4	3.6	2	51.1	49.9	44	74	125	122	30	33	32
Fe <sup>+++</sup>	mg/L	1.00E-07	1.00E-07	1.00E-07	1.00E-07	1.00E-07	1.00E-07	1.00E-07	1.00E-07	1.00E-07	1.00E-07	1.00E-07	1.00E-07
Na <sup>+</sup>	mg/L	155	207	184	41.3	43.5	53	45	43	35.6	88	72	103
Cl <sup>-</sup>	mg/L	33	20	39.4	44	60	60	130	170	185	75	49	99
NO <sub>3</sub> <sup>-</sup>	mg/L	4.00E-01	4	5.6	23	22	14.2	15	11	32	5	40	17
pH	—	8.5	8.7	8.6	8.1	8.1	8.0	8.0	5.2	7.6	7.8	7.7	7.8
T	°C	27.63	27.77	28.8	19.96	19.88	20.78	26.33	19.93	20.28	27.05	20.7	20.72

2-3

\*Compositional group refers to chemical divide diagram as described in the text.

<sup>†</sup>Revised pore water data from Browning et al. (2000). Sample identification nomenclature after Yang et al. (1996, 1998).

<sup>‡</sup>Ambient K<sup>+</sup> concentrations adopted from data in Civilian Radioactive Waste Management System Management and Operating Contractor. 2000.

Note: All solutions have a CO<sub>2</sub> concentration of 10<sup>-3</sup> bars and an O<sub>2</sub> concentration of 0.17 bars.

Browning, L., W.M. Murphy, B.W. Leslie, and W.L. Dam. Thermodynamic interpretations of chemical analyses of unsaturated zone water from Yucca Mountain, Nevada. *Scientific Basis for Nuclear Waste Management XXIII*. R.W. Smith and D.W. Shoosmith, eds. Symposium Proceedings 608. Pittsburgh, PA: Materials Research Society: 237-242. 2000.

Civilian Radioactive Waste Management System Management and Operating Contractor. *Drift-Scale Coupled Processes (DST and THC Seepage) Models*. MDL-NBS-HS-000001. ICN 01. Las Vegas, NV: Civilian Radioactive Waste Management System Management and Operating Contractor. 2000.

Yang I. C., G.W. Rattray, and P. Yu. *Interpretation of Chemical and Isotopic Data from Boreholes in the Unsaturated Zone at Yucca Mountain, Nevada*. U.S. Geological Survey Water Resources Investigations Report 96-4058. 1996.

Yang I. C., P. Yu, G.W. Rattray, J.S. Ferarese, and R.N. Ryan. *Hydrochemical Investigations in Characterizing the Unsaturated Zone at Yucca Mountain, Nevada*. U.S. Geological Survey Water Resources Investigations Report 98-4132. 1998.

Saturated zone groundwaters lie below the proposed repository site and are most relevant to studies involving the transport of radionuclides away from the drift following waste container failure. Samples of saturated zone water pumped from the J-13 Well, as reported by Harrar et al. (1990), have been used extensively by the DOE as a reference to represent Yucca Mountain groundwater compositions in the past (Civilian Radioactive Waste Management System Management and Operating Contractor, 1998, 1999), but J-13 Well water compositions were apparently intended as a proxy for more evolved water compositions output from process-level models that had not yet been developed.<sup>1</sup> The composition of J-13 Well waters is shown in table 2-2 (Civilian Radioactive Waste Management System Management and Operating Contractor, 2000c). Compared to pore water compositions from Yucca Mountain, J-13 Well water is more dilute with higher concentrations of sodium and dissolved C-bearing species and lower concentrations of calcium, chloride, and sulfates. Kerrisk (1987) and Perfect et al. (1995) provide geochemical interpretations and compilations of analytical saturated zone groundwater compositions from the vicinity of Yucca Mountain.

Figure 2-1 compares the compositions of groundwaters from the saturated zone in the vicinity of Yucca Mountain, reported by Kerrisk (1987), with revised perched and pore water data for borehole USW

**Table 2-2. Composition of J-13 Well water\***

Species	Concentration (mg/L)	Concentration (mM)
Ca <sup>++</sup>	13.0 ± 0.99	0.33 ± 0.02
Cl <sup>-</sup>	7.14 ± 0.61	0.20 ± 0.02
F <sup>-</sup>	2.18 ± 0.29	0.11 ± 0.02
HCO <sub>3</sub> <sup>-</sup>	128.9 ± 8.6	2.11 ± 0.14
K <sup>+</sup>	5.04 ± 0.61	0.13 ± 0.02
Mg <sup>++</sup>	2.01 ± 0.21	0.08 ± 0.01
NO <sub>3</sub> <sup>-</sup>	8.78 ± 1.03	0.14 ± 0.02
Na <sup>+</sup>	45.8 ± 2.29	1.99 ± 0.10
SO <sub>4</sub> <sup>2-</sup>	18.4 ± 1.03	0.19 ± 0.01
Si <sub>(aq)</sub>	28.5 ± 1.85	1.02 ± 0.07
pH	7.41 ± 0.44	—

\* Civilian Radioactive Waste Management System Management and Operating Contractor. *Environment on the Surfaces of the Drip Shield and Waste Package Outer Barrier*. ANL-EBS-MD-000001, ICN 01. Revision 00. Las Vegas, NV: Civilian Radioactive Waste Management System Management and Operating Contractor. 2000.

<sup>1</sup>Reamer, C.W. *Summary Highlights of NRC/DOE Technical Exchange and Management Meeting on Key Technical Issue: Evolution of the Near-Field Environment*. Letter (January 26) to D. Brocoum, U.S. Department of Energy. Washington, DC: U.S. Nuclear Regulatory Commission. 2001.

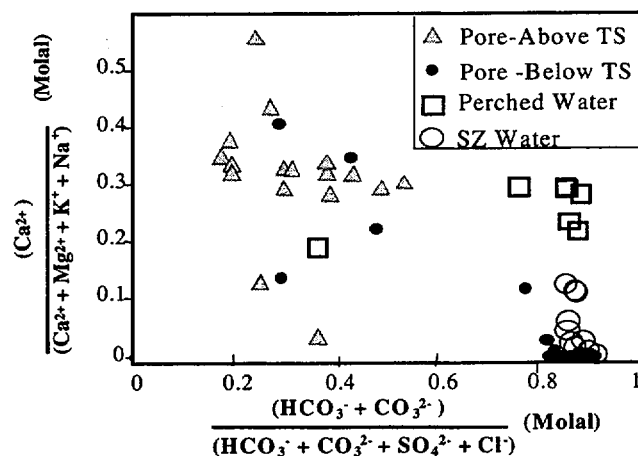


**Figure 2-1. Comparison between revised pore and perched water compositions from borehole USW UZ-14 and saturated zone water compositions from Yucca Mountain (Yang et al., 1996; Kerrisk, 1987)**

UZ-14. Below the Topopah Spring Tuff, the concentrations of  $\text{SO}_4^{2-}$ ,  $\text{Ca}^{2+}$ , and  $\text{Mg}^{2+}$ , which are probably derived predominantly from the ground surface, are significantly diminished. The compositions of perched waters, deep pore waters, and saturated zone waters differ from near-surface pore waters by low relative proportions of  $\text{Ca}^{2+}$  and high proportions of total carbonate relative to other anions. Despite possible differences in their flow path and residence times, these three groundwater types have evolved to similar compositions. Pore waters are generally more concentrated than perched waters, and pore water concentrations increase with depth (Yang et al., 1996). The  $\text{Cl}^-$  concentrations in perched waters and saturated zone waters are lower than in the adjacent pore waters, which led Yang et al. (1996) to conclude that perched waters experienced less water-rock interaction and, therefore, must be supplied by fast fracture flow. Although perched waters may be supplied predominately by fracture flow,  $\text{Cl}^-$  is unlikely to be affected strongly by water-rock interactions. Elevated pore water concentrations might be an artifact of the compression techniques used to extract the waters from the unsaturated zone core for chemical analysis. Compression techniques were not used to collect either perched or saturated zone waters. Evaporation would cause unsaturated zone pore waters to become more concentrated, particularly in nonvolatile anions, but would have a lesser effect on adjacent perched waters replenished by fast pathway fracture flow.

Rock-water interactions over extended periods can also lead to leaching of specific detrimental species that may become concentrated in the water dripping on the drip shield and waste packages. Among these potential detrimental species, Pb has been found to promote stress corrosion cracking and enhance localized corrosion of Alloy 22.<sup>2</sup> Therefore, it is important to examine the existence of minerals that may become a significant source of Pb. In particular, since fractures may act as transport pathways or conduits for fluids moving through and away from the proposed repository horizon, the nature of minerals lining the walls of fractures is of great importance. In a series of studies, Carlos et al. (1990, 1993, 1995) observed the

---

<sup>2</sup>Barkatt, A., and J.A. Gorman. Tests to explore specific aspects of the corrosion resistance of C-22. *Presentation to Nuclear Waste Technical Review Board*. August 1, 2000. Carson City, NV. 2000.

presence of Mn-oxide minerals in the silicic tuff prevailing in several stratigraphic units at Yucca Mountain. There were several Mn-oxide minerals identified, and the Mn-oxide mineralogy seemed to be controlled both by stratigraphy and position relative to the water table. In addition, the mineral chemistry was found to vary widely over short distances suggesting a strong influence of variations in water chemistry. Pb was mostly contained in coronadite  $[Pb(Mn^{4+}, Mn^{3+})_8O_{16} \cdot 0.3-0.8H_2O]$ , in which PbO reached about 23 percent, and in Pb-hollandite  $[Ba(Mn^{4+}, Mn^{3+})_8O_{16} \cdot 0.3-0.8H_2O]$ , in which substitution of Pb for Ba reached up to 10 percent of PbO (Carlos et al., 1990). In other Mn-oxide minerals, Pb was only found in trace amounts or at the most between 0.1 and 1 percent. Thick (up to 2 mm), continuous coatings of Mn-oxides were found predominantly in densely welded portions of the Crater Flat Tuff (Carlos et al., 1995), which is located below the water table. In the Paintbrush Tuff, Mn oxides only formed small crusts and dendrites. In summary, although in minor proportion, Pb was found as a component of some Mn-oxide minerals that are lining rock fractures in the vicinity of the proposed repository at Yucca Mountain. More detailed studies are needed to establish if indeed Pb can be found in greater proportions in fractures that may be a preferential path for water dripping into the emplacement drifts.

Groundwater in the Yucca Mountain region has been shown to have measurable concentrations of trace elements such as lead and mercury (Perfect et al., 1995). Table 2-3 lists the lead concentrations in groundwater in the Yucca Mountain region. It should be noted that mercury values were either zero or below the detection limit. The concentration of lead and mercury in the host rock samples collected from several locations near Yucca Mountain has been reported by Weiss et al. (1994) and Castor et al. (1994). Borehole samples collected within the Yucca Mountain controlled area boundary range had lead concentrations of 1.9 to 22.6 ppm and mercury concentrations in the range of <0.02 to 0.815 ppm. Mercury concentrations from rock samples collected from the Trench 14 Bow Ridge fault range from <0.050 to 3.08 ppm (Weiss et al., 1994). Nonpyritic tuff was reported to have lead concentrations of 0.9 to 97 ppm and mercury concentrations of 0.1 to 0.38 ppm (Castor et al., 1994).

**Table 2-3. Lead concentration in groundwater near Yucca Mountain**

Location	Lead Concentration in ppm
Well J-11 (Jackass Flat)	0.300
Well J-12 (Busted Butte)	0.016
Devils Hole	0.100
Amargosa Flat	0.100
Yucca Lake (Yucca Flat)	0.026
Yucca Flat, Well A	0.056
Fallout Hills NW (Fallout Hills, Obsidian Butte is on Pahute Mesa)	2.90 to 3.10

## 2.2 DELIQUESCENT BEHAVIOR OF SALT MIXTURES AND FORMATION OF AQUEOUS FILM AT LOW RELATIVE HUMIDITIES

There are several scenarios for aqueous solution formation on the engineered barrier system components. These scenarios include seepage flow into the drifts, episodic water flow, and water sorption by deposited hygroscopic salts. Hygroscopic salts may be deposited by evaporation of groundwater that contacts the waste package and drip shield or from dust or aerosols entrained in the drift air.

The evaporative deposition is more likely to take place on the surface of the heat transfer surfaces, such as the waste package and drip shield, than on the surfaces of the nonheat transfer surfaces, such as the steel supports and the gantry rail. This deposition occurs because the heat transfer components are usually hotter than the nonheat transfer components, and thus the RH on the surfaces of the heat transfer components is lower.

Natural waters on the surfaces of components maintained at elevated temperatures will be concentrated because the effective RH in the vicinity of these components will be low. The degree of solution concentration increases with decreasing RH until the deliquescence point is reached. At RHs below the deliquescence point, aqueous salt solutions are not thermodynamically stable, and, hence, solid salts can be deposited on the surface of engineered barrier system components. Inorganic salts comprise 25 to 50 percent of the atmospheric fine aerosol mass in polluted urban environments, and most of the salts exhibit deliquescence behavior upon exposure to a humid environment (Ge et al, 1996, 1998; Tang, 1980). The salts in the aerosols that have been studied include NaCl, KCl, NaNO<sub>3</sub>, (NH<sub>4</sub>)<sub>2</sub>SO<sub>4</sub>, NH<sub>4</sub>NO<sub>3</sub> (Ge et al., 1998), NH<sub>4</sub>HSO<sub>4</sub> (Tang et al., 1978), and MgCl<sub>2</sub> (Tang, 1976). The atmospheric NaCl comes from the evaporation of sea spray produced by bursting bubbles or wind-induced, wave-breaking action (Pandis et al., 1995). The reactions of NaCl aerosols with NO<sub>2</sub>, HNO<sub>3</sub>, and N<sub>2</sub>O<sub>5</sub> in the atmosphere produce NaNO<sub>3</sub> solids (Vogt and Finlayson-Pitts, 1994). These aerosol salts may be transported to the surfaces of the engineered barrier system components by ventilation. These salts on the surfaces of the engineered barrier system components, whether formed by evaporation or by aerosol deposition, will absorb moisture from the air when the RH is above a critical deliquescence RH value.

In the DOE analysis of the engineered barrier system environment, it is assumed that sodium and potassium will be the major cations in the concentrated Yucca Mountain waters, with sodium ions generally in excess of potassium ions (Civilian Radioactive Waste Management System Management and Operating Contractor, 2000c). Therefore, the hygroscopic salts on the engineered barrier system are limited to either sodium or potassium salts. As a bounding condition, it was assumed by DOE that sodium nitrate (NaNO<sub>3</sub>)—the salt with the lowest deliquescence point at elevated temperature (figure 2-2) will determine the minimum RH at which aqueous films will form on the drip shield and waste package outer barrier. The lowest deliquescence point of NaNO<sub>3</sub> was determined to be 50 percent at the boiling point of the repository horizon.

The use of the lowest deliquescence point for NaNO<sub>3</sub> as the bounding minimum RH (also called critical RH, RH<sub>crit</sub>) for salt mixtures that may contain significant amount of ions other than Na<sup>+</sup>, and NO<sub>3</sub><sup>-</sup>, such as K<sup>+</sup> and Cl<sup>-</sup>, ignores the interactions among these ions. Figure 2-3 shows the RH at saturation of an aqueous solution of NaCl and NaNO<sub>3</sub> at 25 °C (Ge et al., 1998). As shown in figure 2-3, a pure salt, either NaCl (x<sub>NaCl</sub> = 1) or NaNO<sub>3</sub> (x<sub>NaCl</sub> = 0) always has a well-defined RH or deliquescent point, and the salt

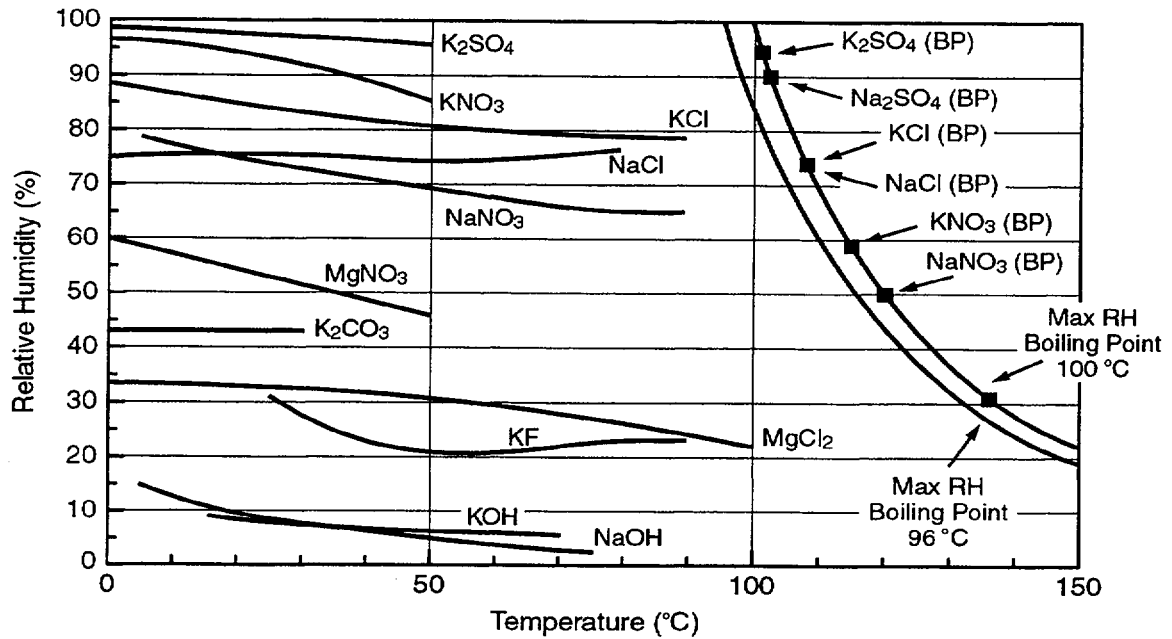


Figure 2-2. Deliquescent points (Civilian Radioactive Waste Management System Management and Operating Contractor, 2000c)

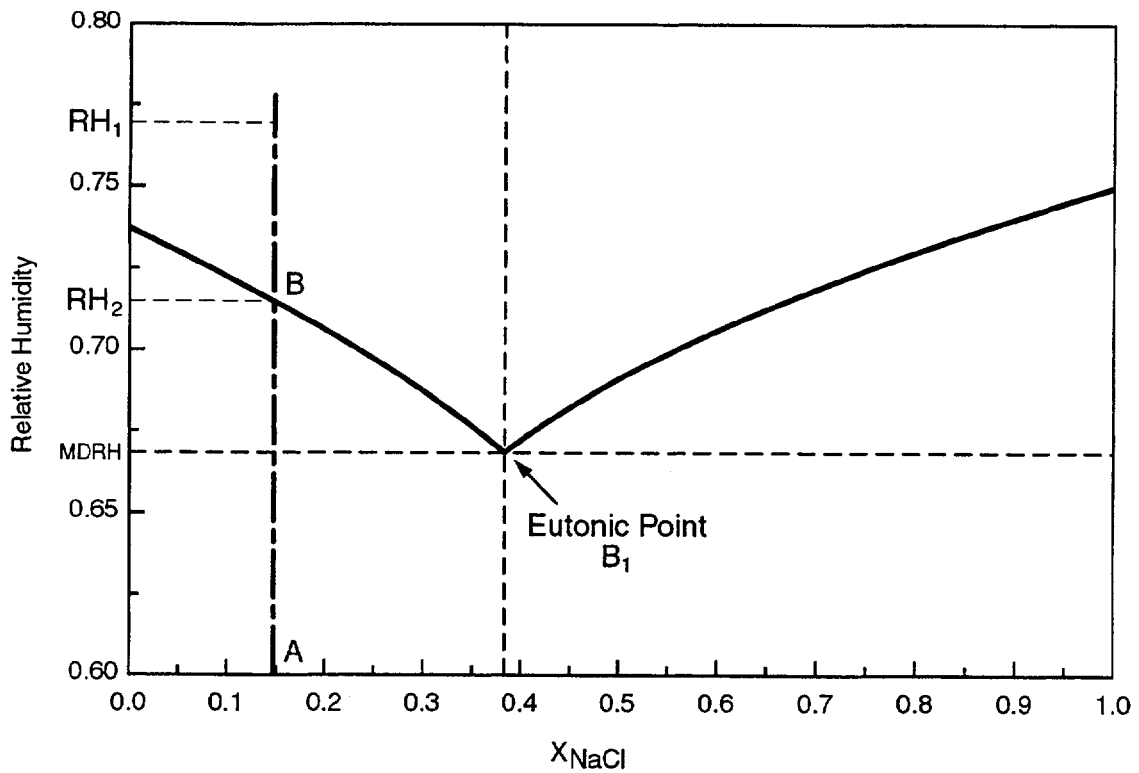


Figure 2-3. Relative humidity(RH) at saturation of an aqueous solution of  $\text{NaNO}_3$  and  $\text{NaCl}$  at  $25^\circ\text{C}$  (Ge et al., 1998) (MDRH = mutual deliquescence RH)

becomes dry if the RH is slightly decreased or becomes hydrated if the RH is slightly increased. For any other composition, the mutual deliquescence RH determines when a salt mixture starts to absorb water or becomes dry. For instance, a liquid composition A, on drying under equilibrium condition from RH<sub>1</sub>, will be a homogenous liquid until RH<sub>2</sub> is reached which is when the first infinitesimal amount of the solid NaNO<sub>3</sub> will crystallize. Upon further drying, NaNO<sub>3</sub> will continue to crystallize while the composition of the liquid follows the curve B-B<sub>1</sub> until the mutual deliquescence RH is reached. At the mutual deliquescence RH, the liquid will crystallize into a solid mixture of NaCl and NaNO<sub>3</sub>. If a solid mixture, having a composition represented by point A, is placed in an humidity chamber and the RH is being increased, no significant absorption of water will take place until the mutual deliquescence RH is reached. At the mutual deliquescence RH, a liquid of composition B<sub>1</sub>, which contains both NaNO<sub>3</sub> and NaNO<sub>3</sub>, is formed. As the RH is further raised, the amount of solid decreases and the amount of liquid increases with the liquid becoming richer in NaNO<sub>3</sub>. At an RH slightly below RH<sub>2</sub>, only a small amount of solid NaNO<sub>3</sub> will remain and the composition of the liquid will change from B<sub>1</sub> to B. At RH<sub>2</sub>, the solid is completely dissolved and the liquid is of composition A.

Based on the above analysis, the minimum deliquescent point used in the DOE analysis may not be realistic although its value is the lowest among the pure salts that may be deposited on the surfaces of the engineered barrier system components. The minimum mutual deliquescence RH of the salt mixture may be a more realistic RH. Table 2-4 shows that the NaCl-NaNO<sub>3</sub>-KNO<sub>3</sub> system has a mutual deliquescence RH of 30 percent, which is significantly lower than the critical RH assumed by the DOE (50 percent). These three salts are abundantly present in the evaporated Yucca Mountain waters (see section 2.3) and also can be found in contaminated air aerosols (Civilian Radioactive Waste Management System Management and Operating Contractor, 2000c; Weast and Astle, 1981; Ge et al., 1998). They may be deposited onto the surface of the waste package or the drip shield during the dry thermal period. The temperature and RH values from a simulation by the DOE are given in figure 2-4 (Civilian Radioactive Waste Management System Management and Operating Contractor, 2000h). After the emplacement, the temperature increases to about 100 °C and then decreases during the ventilation period. Upon the termination of ventilation and drift closure 50 yr after the emplacement, the temperature increases, reaching a maximum of 160 °C. The minimum RH, which is corresponding to the 160 °C peak temperature, is approximately 20 percent. If the deposited salts

**Table 2-4. Deliquescent point for salts and salt mixtures at 16.5 °C**

Salts	Deliquescence Point (Percent)
NaCl	76*
NaNO <sub>3</sub>	78*
KNO <sub>3</sub>	95
Mixture of above three (with composition corresponding to a saturated solution of the three salts)	30.5 <sup>†</sup>

\*Civilian Radioactive Waste Management System Management and Operating Contractor. *Environment on the Surfaces of the Drip Shield and Waste Package Outer Barrier*. ANL-EBS-MD-000001, ICN 01. Revision 00. Las Vegas, NV: Office of Civilian Radioactive Waste Management System Management and Operating Contractor. 2000.

<sup>†</sup>Weast, R.C., and Astle, M.J., eds. *CRC Handbook of Chemistry and Physics: A Ready Reference Book of Chemical and Physical Data*. 62<sup>nd</sup> Edition. Boca Raton, FL: CRC Press. 1981.

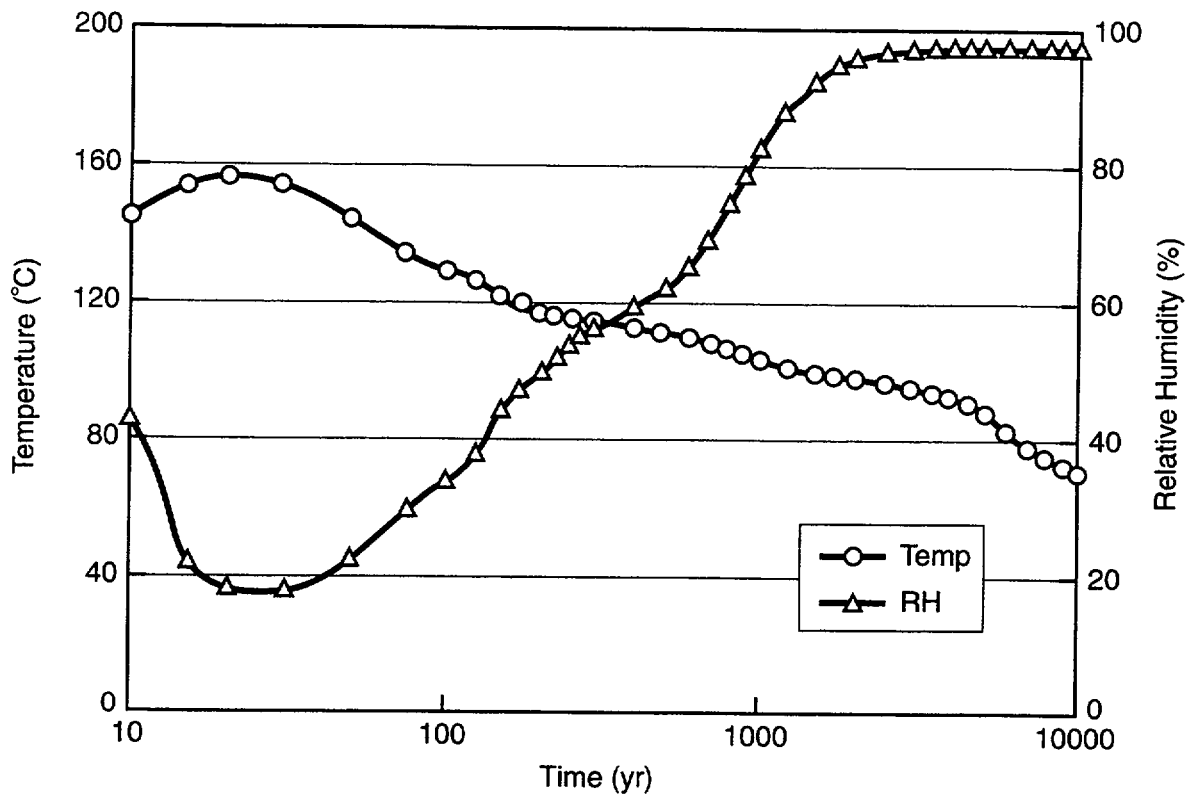


**Figure 2-4. Previous predictions of relative humidity and temperature on the waste package over time after closure (Civilian Radioactive Waste Management System Management and Operating Contractor, 2001)**

produce aqueous salt films at RHs close to 20 percent, aqueous corrosion may take place during the entire emplacement period, and the temperature at which the aqueous corrosion takes place may be as high as 160 °C. Critical RH for the salt mixtures that are likely to be present on the surfaces of the waste package and drip shield should be examined based on the mutual deliquescence RH. The presence of highly hygroscopic salts, such as  $\text{CaCl}_2$  and  $\text{MgCl}_2$ , should be considered because they may significantly lower the mutual deliquescence RH of salt mixtures.

### **2.3 EVAPORATIVE/BOILING CONCENTRATING OF YUCCA MOUNTAIN WATERS**

Because of the heat generated by the spent nuclear fuel, the temperature of the drift would be high and the RH would be low for many hundred years. As shown in figure 2-4, RH on the waste package surface would be less than 85 percent for about 1,000 yr after the emplacement of the nuclear waste. Because of the low RH in the drift, the water near the drift or in contact with the waste package and drip shield will be concentrated by evaporation. Experiments have been conducted by the DOE under selected temperature and RH conditions (Civilian Radioactive Waste Management System Management and Operating Contractor, 1999) using simulated J-13 Well water and pore water (Civilian Radioactive Waste Management System Management and Operating Contractor, 2000c; Rosenberg et al., 2001). The temperatures of the tests range

from 85 to 120 °C, and the RH ranges from 85 percent to values corresponding to a slow boil of solutions in the atmosphere (the RH was not measured but it is expected to be low). In the test conducted in the atmosphere, the evaporation was terminated at a predetermined concentration factor (157 to approximately 1,000) (Civilian Radioactive Waste Management System Management and Operating Contractor, 1999).

The experimental results of Rosenberg et al. (2001) indicate that J-13-like waters evaporate to high pH,  $\text{Na}^+\text{-HCO}_3^-\text{-CO}_3^{2-}$  brines. The highest  $\text{Cl}^-$  concentrations were measured when evaporation occurred in the presence of tuff (e.g., 850 times the original  $\text{Cl}^-$  concentration of 7.2 mg/L). At the same overall concentration ratio (e.g., 1,000 times), there was no significant difference in measured fluoride concentrations from experiments with and without tuff (e.g., 705 times the initial concentration of 2.3 mg/L for experiments with water alone, versus a concentration ratio of 691 for J-13-like waters evaporated with tuff). For experiments starting with J-13-like waters and pore waters, a larger number of minerals precipitate when tuff is present than when the waters are evaporated alone. The Rosenberg et al. (2001) experiments showed that pore waters evaporate to more neutral solutions than J-13-like waters. The maximum  $\text{Cl}^-$  concentration resulting from the evaporation of pore water occurred in the presence of tuff at an overall concentration factor of 1000x (e.g., 681 times the original  $\text{Cl}^-$  concentration of 76.6 mg/L). When the pore water solutions were concentrated to 1000x, measured  $\text{F}^-$  concentrations remained below 250x of their initial concentration regardless of whether tuff was present or not. There are mass balance inconsistencies in the evaporated water compositions reported by Rosenberg et al. (2001). For a concentration ratio of 1000x in the evaporation of J-13-like water without tuff, for example, the chloride concentration ratio was found to be 701 although no Cl-bearing phases were reported to have precipitated.

Tables 2-5 and 2-6 list typical results from evaporation experiments. As shown in tables 2-5 and 2-6, chloride can be significantly concentrated from both the synthetic 100x J-13 Well water and the synthetic pore waters; fluoride can be significantly concentrated from the synthetic 100x J-13 Well water but not from the synthetic pore water. On the basis of the chemical divide theory (see following paragraph), the fluoride in the pore water was believed to precipitate as  $\text{CaF}_2$  during the evaporation because of the high content of calcium relative to the bicarbonate in the pore water (Civilian Radioactive Waste Management System Management and Operating Contractor, 2001).

The evaporation/precipitation experiments of Rosenberg et al. (2001) focus on crucial issues related to drip shield and waste package degradation. However, there are several reasons why the individual evaporated water compositions resulting from that work are unlikely to be either bounding or representative of those that might contact the drip shields and waste packages in the proposed Yucca Mountain repository. First, as noted previously, water seeping into the proposed repository is unlikely to have either pore water or J-13 composition because it will have responded chemically to the thermal pulse experienced in the overlying rock. In addition, there are no representative pore water compositions at Yucca Mountain. Instead, pore water compositions vary significantly both laterally and vertically (Browning et al., 2000). Thus, experimental evaporation of a single pore water provides data on one point in the range of possible evolved pore water compositions. For example, chloride concentrations as high as 185 mg/L were measured by Yang et al. (1998) in the borehole NRG-6, but the Rosenberg et al. (2001) experiments use an initial chloride concentration of 76.6 mg/L. Similarly, the experiments were conducted within a narrow range of subboiling temperatures, providing limited information on the range of evaporated solution compositions that might exist in a repository setting. More generally, analytical data on minor and trace components in the unsaturated zone groundwaters at Yucca Mountain are lacking despite their importance to the characterization of drip shield and waste

**Table 2-5. Evaporative concentrating of synthetic 100x J-13 Well water\***

Ion	Synthetic J-13 Well Water*		Evaporated Synthetic J-13 Well Water*	
	mg/L	mM	mg/L	mM
Ca <sup>2+</sup>	5	0.13	36	0.9
K <sup>+</sup>	513	13.2	10,832	277
Mg <sup>2+</sup>	2	0.08	0	0
Na <sup>+</sup>	4,032	175	76,314	3,319
Cl <sup>-</sup>	730	20.6	14,419	406
F <sup>-</sup>	208	10.9	3,630	191
HCO <sub>3</sub> <sup>-</sup>	4,142	67.9	54,614	895
NO <sub>3</sub> <sup>-</sup>	732	11.9	14,085	227
SO <sub>4</sub> <sup>2-</sup>	1,632	17.0	29,783	310
SiO <sub>2</sub>	—	—	—	—

\*Civilian Radioactive Waste Management System Management and Operating Contractor. *In-Drift Precipitate/Salts Analysis*. ANL-EBS-MD-000045, ICN 02. Revision 00. Las Vegas, NV: Office of Civilian Radioactive Waste Management System Management and Operating Contractor. 2001.

package degradation, and it cannot be assumed that these groundwater components will behave conservatively during heating and evaporation.

The types and amount of salts that precipitate, brine compositions, and deliquescence points are all dependent on the composition of seepage waters that enter the drift. Simple mass balance calculations were performed on a compilation of more than 100 revised pore water compositions from Browning et al. (2000) to bound the range of compositions resulting from their evaporation. The approach used was based on the chemical divide model of Hardie-Eugster (1970). The chemical divide model is based on the idea that when two ions are involved in the precipitation of a binary salt during evaporation, the concentration of one will increase while the other decreases. The chemistry of a water undergoing evaporation is conceptualized as evolving along a series of chemical divides, which appear as branches in a flow chart (figure 2-5). Table 2-1 provides the results of these calculations. The pore water compositions in table 2-1 are separated into compositional groups that are numbered according to the chemical divide approach shown in figure 2-5. Sample identification numbers referred to those of Yang et al. (1996, 1998).

A few observations can be made as a result of performing the chemical divide calculations on the complete set of revised pore water data from Browning et al. (2000). Evaporated pore waters may occupy any of the compositional categories represented in the chemical divide model. Most reinterpreted pore water

**Table 2-6. Evaporative concentrating of synthetic pore water\***

Ion	Synthetic Pore Water <sup>†</sup>		Evaporated Synthetic Pore Water <sup>†</sup>	
	mg/L	mM	mg/L	mM
Ca <sup>2+</sup>	57.2	1.43	15,629	391
K <sup>+</sup>	4.2	0.108	2,779	71
Mg <sup>2+</sup>	11.7	0.488	5,478	228
Na <sup>+</sup>	8.2	0.356	5,961	259
Cl <sup>-</sup>	78.0	2.20	53,084	1.497
F <sup>-</sup>	2.3	0.121	<577	<30
HCO <sub>3</sub> <sup>-</sup>	16.2	0.266	<35	<0.6
NO <sub>3</sub> <sup>-</sup>	11.0	0.177	not measured	not measured
SO <sub>4</sub> <sup>2-</sup>	81.7	0.851	2,077	22
SiO <sub>2</sub>	9.8	0.163	513	8.6

\*Civilian Radioactive Waste Management System Management and Operating Contractor. *In-Drift Precipitate/Salts Analysis*. ANL-EBS-MD-000045, ICN02. Revision. 00. Las Vegas, NV: Office of Civilian Radioactive Waste Management System Management and Operating Contractor. 2001.

<sup>†</sup>Rosenberg, N.D., K.G. Knauss, and M.F. Dibley. *Evaporation of Topopah Spring Tuff Pore Water*. UCRL-ID-135765. Livermore, CA: Lawrence Livermore National Laboratory. 1999.

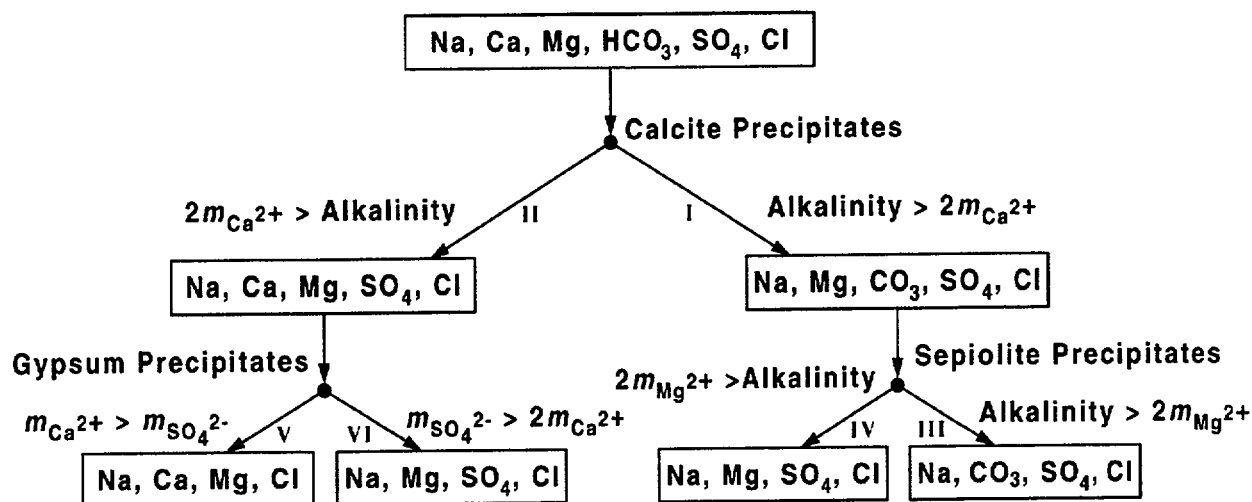


**Figure 2-5. Chemical divide diagram**

compositions, however, fall on the right side of the chemical divide diagram, suggesting that  $\text{Na}^+$ ,  $\text{CO}_3^{2-}$ ,  $\text{SO}_4^{2-}$ , and  $\text{Cl}^-$  brine compositions would result from their evaporation. A smaller proportion of  $\text{Na}^+$ ,  $\text{Ca}^{2+}$ ,  $\text{Mg}^{2+}$ , and  $\text{Cl}^-$  brines are most likely to form from the evaporation of pore waters that were extracted from the uppermost portions of boreholes. The partial pressure of  $\text{CO}_2$ ,  $p\text{CO}_2$ , was fixed during the reinterpretation of analytical pore water compositions, so this trend results from a general decrease in  $\text{Ca}^{2+}$  concentration with depth (see figure 2-5). Caliche and other near-surface materials probably represent the most significant source of dissolved calcium in the infiltrating waters, and the trend is likely caused as the percolating waters leave calcite behind. Consequently, the shallower the collection site for the pore waters, the more likely it is for these waters to evaporate toward solution compositions on the left side of the chemical divide. Evaluations of figure 2-5 (on chemical divides) and table 2-1 (on pore water compositions) indicate the importance of  $p\text{CO}_2$  in controlling the chemical composition of evolving brines in a proposed nuclear waste repository.

To predict the evaporation concentration of the waters in contact with the drip shield and waste package outer barrier over a wide range of temperature and RH conditions, a model was developed by DOE. The approach for the development of the model is documented in the in-drift precipitates/salts Analysis/Model Report (Civilian Radioactive Waste Management System Management and Operating Contractor, 2001). The model is intended to predict the pH, chloride concentration, ionic strength, and the minimum deliquescence RH.

The precipitates/salts model is composed of two submodels, a high RH model and a low RH model. The high RH model is the EQ3/6 Pitzer model, which calculates the speciation and precipitation of salts in aqueous solutions according their thermodynamic properties. Because the EQ3/6 Pitzer model has an upper limit in ionic strength of 10 molal, the high RH model can only be used for RHs above 85 percent. The low RH is for RHs lower than 85 percent.

The solutions concentrated in the evaporation experiments are within the high RH model range, and, therefore, they can be used to verify the high RH model. The results for  $\text{Na}^+$ ,  $\text{F}^-$ ,  $\text{HCO}_3^-$ ,  $\text{Cl}^-$ ,  $\text{K}^+$ ,  $\text{NO}_3^-$ , and  $\text{SO}_4^{2-}$  from the high RH model compare well with the results from the evaporation experiments. However, there are significant discrepancies for  $\text{Si}$ ,  $\text{Ca}^{2+}$ , and  $\text{Mg}^{2+}$  and pH. These discrepancies were attributed to the errors or uncertainties in the thermodynamic database or the kinetic limitations of precipitation reactions (Civilian Radioactive Waste Management System Management and Operating Contractor, 2001).

As mentioned earlier, the RH on the waste package surface has been predicted to be lower than 85 percent for 1,000 yr when the temperature is high and localized corrosion of Alloy C-22 may occur. Therefore, the low RH model is important for assessing the possible effect of the environment on the mode and rate of corrosion. At the present time, there are no experimental data available to compare with the low RH model results. However, based on the model assumptions and thermodynamic principle, the low RH model has the following shortcomings:

- (i) It underestimates the amount of salts during the initial stage of emplacement when the drift is hot. The model calculates the mass balance during each time interval and assumes that, as soon as the critical RH is reached, half of the dissolved salts in a time interval would be washed away. In reality, during the initial stage, solid salt deposits would be accumulated on the drip shield or waste package outer barrier surfaces and only a small amount of

concentrated liquid can be present after the deliquescent humidity is reached. The concentrated liquid would stay and accumulate in the pores of the deposits until the liquid volume reaches a point where the solid deposit could no longer hold the liquid.

- (ii) It underestimates the concentrations of the  $\text{Cl}^-$ ,  $\text{SO}_4^{2-}$ , and  $\text{CO}_3^{2-}$  in the initial time period. The model assumes that only a small amount of these salts dissolves, but calculates their concentrations by dividing the small amounts of dissolved salts by a large volume of water.
- (iii) The model assumes that the minimum RH is 50 percent and that there is no hydration below 50-percent RH. As discussed in section 2.2, the minimum RH may be lower than 30 percent, and, hence, the aqueous film formation may start earlier.

## **2.4 AQUEOUS SOLUTIONS FOR CORROSION TESTING**

Based on the preliminary analysis of the deliquescence behavior of salts and the evaporation of Yucca Mountain waters, several aqueous solutions were formulated by the DOE as the bounding types of solution chemistries for waters that would contact the engineered barrier system components. These aqueous solutions were used for the corrosion testing of the engineered barrier system component materials in the long-term corrosion test facility and in complementary testing. The compositions of these aqueous solutions are listed in tables 2-7 and 2-8.

The composition of the saturated aqueous solutions used for corrosion testing were derived on the assumption that the minimum RH is 50 percent. As mentioned in section 2.3, the minimum RH of a salt mixture may be close to 20 percent. The aqueous solution that would contact the engineered barrier system components may be more concentrated, and the temperature at which aqueous corrosion occurs may be as high as 160 °C.

In addition, because the nitrate salts have the highest solubilities, the brine solutions dripping onto the surface of the drip shield or the waste package are likely to be nitrate-rich salt mixtures. However, as mentioned in section 2.2, dripping is not the only mechanism for the salt to be deposited on the drip shield or waste package. Salt mixtures deposited on the drip shield and waste package by other mechanisms, such as by aerosol, may contain less nitrates. The saturated waters in tables 2-7 and 2-8 may not bound the solution chemistry realistic because they contain a high concentration of nitrates and nitrates may have an inhibiting effect on localized corrosion. Therefore, a highly concentrated chloride solution with a low nitrate content should also be included in the text matrix in the assessment of corrosion.

## **2.5 EFFECT OF MICROBIAL ACTIVITY ON THE ENVIRONMENT**

Evidence exists that the effect of bacteria on the average bulk environment is small, but this conclusion cannot be extrapolated to local environmental effects. Arguments based on low microbial activity because of limited nutrients, water, energy, or other component of the metabolic process do not represent how localized impacts can be distributed in the repository, drift, or over a waste package surface. To adequately characterize the effects of microbial activity on the environment, the distribution of components or effects, including development of biofilms, needs to be considered. The effects of localized impacts such as biofilm development, colloid formation, and the production of inorganic acids, methane, organic byproducts, carbon

**Table 2-7. The composition of several aqueous solutions used for corrosion testing\***

Ion	Concentration							
	Simulated Dilute Water		Simulated Concentrated Water		Simulated Acidified Water		Simulated Saturated Water	
	60 and 90 °C		60 and 90 °C		60 and 90 °C		100 °C	
	mg/L	mM	mg/L	mM	mg/L	mM	mg/L	mM
K	34	0.87	3,400	87	3,400	87	142,000	3,632
Na <sup>+</sup>	40	17.8	40,900	1,780	40,900	1,780	487,000	21,182
Mg <sup>2+</sup>	1	0.04	<1	20.04	1,000	41	0	0.00
Ca <sup>2+</sup>	0.5	0.01	<1	20.01	1,000	25	0	0.00
F <sup>-</sup>	14	0.74	1,400	74	0.00	0.00	0	0.00
Cl <sup>-</sup>	67	1.89	6,700	189	24,250	684	128,000	3,610
NO <sub>3</sub> <sup>-</sup>	64	1.03	6,400	103	23,000	371	1,313,000	21,175
SO <sub>4</sub> <sup>2-</sup>	167	1.74	16,400	174	38,000	396	0	0.00
HCO <sub>3</sub> <sup>-</sup>	947	15.52	70,000	1,148	0.00	0.00	0	0.00
Si	27 (60 °C) 49 (90 °C)	—	27 (60 °C) 49 (90 °C)	—	27 (60 °C) 49 (90 °C)	—	—	—

\*Civilian Radioactive Waste Management System Management and Operating Contractor. *Environment on the Surfaces of the Drip Shield and Waste Package Outer Barrier*. ANL-EBS-MD-000001, ICN 01. Revision 00. Las Vegas, NV: Office of Civilian Radioactive Waste Management System Management and Operating Contractor. 2000.

dioxide, and other chemical species that could change the longevity of materials and the transport of radionuclides from the near field have not been investigated by the DOE (Civilian Radioactive Waste Management System Management and Operating Contractor, 2000d). In addition, utilization of repository construction and structural materials should be considered as possible nutrient and energy sources.

Details about bacteria relevant to the potential Yucca Mountain repository and their characteristics can be found in Amy and Haldeman (1997), Banfield and Nealson (1997), or Pedersen and Karlsson (1995). Bacteria expected in the potential Yucca Mountain repository environment can catalyze reactions and utilize the energy (i.e., they are chemotrophs). Any sufficiently slow reaction allows bacteria to compete, so any redox couple that yields energy can be exploited. Metabolic processes can include aerobic respiration, nitrification and denitrification, methane oxidation, manganese and iron oxidation, sulfur oxidation, manganese and iron reduction, sulfate reduction, and methanogenesis. To grow, microbes need to incorporate carbon (organic or CO<sub>2</sub>), nitrogen, phosphorous, and sulfur. Combinations of metabolic pathways can give great versatility to organisms in nutrient-limited environments. In the absence of nutrients, evidence exists that microbial populations can survive for millions of years without sufficient energy for growth and reproduction until an environment for energy production returns. Finally, bacteria cannot grow without water.

**Table 2-8. Recipe for basic saturated water\***

Chemicals	Grams	M
KCl	9.7	2.32
NaCl	8.8	2.69
NaF	0.2	0.085
NaNO <sub>3</sub>	13.6	2.86
Na <sub>2</sub> SO <sub>4</sub>	1.4	0.176
H <sub>2</sub> O	56.0	—
Na <sub>2</sub> CO <sub>3</sub>	10.6	1.786
Na <sub>2</sub> SiO <sub>3</sub> · 9H <sub>2</sub> O	4.0	0.251

\*Civilian Radioactive Waste Management System Management and Operating Contractor. *Environment on the Surfaces of the Drip Shield and Waste Package Outer Barrier*. ANL-EBS-MD-000001. Revision 00. ICN 01. Las Vegas, NV: Office of Civilian Radioactive Waste Management System Management and Operating Contractor. 2000.

Evidence exists that available nutrients and/or energy for microbial growth limits the effect of bacteria on the bulk environmental chemistry (Civilian Radioactive Waste Management System Management and Operating Contractor, 2000d). The exception to this possible limitation is an increase in carbon dioxide, which depends on the rate of repository ventilation. Cases are made for limited nutrients, energy, and water. However, effects on local environments have not been characterized.

When biofilms are formed, bacteria create local environments that differ from the bulk. Microorganisms can create living conditions to which they are suited even if these conditions differ from the bulk. The biofilm can maintain an environment at the biofilm/surface interface that differs from the bulk in terms of pH, dissolved oxygen, and other organic and inorganic species. In some cases, these interfacial conditions could not be maintained in the bulk medium. The bulk can then serve as a larger source of nutrients and energy that normally would not be expected to support growth. Minerals and mineral replacement reactions can occur that are not predicted by thermodynamic arguments based on the chemistry of the bulk medium (Little et al., 1997).

Cases have been made for limited carbon, nitrogen, sulfur, and phosphorous as nutrients (Civilian Radioactive Waste Management System Management and Operating Contractor, 2000c). The results do not consider nutrients that originate from materials used in the construction of the repository or that may be nonuniformly distributed or consumed through the action of biofilms. In addition, available carbon is considered to be dissolved organic carbon available in the groundwater entering the drift (i.e., approximately 1 ppm). The effects of hydrocarbons left in the repository during construction and the ability of certain bacteria to use carbon dioxide as a carbon source (Geesey, 1993) are not clear. Some microorganisms (chemoautotrophs) in the deep subsurface are capable of deriving their carbon requirement through the fixation of carbon dioxide; many methanogens, sulfur oxidizers, and ammonia oxidizers utilize carbon dioxide (Geesey, 1993). The DOE

calculations (Civilian Radioactive Waste Management System Management and Operating Contractor, 2000d) suggest that if dissolved organic carbon limits the growth of bacteria, there would exist sufficient bacteria to uniformly cover all waste packages and waste forms. Based on this argument and the nonuniform growth of biofilm, it is reasonable to expect sufficient bacteria to create nonuniform coverage with significant thickness.

To grow bacteria require available energy acquired through free energy released from oxidation/reduction reactions. When considering energy as a limitation, only sufficient energy to create a modified local environment is required. In addition, energy sources, such as steel used as repository structural material, can serve this role.

Low water activity in the repository cannot be used to discount microbial activity because measuring or predicting the humidity of the drift gas does not represent local water activity. Microbes cannot grow without water, and elevated temperatures of the emplaced waste packages will reduce humidity in the drift. However, dripping water will increase the local humidity (i.e., local saturation) and continuously carry new bacteria into the drift. This effect will increase as the repository cools over time.

## **2.6 EVOLUTION OF CHEMISTRY IN LABORATORY-SCALE HEATER TEST**

The laboratory-scale heater test at the CNWRA (Brossia et al., 2000) was initiated to examine three primary items: (i) the evolution of chemistry over time in the presence of a thermal source (ii) evaluation of corrosion information related to Alloy 22 including corrosion potential over time and (iii) evaluation of possible methods that DOE may utilize to confirm waste package performance. The discussion in this section will focus on the first item.

The main method utilized to monitor chemistry thus far has been potentiometric methods that rely on the measurement of a potential difference between a sensing electrode and a stable reference. The potentiometric methods employed thus far include monitoring of the pH and chloride concentration using an oxidized tungsten wire for pH and a chloridized silver wire for chloride. These wires along with Alloy 22 and Type 316L stainless steel wires to measure open circuit potentials have been incorporated into a sensor array cell designed to capture incoming water percolating through crushed tuff in a laboratory-scale drift heater test. A saturated calomel electrode connected to the array cell through a long salt bridge/luggin probe has been used as a reference electrode.

Measurement of pH and chloride concentrations using potentiometric methods was found to be accurate and predictable over a range of 2 to 10 for pH and from  $10^{-3}$  to 1 M in chloride concentration. It has been noted that when emplaced in the laboratory-scale heater test, a range of wet and dry periods were observed. During one wet period, the initial pH and chloride concentrations, measured using the sensor, were 8.4 and  $2 \times 10^{-3}$  M. These values are in agreement with measurements taken from solutions extracted from the laboratory-scale heater test near the vicinity of the sensor (pH 8.0–8.6 and 2 to  $8 \times 10^{-3}$  M for chloride). As evaporation and dryout occurred, both the pH and the chloride concentrations increased as shown in figure 2-6. The increase in the pH is thought to result from exsolution of  $\text{CO}_2$  with increased time. In the present case, the chloride concentration increased to  $\sim 0.6$  M, however, in other tests, the chloride concentration was noted to increase to values approaching 3.5 M. It is clear from these experiments that the chemistry of the incoming water can change significantly, and higher concentrations of species than those reported for the local groundwater may potentially develop.

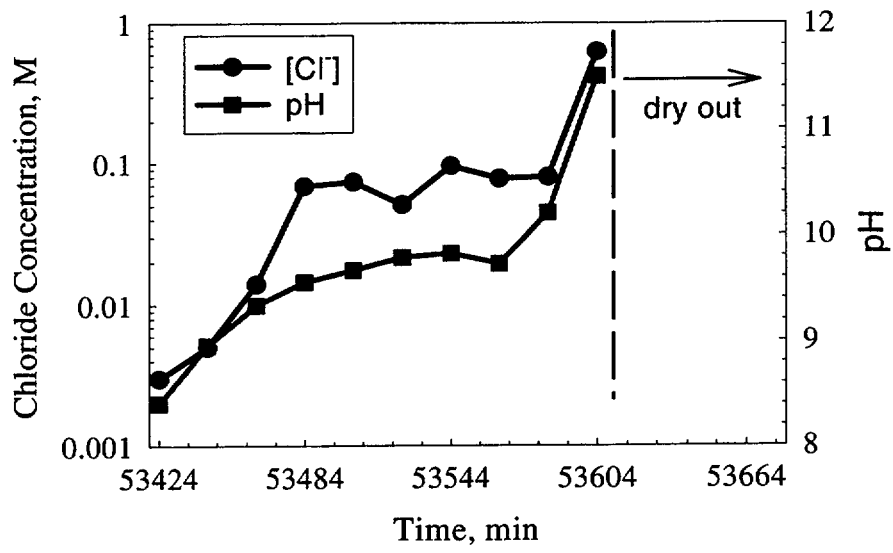


Figure 2-6. Response of pH and chloride concentration to evaporation and dryout

### 3 CORROSION OF CANDIDATE CONTAINER MATERIALS

One of the principal factors in the DOE Repository Safety Strategy for the proposed repository at Yucca Mountain (Civilian Radioactive Waste Management System Management and Operating Contractor, 2000a) is the performance of the waste package barriers. Alloy 22, presently the material of choice for the waste package outer barrier, is considered to be extremely resistant to various modes of aqueous corrosion over broad ranges of temperature, pH, and concentration of anionic and oxidizing species. Several degradation processes are considered in the DOE performance assessment including dry-air oxidation, humid-air corrosion, passive aqueous corrosion, localized corrosion, and stress corrosion cracking. Dry-air oxidation is not considered to be a process that would limit the lifetime of the Alloy 22 waste package outer barrier (Civilian Radioactive Waste Management System Management and Operating Contractor, 2000h) and is not discussed in this report. An assessment of the DOE approach on the degradation of the waste packages by dry-air oxidation is included in the Container Life and Source Term Issue Resolution Status Report (U.S. Nuclear Regulatory Commission, 2001). The corrosion-degradation processes may be accelerated as a result of the thermal instability of Alloy 22. Microbial influenced corrosion is also considered as a corrosion process in which the metabolic generation of a specific environment may accelerate the degradation of the Alloy 22 waste packages.

Corrosion-resistant Ni-Cr-Mo alloys have been used in a variety of applications that require high resistance to localized attack. As a result, these alloys have been used extensively in chemical-process industries, power plants, oil and gas production, and offshore applications where other materials, such as stainless steels undergo rapid degradation in the form of localized corrosion. The localized corrosion resistance and thermal stability of the Ni-Cr-Mo alloys are dependent on alloy composition. A summary of the effect of alloying elements on the corrosion resistance and thermal stability of Ni-Cr-Mo alloys is provided in Cragolino et al. (1999).

The excellent corrosion resistance of Alloy 22 can be attributed to a protective passive film that restricts the dissolution of the alloy components. For stainless steels and Ni-Cr-Mo alloys, the protective film consists of an inner oxide film that is rich in chromium oxide and an outer oxyhydroxide layer formed by deposition. The stability of the passive film is enhanced by the addition of Cr, Mo, and W to the alloy. In conditions in which the protective oxide film is stable, the corrosion rate of passive metals and alloys is not strongly dependent on temperature, environmental composition, and redox potential (Cragolino et al., 1999).

Breakdown of the oxide film can lead to the initiation and rapid penetration of the material by localized corrosion. Although the mechanisms of localized breakdown of the passive films and initiation of localized corrosion on Ni-Cr-Mo alloys are not clearly understood, empirical correlations to alloy composition, temperature, and exposure environment composition have been derived. In general, localized corrosion of Ni-Cr-Mo alloys is possible in environments that contain aggressive anions such as chloride. Reduced-sulfur species and heavy metals such as Pb, Hg, and Sn are also known to be aggressive to these alloys (Klöwer, 1998). In general, the resistance of Ni-Cr-Mo alloys to localized corrosion increases with the addition of Cr, Mo, and W and decreases with temperature and concentration of aggressive species. Fabrication methods, particularly welding, and high-temperature (> 600 °C) exposure are important factors that can significantly decrease localized corrosion resistance (Sridhar, 1990) and impact strength (Hoffmann, 1998) of Ni-Cr-Mo alloys.

### 3.1 U.S. DEPARTMENT OF ENERGY INVESTIGATIONS

Investigations conducted by the DOE at Lawrence Livermore National Laboratory have focused on measurement of corrosion rates and prediction of localized corrosion. Because of the evolution of waste package design and corresponding changes to the candidate container materials, a range of Ni-rich and Ni-base candidate container alloys have been tested including Alloys 825, 625, and 22 as well as other Ni-rich and Ni-base alloys, such as G30 and C4 (McCright 1998; Civilian Radioactive Waste Management System Management and Operating Contractor, 2000e). The test environments consist of a variety of solutions that are based on the predicted evolution of J-13 Well water including simulated acidified water, simulated dilute water, simulated concentrated water, simulated saturated water, and basic saturated water as discussed in section 2.4. The compositions of these solutions are provided in table 2-7. Below 100 °C, the composition of water that contacts the waste package surface is assumed to be simulated dilute water, whereas simulated saturated water is assumed to be present above 100 °C. Basic saturated water has also been identified as another plausible water chemistry that may develop on the waste package surface as a result of dripping and evaporation (Civilian Radioactive Waste Management System Management and Operating Contractor, 2000f).

#### 3.1.1 Humid-Air Corrosion

Humid-air corrosion is assumed to occur when the RH is greater than the  $RH_{critical}$  (Civilian Radioactive Waste Management System Management and Operating Contractor, 2000c). The  $RH_{critical}$  is based on the deliquescence point (lowest RH at which a saturated solution of the salt can be maintained at a given temperature) for sodium nitrate ( $NaNO_3$ ) (Civilian Radioactive Waste Management System Management and Operating Contractor, 2000c) defined by

$$RH_{critical} = -3.5932 \times 10^{-5} T^3 + 5.9649 \times 10^{-3} T^2 - 0.45377T + 81.701 \quad (3-1)$$

where  $T$  is in °C. At 20 °C, the deliquescence point for  $NaNO_3$  occurs at a RH of 75 percent. Because of the dependence on temperature at 90 °C, the deliquescence point is lowered to a RH of 65 percent, and at 120 °C (the boiling point of a saturated  $NaNO_3$  solution at atmospheric pressure), the deliquescent point occurs at a RH of 50 percent. The deliquescence point of  $NaCl$  is not strongly dependent on temperature and occurs at a RH of 74 to 76 percent. The groundwater at the proposed repository site may also contain  $Ca^{2+}$  and  $Mg^{2+}$ , which are capable of forming salts at lower deliquescence points than  $NaNO_3$ . It is anticipated, however that these divalent cations will form precipitated salts such as carbonates or silicates that do not have deliquescence points below that measured for  $NaNO_3$ . These assumptions have been questioned and are discussed in section 2.2.

Rates of humid-air corrosion were calculated from the weight loss of specimens exposed above the solution level in vessels in the long-term corrosion test facility using the test solutions listed in table 2-7. Specimens were also exposed at the waterline, and completely immersed specimens were used to determine aqueous corrosion rates. A comparison of the average corrosion rates of specimens exposed in the vapor phase, at the waterline, and in the aqueous phase for exposure times of 6 mo and 1 yr indicates that water composition, temperature, and exposure conditions do not significantly affect the corrosion rate of Alloy 22 (McCright, 1998). Although the 2-yr data from the long-term corrosion test facility have been reported (Civilian Radioactive Waste Management System Management and Operating Contractor, 2000e), a

comparison of the corrosion rates for specimens exposed in the vapor phase to those exposed in the aqueous phase was not provided. In addition, the corrosion rates calculated for Alloys G30, C4, and 625 do not show a dependence on water composition, temperature, or exposure conditions. Based on these observations, the DOE model of corrosion of the Alloy 22 waste package outer barrier assumes that the corrosion rate and the distribution of corrosion rates under these conditions are the same as for aqueous corrosion and are independent of time (Civilian Radioactive Waste Management System Management and Operating Contractor, 2000f).

### 3.1.2 Uniform Corrosion

General passive corrosion is assumed to occur when the  $E_{\text{corr}}$  is less than the critical potential ( $E_{\text{critical}}$ ) for the initiation of localized corrosion. The general corrosion rates are derived from data obtained from the long-term corrosion test facility, where numerous test specimens have been exposed to aqueous solutions based on modifications of J-13 Well water (Civilian Radioactive Waste Management System Management and Operating Contractor, 2000e; McCright, 1998). Corrosion rates of specimens exposed in the long-term corrosion test facility were calculated by measuring the weight loss of the specimens (American Society for Testing and Materials, 1997) after 6 mo, 1 yr, and 2 yr of exposure in simulated dilute water, simulated concentrated water, simulated acidified water, and simulated cement-modified water. The tests were conducted at 60 and 90 °C and included specimens that were fully immersed, partially immersed, and those exposed only to the vapor phase. Creviced and welded specimens were also tested. No localized corrosion was observed on any Alloy 22 test specimen. It should be noted, however, that small pits were observed in the crevice regions on Alloy 825 specimens after testing for 6 mo in simulated acidified water at both 60 and 90 °C (McCright, 1998). The corrosion rates for the Alloy 22 calculated by weight loss are not strongly dependent on temperature or water composition.

For specimens not fitted with crevice-forming washers, the penetration rate, calculated using weight loss, ranged from -31 to 37 nm/yr after the 2-yr exposure to the long-term corrosion test facility-simulated waters. By comparison, specimens fitted with crevice-forming washers had calculated penetration rates that ranged from -9 to 73 nm/yr after the 2-yr exposure. When all exposure times and conditions were considered, the corrosion rates for Alloy 22 range from -60 to 731 nm/yr. The highest corrosion rates were observed in the 6-mo exposure specimens. Corrosion rates above 200 nm/yr were observed only for a few specimens. The average corrosion rates of the Alloy 22 specimens tend to decrease with time from 50 nm/yr after 6 mo to 30 nm/yr after 1 yr to 10 nm/yr after 2 yr, based on weight-loss measurements. Weight gain was observed on 25 percent of the Alloy 22 weight-loss specimens as a result of the deposition of silica (assumed to be amorphous  $\text{SiO}_2$ ) on the surface of the specimens (Civilian Radioactive Waste Management System Management and Operating Contractor, 2000e,f).

Recently, the DOE has evaluated Alloy 22 corrosion rate data obtained from the University of Virginia (Civilian Radioactive Waste Management System Management and Operating Contractor, 2001b). The corrosion rates were potentiostatically measured in LiCl solutions with 10:1 and 100:1 chloride-to-sulfate ion ratios (pH 2.75 to 7.750). The activation energy for passive dissolution was determined to be 36 kJ/mole using data obtained at 80, 85, and 95 °C. Using the calculated  $\pm 1$  standard deviation over the 80 to 95 °C temperature range, the activation energy could be as low as 11 kJ/mole, which would yield calculated passive dissolution rates that are not as strongly dependent on temperature. Using an activation energy of 36 kJ/mole,

distributions of corrosion rates at 25, 60, and 125 °C were subsequently calculated. The 50<sup>th</sup> percentile corrosion rates were calculated to be  $9.5 \times 10^{-6}$  mm/yr at 25 °C,  $4.5 \times 10^{-5}$  mm/yr at 60 °C, and  $3.8 \times 10^{-4}$  mm/yr at 125 °C.

### 3.1.3 Microbially Influenced Corrosion

Microbially influenced corrosion is recognized as a phenomenon that may affect the performance of waste package materials (Geesey and Cragnolino, 1995). At present, limited information is available on microbially influenced corrosion of Ni-base alloys, such as Alloy 22 (Geesey, 1993). It appears that the resistance of these alloys to microbially influenced corrosion is related to their resistance to localized corrosion in abiotic environments. Alloy 22 is quite resistant to localized corrosion and microbially influenced corrosion has not been reported for this alloy (Geesey and Cragnolino, 1995). Microbially influenced corrosion has been reported for Alloy 825 (42Ni-30Fe-21Cr-3Mo) in lake water that contained 35-ppm chloride and 25-ppm sulfate (Brennenstuhl et al., 1990).

Bacteria involved in microbially influenced corrosion have been divided into three broad phenotypic groups: (i) acid-producing bacteria, (ii) sulfate-reducing bacteria, and (iii) iron-oxidizing bacteria (Little et al., 1991). Bacteria representatives of each phenotypic group have been identified as part of the natural flora at the proposed HLW repository site at Yucca Mountain (Pitonzo et al., 1996; Horn et al., 1999; Lian et al., 1999a). Microbial biofilms are known to grow in environments in which nutrients are present only at growth-limiting levels (Costerton et al., 1995). Bacteria are able to grow because of the efficiency with which biofilms are capable of scavenging the available nutrients. The limited concentration of phosphate in the groundwater has been identified as a possible limitation to microbial growth in the proposed repository at Yucca Mountain (Civilian Radioactive Waste Management System Management and Operating Contractor, 2000e).

The corrosion rates of Alloy 22 in the presence of bacteria were evaluated and compared to corrosion rates obtained in sterile solutions (Civilian Radioactive Waste Management System Management and Operating Contractor, 2000e,f). Similar tests were also conducted using Alloy 625 and Type 304 stainless steel. Test solutions consisted of variants of J-13 Well water that were either maintained under sterile conditions or inoculated with microbes obtained from the Yucca Mountain region. Bacteria used to inoculate the test solutions consisted of 12 strains obtained from the Yucca Mountain region and included four acid-producing bacteria, five slime-forming bacteria, two iron-oxidizing bacteria, and one sulfate-reducing bacteria (Lian et al., 1999a). In addition to Alloy 22, several other candidate container materials have been evaluated, such as Alloy 625 and carbon steel (Horn et al., 1999, 2000; Lian et al., 1999a,b). The corrosion rates of the candidate container materials were obtained using linear polarization. The test solutions were analyzed for metal corrosion products using inductively coupled plasma spectroscopy (Lian et al., 1999a). During an exposure time of 160 d, the corrosion rate of Alloy 22 in sterile solution was measured using linear polarization to be in the range of 0.006 to 0.012  $\mu\text{m}/\text{yr}$ . In the inoculated solutions, the corrosion rate of Alloy 22 increased to 0.014 to 0.036  $\mu\text{m}/\text{yr}$ . Based on linear polarization measurements reported by Lian et al. (1999a) and assuming no localized corrosion, the corrosion rate of Alloy 22 appears to be two to six times greater in the inoculated solutions compared to abiotic solutions. The analyses of solutions following the conclusion of the tests showed significant concentration in solution of Cr for all alloys, including Alloy 22. The increased Cr concentration in the test solutions suggests that preferential dissolution of Cr from the passive film on the alloys has occurred. The preferential dissolution of Cr has also been observed for Alloy 800 (Brennenstuhl et al., 1990).

Linear polarization may be questionable as a valid method to measure corrosion rates of passive alloys. In general, linear polarization has been used for alloys that are not passive. For passive materials, significant measurement errors may occur from the charging of the passive film during polarization. In addition, because of insufficient measurement resolution, the low corrosion rates typically observed on passive alloys may prevent accurate measurements using linear polarization. In the case of microbially influenced corrosion, linear polarization would not have captured the variations in corrosion rates that may have occurred as a result of biofilm formation. Areas where biofilms formed may have much higher corrosion rates than areas without biofilms.

### 3.1.4 Effect of Thermal Aging on Corrosion

The effect of thermal aging on the corrosion of Alloy 22 was assessed by measuring the anodic polarization response of specimens thermally aged for 10 and 173 h at 700 °C. It is not clear from the description of the DOE data if the specimens tested included crevice geometries or were traditional anodic polarization specimens with no crevices. According to the thermal stability data provided by Heubner et al. (1989) and data reported by the DOE (Civilian Radioactive Waste Management System Management and Operating Contractor, 2000f,g), the grain boundary regions after 10 h at 700 °C are partially covered by topologically closed, packed-phase precipitates such as  $\sigma$ ,  $\mu$ , and P-phase, which can contain more than 34 percent Mo (Cieslak et al., 1986) and thus deplete the Mo concentration in the grain boundary regions. After 173 h at 700 °C, the grain boundaries are completely covered with topologically closed-packed phases accompanied by significant precipitation in the grain interiors (Heubner et al., 1989; Civilian Radioactive Waste Management System Management and Operating Contractor, 2000f). The thermally aged specimens were tested in simulated acidified water and simulated dilute water at 90 °C and in basic saturated water at 110 °C. In the simulated acidified water and basic saturated water, the  $E_{critical}$  was determined by the potential at which the anodic current increases dramatically and is no longer independent of potential (termed Type 1 behavior). For simulated acidified water, the  $E_{critical}$  was approximately 650 mV vs Ag/AgCl (605 mV<sub>SCE</sub>)<sup>1</sup> for the 173 h aged material and very close to the value measured for the base alloy without thermal aging. The anodic current density for the thermally aged material was about 2.5 times that of the base alloy. In basic saturated water, the critical potential was reduced to 350 mV versus Ag/AgCl (305 mV<sub>SCE</sub>) for the 173 h aged material. The anodic current densities were similar for the thermally aged material and the base alloy. The anodic behavior of Alloy 22 is different in simulated dilute water, and the anodic polarization scan is characterized by an anodic peak in the range of 200 to 400 mV vs Ag/AgCl (155 to 355 mV<sub>SCE</sub>) (termed Type 2 behavior). For the thermally aged specimens in simulated dilute water, the  $E_{critical}$  was again similar to the base metal, and the anodic current densities were similar for the thermally aged material and the base alloy. Reductions in the  $E_{corr}$  on the order of 100 mV were observed for all thermally aged specimens in all solutions. Again, although it is not explicitly stated, it is implied that the  $E_{corr}$  values for the thermally aged specimens were measured in air-saturated solutions. The reduction in the  $E_{corr}$  was suggested to offset or compensate for any apparent reduction in the  $E_{critical}$ . As a result, it was considered that the resistance of Alloy 22 to localized corrosion was not compromised by thermal aging.

---

<sup>1</sup>mV<sub>SCE</sub> is millivolts versus a saturated calomel electrode.

### 3.1.5 Localized Corrosion

The susceptibility of Alloy 22 and other Ni-base alloys to localized corrosion was evaluated by comparing the corrosion potential ( $E_{\text{corr}}$ ) with the critical potential for the initiation of localized corrosion ( $E_{\text{critical}}$ ). These potentials were measured in short-term tests conducted in aerated simulated dilute water, simulated concentrated water, simulated acidified water, simulated saturated water, and basic saturated water solutions. The test method was based on American Society for Testing and Materials (ASTM) G5 (American Society for Testing and Materials, 1999a) for potentiodynamic anodic polarization curves, although cyclic polarization tests similar to the method described in ASTM G61 (American Society for Testing and Materials, 1999b) were also used. Alloy 22 was evaluated using only the base alloy without welds or thermal processing to simulate waste package fabrication effects. Cyclic polarization tests, used to obtain  $E_{\text{critical}}$  values as a function of solution composition and temperature, were conducted with cylindrical specimens that were free of crevices. Although several scan rates were initially investigated (McCright, 1998), most tests were conducted using the ASTM G61 specified scan rate of 0.167 mV/s (600 mV/h).

Two types of responses were measured for the Ni-base alloys. For the Type 1 response, the material was passive until the potential for transpassive dissolution was reached (figure 3-1). Type 1 response was observed for Alloy 22 in simulated acidified water, simulated saturated water (Civilian Radioactive Waste Management System Management and Operating Contractor, 2000e), and basic saturated water (Civilian Radioactive Waste Management System Management and Operating Contractor, 2000f). The difference between  $E_{\text{critical}}$  and  $E_{\text{corr}}$  was compared for simulated acidified water at temperatures of 30, 60, and 90 °C.

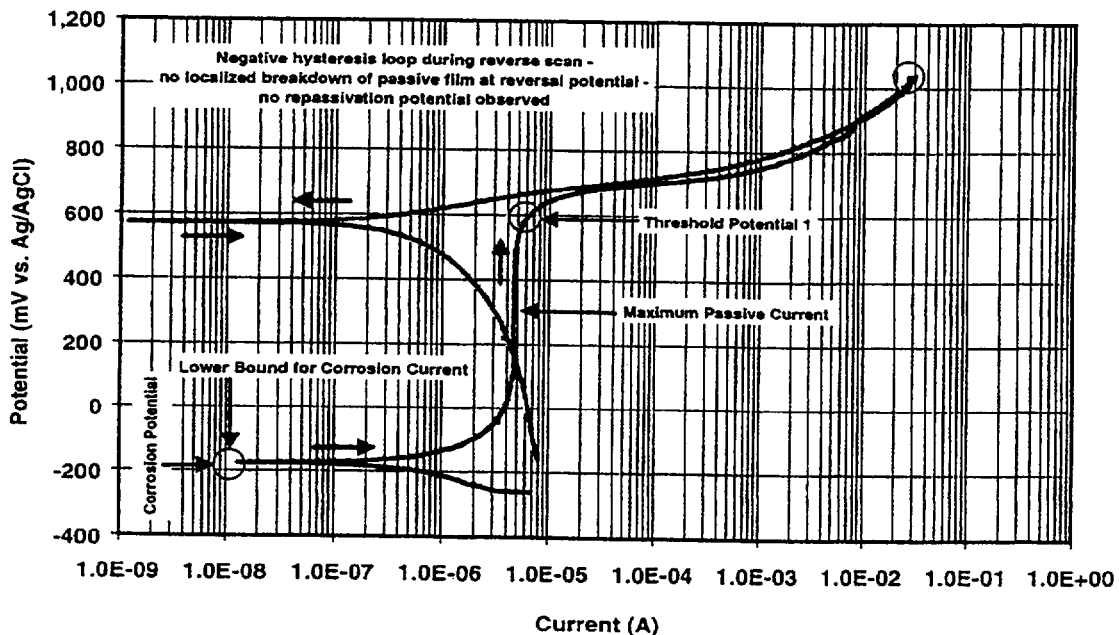


Figure 3-1. Example of Type 1 polarization behavior for Alloy 22 (Civilian Radioactive Waste Management System Management and Operating Contractor, 2000f)

Values of  $E_{\text{corr}}$  and  $E_{\text{critical}}$  were measured using an Ag/AgCl/KCl-saturated reference electrode. The potential for the Ag/AgCl/KCl-saturated reference electrode is -45 mV with respect to the saturated calomel electrode (SCE). In simulated acidified water, the  $E_{\text{critical}}$  was always in the range of 550 to 650 mV versus Ag/AgCl (505 to 605 mV<sub>SCE</sub>) and the  $E_{\text{corr}}$  was in the range of -50 to -200 mV versus Ag/AgCl (-95 to -245 mV<sub>SCE</sub>). Both  $E_{\text{corr}}$  and  $E_{\text{critical}}$  decreased with temperature. As a result, the difference between  $E_{\text{corr}}$  and  $E_{\text{critical}}$  was observed to be greater than 600 mV for all temperatures. For simulated saturated water,  $E_{\text{critical}}$  values ranged from 200 to 800 mV versus Ag/AgCl (155 to 755 mV<sub>SCE</sub>) over the temperature range of 100 to 120 °C, whereas the  $E_{\text{corr}}$  ranged from -220 to -320 mV versus Ag/AgCl (-265 to -365 mV<sub>SCE</sub>), yielding a difference of at least 420 mV between  $E_{\text{critical}}$  and  $E_{\text{corr}}$ . The response of Alloy 22 in basic saturated water is similar to that shown in simulated saturated water. Differences between  $E_{\text{critical}}$  and  $E_{\text{corr}}$  measured in short-term tests are on the order of 400 mV.

In both simulated dilute water and simulated concentrated water, a Type 2 response was observed for Alloy 22 as shown in figure 3-2 (Civilian Radioactive Waste Management System Management and Operating Contractor, 2000e). Type 2 response was characterized by the occurrence of an anodic peak at intermediate potentials between 200 and 400 mV versus Ag/AgCl (155 to 355 mV<sub>SCE</sub>). At higher potentials, the potential for breakdown or transpassive dissolution was observed. For the Type 2 response several potentials were identified as critical potentials as indicated in figure 3-2. It should be noted, however, that the threshold potential 1 on the Type 2 response, was not considered to be a critical potential for the initiation of localized corrosion. The basis for this assessment was a short-term test (less than 24 h) in which an Alloy 22

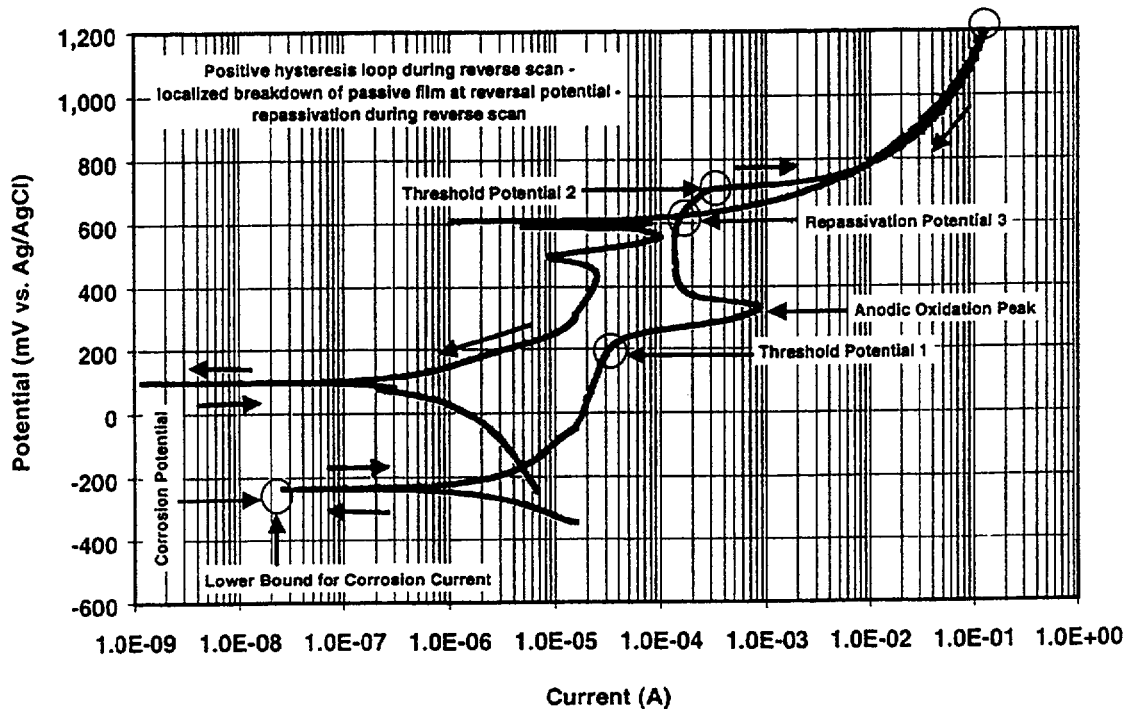


Figure 3-2. Example of Type 2 polarization behavior for Alloy 22 (Civilian Radioactive Waste Management System Management and Operating Contractor 2000f)

test specimen was maintained at 200 mV versus Ag/AgCl (155 mV<sub>SCE</sub>) in simulated dilute water at 90 °C. Although a large current peak occurred during the first half of the test, no localized corrosion was observed on the specimen. For simulated dilute water, the differences between  $E_{critical}$  and  $E_{corr}$  range from 500 mV at 30 °C to less than 400 mV at 90 °C. For simulated dilute water, the difference between  $E_{critical}$  and  $E_{corr}$  is 600 mV at 30 °C and 500 mV at 90 °C. The absence of a crevice-forming device on test specimens used to determine  $E_{critical}$  values does not permit the initiation of crevice corrosion. Initiation and early penetration of the waste packages by localized corrosion are more likely to occur as a result of crevice corrosion, which is much easier to initiate compared to pitting corrosion, especially on corrosion-resistant Ni-Cr-Mo alloys. Values of  $E_{critical}$  measured when no localized corrosion is initiated are not conservative because these potentials are associated with transpassive dissolution or oxygen evolution. Conservative values of  $E_{critical}$ , which have been shown to predict long-term localized corrosion susceptibility, can be acquired using crevice corrosion repassivation potentials (Cragolino et al., 1999).

The effect of gamma radiolysis on the localized corrosion susceptibility of Alloy 22 was assessed by measuring the  $E_{corr}$  of the alloy in both simulated acidified water and simulated dilute water with the addition of hydrogen peroxide (H<sub>2</sub>O<sub>2</sub>). Although not explicitly stated, it is implied that the  $E_{corr}$  values measured in solutions containing H<sub>2</sub>O<sub>2</sub> are compared to those measured in air-saturated solutions. In simulated dilute water at 25 °C, the  $E_{corr}$  increased from -230 to -40 mV vs Ag/AgCl (-275 to -85 mV<sub>SCE</sub>) after the addition of 72 ppm H<sub>2</sub>O<sub>2</sub>. In simulated acidified water at 25 °C the  $E_{corr}$  increased from -80 to 150 mV vs Ag/AgCl (-125 to 105 mV<sub>SCE</sub>) after the addition of 72 ppm H<sub>2</sub>O<sub>2</sub> (Civilian Radioactive Waste Management System Management and Operating Contractor, 2000e).

### **3.1.6 U.S. Department of Energy Model Abstraction and Predicted Performance**

#### **3.1.6.1 Humid-Air Corrosion**

In the abstraction of waste package performance, the corrosion rates of the waste package materials are assumed to be the same as the aqueous corrosion rates. The lack of measurable differences between corrosion rates of Ni-base alloys including Alloy 22 under humid and aqueous conditions is cited as the basis for this assumption (Civilian Radioactive Waste Management System Management and Operating Contractor, 2000e,f,h).

#### **3.1.6.2 Uniform Corrosion**

Two environmental conditions are considered for the stabilization of an aqueous film on the waste package surface. The presence of an aqueous environment is expected either when the RH in the emplacement drift is greater than the deliquescence point of any salts deposited on the waste package surface and or when dripping of condensed water occurs on the waste package. Below 100 °C, the composition of water that contacts the waste package surface is assumed to be simulated dilute water. Simulated saturated water is assumed to be present above 100 °C. Basic saturated water has also been identified as another plausible water chemistry that may develop on the waste package surface as a result of dripping and evaporation. Compositions of the water chemistry are provided in table 2-7. In addition, it is assumed that  $\gamma$ -radiolysis can increase  $E_{corr}$  of Alloy 22 by 100 mV, based on short-term exposures of specimens to solutions containing H<sub>2</sub>O<sub>2</sub> (Civilian Radioactive Waste Management System Management and Operating Contractor, 2000e,f).

The corrosion rates for Alloy 22 specimens were corrected for the deposition of silica that occurred during testing. Silica deposition occurred because silica was added to the test solutions. Only 2-yr data from the long-term corrosion test facility were used for performance assessment analyses, which have the lowest mean corrosion rate with respect to 6-mo and 1-yr test data. Because negative corrosion rates (from weight gain) are believed to be caused by silica deposition, these rates were not used in the performance assessment. The thick line in figure 3-3 represents data used for the Total System Performance Assessment–Site Recommendation (TSPA–SR) analyses. It has been suggested, based on atomic force microscopy measurements, that weight gain caused by the deposited silica can be corrected by adding a maximum value of  $63 \text{ nm yr}^{-1}$  (Civilian Radioactive Waste Management System Management and Operating Contractor, 2000e,f). Accordingly, corrosion rates in figure 3-3 (thick line) were corrected by adding a constant randomly selected from a uniform distribution between 0 and  $63 \text{ nm yr}^{-1}$ . Resulting corrosion rates were modulated by factors to account for microbial-induced corrosion and thermal aging, as described in sections 3.1.6.3 and 3.1.6.4. An upper bound of  $730 \text{ nm yr}^{-1}$  was assumed for the total effective Alloy 22 corrosion rate. Thus, the abstracted general corrosion rate for the Alloy 22 waste package outer barrier was distributed between 0 and  $7.3 \times 10^{-5} \text{ mm yr}^{-1}$ .

The cumulative distribution function for the general corrosion rate for Alloy 22 was considered to be a mix of uncertainty and variability. Separation of uncertainty and variability was not possible because the low corrosion rates calculated from the measured weight loss were considered to be within the measurement noise (Civilian Radioactive Waste Management System Management and Operating Contractor, 2000f). A technique known as Gaussian Variance Partitioning is used to decompose the general corrosion rate distribution function into multiple distribution functions, providing a scheme to account for uncertainty and variability (Civilian Radioactive Waste Management System Management and Operating Contractor, 2000h).

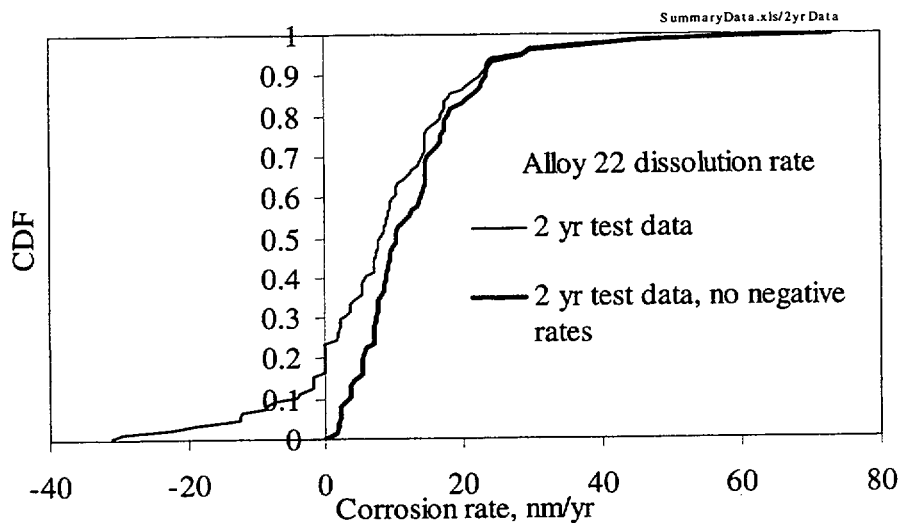


**Figure 3-3. Cumulative distribution function for the corrosion rate of Alloy 22, 2-yr data from the long-term corrosion test facility. The thick line was computed neglecting negative corrosion rates. These data (thick line) were used in the Total System Performance Neglecting Assessment–Site Recommendation analyses. Corrosion rates were increased by a constant randomly sampled from a uniform distribution with 0 and  $63 \text{ nm yr}^{-1}$  as bound values to account for silica deposits. The average corrosion rate, without silica correction, is  $8 \text{ nm yr}^{-1}$  and  $13 \text{ nm yr}^{-1}$  if negative rates are neglected.**

### 3.1.6.3 Microbially Influenced Corrosion

Acceleration of the corrosion rates as a result of microbial activity is treated using an enhancement factor,  $G_{MIC}$ . For Type 316 NG, a  $G_{MIC}$  of 10 is used, based on results obtained with Type 304 SS (Civilian Radioactive Waste Management System Management and Operating Contractor, 2000e). For Alloy 22, experimental results indicate a  $G_{MIC}$  of 2 as discussed in section 3.1.3, based on the corrosion rate measured in short-term exposure tests (Civilian Radioactive Waste Management System Management and Operating Contractor, 2000f). The enhancement factor for Alloy 22 is assumed to have a uniform distribution between 1 and 2. In addition, it is assumed that microbially influenced corrosion of the waste package occurs only when the humidity is greater than 90 percent and sufficient nutrients exist to support microbial activity (Civilian Radioactive Waste Management System Management and Operating Contractor, 2000f). Although the type of nutrients is not explicitly stated in the TSPA-SR, the general corrosion and localized corrosion of the waste package outer barrier Analysis/Model Report (Civilian Radioactive Waste Management System Management and Operating Contractor, 2000a) suggests that low concentration of phosphate in the groundwater in the Yucca Mountain region may have limited the microbial activity.

### 3.1.6.4 Thermal Aging

An enhancement factor, uniformly distributed between 1 and 2.5, is used to model the corrosion rate of thermally aged Alloy 22. As discussed in section 3.1.4, the enhancement factor is based on the passive current density of the thermally aged specimen (700 °C for 173 h) measured in a potentiodynamic polarization test (Civilian Radioactive Waste Management System Management and Operating Contractor, 2000f). It is assumed this enhancement factor affects only the weld area, which is approximately 3 percent of the waste package surface.

### 3.1.6.5 Localized Corrosion

Abstraction of the localized corrosion initiation model was obtained from fitting the difference ( $\Delta E$ ) between the  $E_{critical}$  and the  $E_{corr}$  measured in the test solutions listed in table 2-7 to a multiparameter equation that considers the chloride concentration, temperature, and solution pH (Civilian Radioactive Waste Management System Management and Operating Contractor, 2000i). Because  $\Delta E$  was not observed to be a strong function of either temperature or the log of the chloride concentration, the equation for  $\Delta E$  was simplified to include only pH and  $pH^2$  terms. The minimum value for  $\Delta E$  was determined to be just below 400 mV at a pH of 8. At both lower and higher pH values,  $\Delta E$  increases and was determined to be 800 mV at pH 2 and pH 14. Confidence intervals of  $\pm 3\sigma$  and  $\pm 4\sigma$  indicate that the value of  $\Delta E$  is always greater than 100 mV. Based on these analyses, the start of localized corrosion of Alloy 22 was determined to be unlikely in the range of possible repository environments. As such, localized corrosion of Alloy 22 is not included in the TSPA model abstraction (Civilian Radioactive Waste Management System Management and Operating Contractor, 2000j).

In the event that localized corrosion would occur, the rate of localized penetration of Alloy 22 was estimated using corrosion rates in highly corrosive environments such as 10 percent  $FeCl_3$  at 75 °C; dilute boiling HCl; and a solution containing 7 vol %  $H_2SO_4$ , 3 vol % HCl, 1 wt %  $FeCl_3$ , and 1 wt %  $CuCl_2$  at 102 °C. The distribution of localized corrosion rates is centered around the highest passive current density

of  $10 \mu\text{A}/\text{cm}^2$  which corresponds to a corrosion rate of  $100 \mu\text{m}/\text{yr}$ . The cumulative distribution of penetration rates for localized corrosion is  $12.7 \mu\text{m}/\text{yr}$  for the 0<sup>th</sup> percentile,  $127 \mu\text{m}/\text{y}$  for the 50<sup>th</sup> percentile, and  $1,270 \mu\text{m}/\text{yr}$  for the 100<sup>th</sup> percentile (Civilian Radioactive Waste Management System Management and Operating Contractor, 2000e,f).

### 3.1.6.6 Predicted Performance

The TSPA-SR uses the Waste Package DEgradation (WAPDEG) model (Civilian Radioactive Waste Management System Management and Operating Contractor, 2000k) to evaluate the degradation of the waste packages and drip shields. Corrosion processes for a total of 400 waste package and drip shield pairs are simulated in the model to incorporate the effects of spatial and temporal variation. The uncertainty and variability for each waste package and drip shield pair are incorporated by discretizing the waste package and the drip shield into numerous subareas called patches. The performance of the waste packages and drip shields from the time of repository closure to 100,000 yr after repository closure is simulated using 300 realizations for the basecase scenario.

In the basecase scenario, the first drip shield patch fails around 20,000 yr after repository closure. The mean (of the Monte Carlo simulations of the TSPA-SR) curve of the fraction of drip shield patches failed versus time shows that 50 percent of the patches will fail after 100,000 yr. The first waste package failure occurs around 10,000 yr and is attributed to the effects of manufacturing defects. The upper bound of the TSPA-SR Monte Carlo simulations indicates that 1 percent of the patches will fail after 100,000 yr. The median and the mean curves show that only ~0.1 percent of the patches will fail after 100,000 yr.

Frequently, the number or the fraction of waste packages displaying first-patch penetration is taken as a measure of the system performance. It is important to note that this quantity is not well defined because it is sensitive to the number of patches assumed in the simulation. In fact, in the limit when the number of patches approaches infinity this curve tends to approach a step function. On the other hand, the fraction of penetrated patches or fraction of degraded area versus time is independent of the number of patches. Thus, this quantity is a more objective measurement of the system performance.

The reason the number of waste packages with first-patch failure depends on the number of patches is straightforward. The surface area of each patch is inversely proportional to the number of patches on the waste package surface. Thus, to yield the same extent of degraded surface at any given time, a case with larger number of patches must display a greater number of waste packages with first-patch penetration. Figure 3-4 shows the influence of the number of patches on the computation of the fraction of waste packages with first-patch penetration. Figure 3-4 also includes the fraction of penetrated waste package surface by general corrosion based on corrosion rates in figure 3-3. The fraction of waste packages with first-patch penetration can be obtained from the fraction of degraded surface by multiplying the latter quantity by the number of patches and truncating the product at one. Because of this simple relationship, it is evident that in the limit when the number of patches approaches infinity, the curve "fraction of waste packages with first-patch penetration versus time" approaches a step function. The time at which the step occurs is defined by the upper general corrosion rate (currently  $730 \text{ nm yr}^{-1}$ ). Therefore, the number of waste packages with first-patch failure is an ill-defined quantity.

Sensitivity analyses reported in the TSPA-SR (Civilian Radioactive Waste Management System Management and Operating Contractor, 2000h) were conducted to assess the effect of corrosion parameters

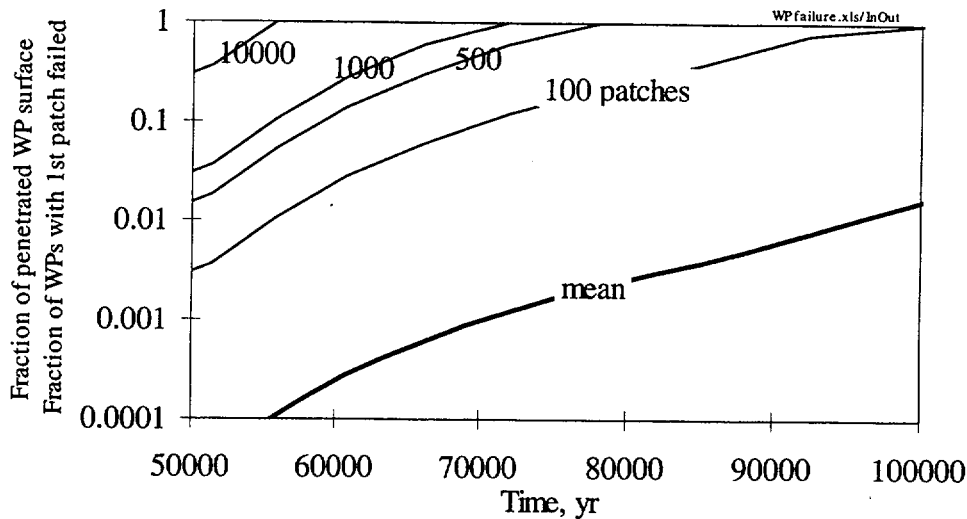


**Figure 3-4. Thick line: fraction of penetrated waste package surface versus time (Center for Nuclear Waste Regulatory Analyses computations based on corrosion rates in figure 3-3). Thin lines: fraction of waste packages with first-patch penetration versus time. All lines represent mean values. The labels on the thin lines indicate the number of patches on the waste package surface.**

on the overall waste package performance. Variations in temperature and RH were not included in the sensitivity analyses because these parameters were assessed to not significantly affect either waste package or drip shield performance except for the RH threshold for the initiation of corrosion. The effect of dripping was not included because the DOE models for general corrosion is not dependent on dripping conditions. As previously indicated, the initiation of localized corrosion of waste packages is not considered possible as a result of the large difference between  $E_{critical}$  and  $E_{corr}$ .

The uncertainty and variability split in the corrosion rate (incorporated by the Gaussian Variance Partitioning scheme into the WAPDEG code) was examined as part of the sensitivity analyses for the TSPA-SR (Civilian Radioactive Waste Management System Management and Operating Contractor, 2000h). WAPDEG samples the corrosion rate for each waste package patch from the variability distribution obtained from the Gaussian Variance Partitioning of the  $SiO_2$  corrected corrosion rate distribution. TSPA-SR sensitivity analyses indicate no relevance of the uncertainty-variability split (i.e., different splits did not affect the number of failed waste packages or the mean dose rate). Nonetheless, these quantities were shown to be strongly dependent on the magnitude of the corrosion rates assumed in the simulations. Even when the corrosion rate is fixed to the 95<sup>th</sup> percentile values of uncertainty variance, the first waste package failure occurs at approximately 12,000 yr and the maximum dose rate at 100,000 yr is 200 mrem/yr (figure 3-5).

A robust analysis for the waste package was also reported in the TSPA-SR (Civilian Radioactive Waste Management System Management and Operating Contractor, 2000h). This analysis modeled the performance of degraded waste packages and enhanced waste packages. Degraded waste packages were modeled by fixing five parameters at the 95<sup>th</sup> percentile of their respective distributions. These parameters included the residual hoop stress and the stress-intensity factor at the closure lid welds, the number of manufacturing defects in the closure lid welds, the Alloy 22 general corrosion rate, and the enhancement

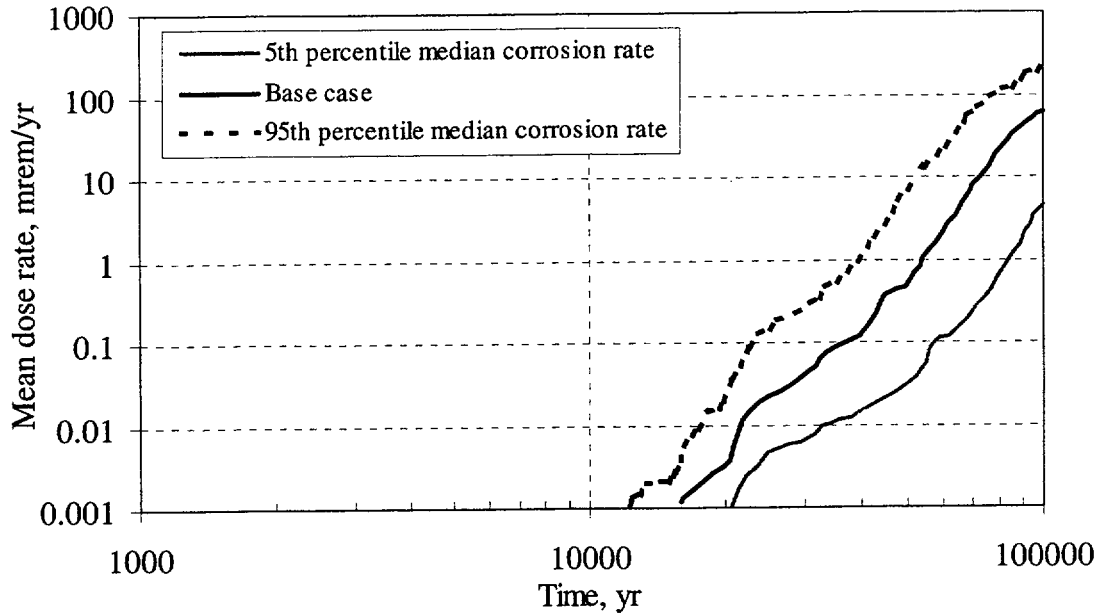


**Figure 3-5. U.S. Department of Energy predicted mean dose rate as a function of time for the basecase corrosion rate, and the 5<sup>th</sup> and 9<sup>th</sup> percentile median corrosion rates is fixed at the 5<sup>th</sup> and 95<sup>th</sup> percentile values of the uncertainty variance**

factors for general corrosion due to microbially influenced corrosion and aging and phase stability. Similarly, the enhanced waste package performance was modeled by fixing the values of these parameters to the 5<sup>th</sup> percentile of their respective distributions. The uncertainty-variability partitioning ratio was set to the 5<sup>th</sup> percentile value, which considers that the variance in the measured corrosion rates is mostly a result of variability for the degraded waste package analyses. For the enhanced waste package analyses, the uncertainty-variability partitioning ratio was set to the 95<sup>th</sup> percentile value, which considers that the variance in the measured corrosion rates is mostly a result of measurement uncertainty.

No waste package failures were predicted to occur during the first 100,000 yr for the enhanced waste package analyses, whereas the first waste package failure occurs at 7,000 yr for the degraded waste package analyses. Correspondingly, there is no dose for the enhanced waste packages in the first 100,000 yr (no waste package failure). For the degraded waste package analyses, the predicted mean dose starts at 8,200 yr compared to 15,000 yr for the basecase. The predicted mean dose for the degraded waste packages is also higher and reaches  $8 \times 10^{-2}$  mrem/yr at 100,000 yr which is about four times larger than the basecase (Civilian Radioactive Waste Management System Management and Operating Contractor, 2000h).

### 3.1.7 Assessment of the U.S. Department of Energy Approach

The DOE approach has been previously assessed. These assessments are provided in the Issue Resolution Status Report (U.S. Nuclear Regulatory Commission, 2001). In addition, technical exchange agreements have been documented and are intended to address the concerns regarding the DOE approach.<sup>2,3</sup>

The DOE engineered barrier subsystem degradation models are based on tests conducted in solutions that are not consistent with the environments predicted to result from the evolution of near-field processes. Distributions of engineered barrier materials uniform corrosion rates and abstraction of the critical potentials for localized corrosion are based on tests conducted using solutions based on variations of J-13 Well water at 60 and 90 °C (Civilian Radioactive Waste Management System Management and Operating Contractor, 2000f). The ratios of chloride and nitrate concentrations used on these tests are similar to the results of groundwater chemistry evolution calculations using EQ3/6, assuming an initial water composition equivalent to J-13 Well (Civilian Radioactive Waste Management System Management and Operating Contractor, 2001). In recent presentations,<sup>4</sup> two types of distinctive water chemistries were identified experimentally as produced by evaporation. Bicarbonate-type waters were generated by evaporation of J-13 and perched waters, whereas chloride-sulfate-type waters were formed by evaporation of pore water (Civilian Radioactive Waste Management System Management and Operating Contractor, 2000k). In the bicarbonate-type waters, the ratio of the fluoride to chloride concentration is similar to that of the original J-13 Well water, but the chloride concentration reaches values around 0.2 M. In the chloride-sulfate type, the concentration of fluoride is in the range of  $10^{-3}$  molal, but the chloride concentration is in excess of 1 molal with low nitrate concentrations. High chloride and fluoride concentrations are also obtained in models of the in-drift environment, taking into account seepage and thermal-hydrological-chemical-coupled processes (Civilian Radioactive Waste Management System Management and Operating Contractor, 2000l). These two types of water chemistries can lead to significant differences in the mode and rate of corrosion of drip shield and waste package materials.

The DOE approach relies on passive dissolution rates of Alloy 22 determined via weight loss measurements. Potentiostatic measurements of the passive dissolution rate, discussed in section 3.1.2, are not used in the DOE model abstraction. Because the passive corrosion rate of Alloy 22 is quite low, the change in mass is also small. For a 1-yr exposure, the change in weight is less than  $2 \times 10^{-3}$  percent. Such small changes in weight can be determined provided there is no substantial interference from a competing process. In the case of the DOE long-term corrosion test facility data, the deposition of silica was shown to interfere with weight loss data. The suggested correction (Civilian Radioactive Waste Management System Management and Operating Contractor, 2000e,f) to the corrosion rates (i.e., addition of a constant between 0 and  $63 \text{ nm yr}^{-1}$ , uniformly sampled) may lead to a nonconservative estimation of the actual corrosion rates

---

<sup>2</sup>Reamer, C.W. *Summary Highlights of NRC/DOE Technical Exchange and Management Meeting on Key Technical Issue: Container Life and Source Term*. Letter (October 4) to D. Williams, U.S. Department of Energy. Washington, DC: U.S. Nuclear Regulatory Commission. 2000.

<sup>3</sup>Reamer, C.W. *Summary Highlights of NRC/DOE Technical Exchange and Management Meeting on Key Technical Issue: Evolution of the Near-Field Environment*. Letter (January 26) to D. Brocoum, U.S. Department of Energy. Washington, DC: U.S. Nuclear Regulatory Commission. 2001.

<sup>4</sup>Ibid.

by undercorrecting the measured rates. Furthermore, the time-dependent changes in corrosion rate that may have occurred after the silica deposition have also not been accounted for. Corrosion rates were computed from weight loss data assuming a constant reactive surface area according to Eq. (3-2):

$$CR = \frac{\Delta w}{\rho A t} \quad (3-2)$$

where  $\Delta w$  is the weight loss (kg),  $\rho$  is Alloy 22 density,  $A$  is the surface area of the coupon sample (30.65 and 57.08 cm<sup>2</sup> for noncreviced and creviced samples, respectively), and  $t$  is the duration of the weight loss test (yr). The reactive surface area may decrease with time as a consequence of the silica deposits. Because the corrosion rate is inversely proportional to the surface area, use of a larger surface area may result in underestimation of corrosion rates. In addition, the mean value of the correcting silica term (i.e., 31.5 nm yr<sup>-1</sup>) is more than twice the value of the mean corrosion rate (equal to 13 nm yr<sup>-1</sup>, see figure 3-3); thus, the value of the experimental data is questionable.

Because Eq. (3-2) yields average rates over a reference surface its use is not valid in case of existence of small zones of enhanced dissolution (this equation underestimates the corrosion rate of the enhanced dissolution zones). The relative corrosion rates of welded and base metal Alloy 22 were determined using weight loss specimens. However, welded specimens were exposed along with the base alloy. Because the area of the welded region is quite small (approximately 10–15 cm<sup>2</sup>) and accounts for less than 25 percent of the total specimen surface area, accelerated corrosion rates of the welded region would be masked by the much larger area of the base alloy. Similarly for creviced samples, the area of the crevice is smaller than the base alloy surface. Therefore, potentially higher corrosion rates of crevice zones are masked by the much larger area of the base alloy. It must be noted that creviced samples in the long-term corrosion test facility in general yielded higher corrosion rates [computed on the basis of Eq. (3-2)] than noncreviced samples. If the difference in the corrosion rates with respect to noncreviced samples is due to higher dissolution rates on the crevices, reported values of corrosion rates for creviced samples are questionable.

The distribution of passive corrosion rates used by the DOE is not supported by the electrochemical measurements conducted within the Yucca Mountain project and is lower than corrosion rates measured in a variety of service environments. Corrosion rates reported from tests conducted in the long-term corrosion test facility have been compared to values published in the literature (Cragolino et al., 1999). In general, the corrosion rates used to assess long-term waste package performance (Civilian Radioactive Waste Management System Management and Operating Contractor, 2000f,g,h) are much lower than the corrosion rate for pure Cr and Fe-Cr alloys (Kirchheim et al., 1989); Ni-base alloys including Alloys 625, C4, and C-276 in high-temperature groundwater and brines (Smailos, 1993; Harrar et al., 1977, 1978); and Alloy 22 in environments containing Cl<sup>-</sup>, F<sup>-</sup>, SO<sub>4</sub><sup>2-</sup> (Bickford and Corbett, 1985).

General corrosion rates measured during a period of 2 yr were used in the TSPA-SR computations, disregarding data gathered after 0.5 and 1 yr. In general, corrosion rates seem to decrease with exposure time. The DOE has defined or suggested that the reason this apparent decrease is due to the presence of an oxide layer that thickens with time. No evidence has been presented that this oxide layer is the reason for the decreased corrosion rates. Increasing coverage with silica deposits could also result in corrosion rates [computed via Eq. (3-2)] that apparently decrease with time. Based on the premise of intrinsic corrosion rates decreasing with time, selection of 2-yr test data for TSPA-SR computations has been suggested as a

conservative approach. Evidence is needed (as agreed to with DOE), showing that intrinsic corrosion rates do decrease with time independently of the effect of silica and other corrosion product deposits. As previously mentioned, reported long-term corrosion test facility corrosion rates for 0.5- and 1-yr exposures are lower than rates reported for alloy systems comparable to Alloy 22. Use of these data could have an important impact in performance assessment computations as suggested in figure 3-6.

The corrosion rate data used by the DOE do not consider the effects of long-term changes to the composition of the oxide films. Previous investigations (Lorang et al., 1990) indicated that the composition of the oxide film, which acts as a barrier for mass transport, becomes enriched in Cr and depleted in Mo and Ni. The long-term effects of preferential dissolution of alloying elements may include changes to the oxide film composition that could, in turn, alter the passive corrosion rate, or promote an increase in the susceptibility of the alloy to localized corrosion. Information on the preferential dissolution of alloying elements has not been obtained from long-term corrosion test facility specimens.

Data used by the DOE as the basis to model the enhancement factor for microbially influenced corrosion are not sufficient to assess the effects of microbial activity on the long-term performance of the

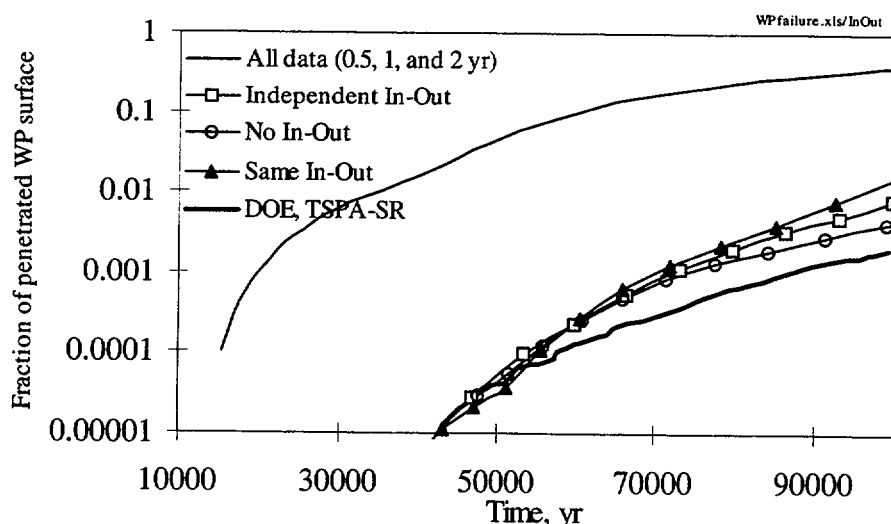


**Figure 3-6. Fraction of penetrated waste package surface by general corrosion versus time. The upper line was derived considering long-term corrosion test facility general corrosion rates from 0.5-, 1-, and 2-yr exposure periods. The lower thick line is the mean curve in figure 3.4 (Civilian Radioactive Waste Management System Management and Operating Contractor, 2000h). The other data were generated from corrosion rates in figure 3-3. A simplified model that accounts for enhancement factors for microbially influenced corrosion and thermal aging of closure lid welds and corrosion from the inside-out after first-patch penetration was implemented to determine the fraction of penetrated patches (or fraction of penetrated surface). Three variants of the model were considered. In one case, there was no inclusion of corrosion from the inside-out; in a second case, the in-out corrosion rate was selected equal as the out-in rate, and in a third case, the in-out rate was selected independently from the out-in rate. There is no consideration of relative humidity terms in the simplified model, but this is not relevant in the 100,000-yr simulations.**

Alloy 22 waste package outer barriers. The enhancement factor for microbially influenced corrosion,  $G_{MIC}$ , was calculated from the linear polarization results of specimens exposed to sterile and inoculated solutions (Civilian Radioactive Waste Management System Management and Operating Contractor, 2000e,f). No information is provided on the possible preferential dissolution of alloying elements or on localized corrosion susceptibility as a result of microbial activity. In addition, the effects of temperature and environmental variations on the value of  $G_{MIC}$  are not available. The selection of a microbially influenced corrosion enhancement factor for general corrosion (uniformly distributed between 1 and 2) is based on the assumption of a homogeneous and stoichiometric dissolution process. This approach is not necessarily conservative in the event that enhanced dissolution occurs along preferential paths such as grain boundaries.

Data used in the DOE assessment of Alloy 22 localized corrosion resistance are insufficient to evaluate the susceptibility of the waste packages to localized corrosion. The DOE assessment compares the corrosion potentials and initiation potentials measured in short-term tests. Data used as criteria to evaluate the localized corrosion susceptibility of the waste package outer barrier are limited to potentials associated with transpassive dissolution and evolution of oxygen (Civilian Radioactive Waste Management System Management and Operating Contractor, 2000e). The approach used does not consider many important factors to assess properly localized corrosion susceptibility. In addition, confirmatory tests designed to determine the validity of the critical potential approach have not been reported. It is well established that the initiation of crevice corrosion occurs preferentially to pitting corrosion. For example, in ferric chloride the critical pitting temperature for Alloy 22 is 85 °C, whereas the critical crevice temperature is 55 °C (American Society for Testing and Materials, 2000). NRC staff review (U.S. Nuclear Regulatory Commission, 2001) of the General Corrosion and Localized Corrosion of Waste Package Outer Barrier Analysis/Model Report (Civilian Radioactive Waste Management System Management and Operating Contractor, 2000e) and the Waste Package Degradation Process Model Report (Civilian Radioactive Waste Management System Management and Operating Contractor, 2000f) concluded that the DOE selection of critical potentials and the assessment of corrosion potentials are not based on the most likely corrosion mode for the alloy and do not consider environmental effects of temperature, solution chemistry, trace elements (e.g., Pb, As, and Hg), and the effects of material property variations such as long-term evolution of the oxide film. As a result, DOE has agreed to provide additional data or provide further technical bases for this issue.

Data used by the DOE to model waste package performance are insufficient to assess the possible detrimental effects of long-term thermal aging as a consequence of prolonged exposure to elevated temperatures and fabrication processes, including cold-working, welding, laser peening, and induction annealing, on the uniform corrosion rate and localized corrosion resistance of Alloy 22. The enhancement factor for the thermally aged specimens is based solely on short-term data and does not consider the effects of preferential corrosion that may occur at the grain boundary regions as indicated in previous investigations (Heubner et al., 1989). Previous investigations identified the formation of topologically closed-packed phases in both thermally aged (Heubner et al., 1989) and welded (Cieslak et al., 1986) Alloy 22. Observations of preferential initiation of localized corrosion in weldments and at grain boundary attack on the thermally aged material (Heubner et al., 1989) as well as lower critical pitting temperature for welded Alloy 22 (Sridhar, 1990) do not support the DOE conclusion of no reduced susceptibility to localized corrosion after thermal aging. The reduction of the  $E_{corr}$  after thermal aging suggests an increase in the passive current density. As previously indicated, this increase may be a result of significantly enhanced dissolution at grain boundaries. The increased current density, measured during an anodic polarization scan of an Alloy 22 specimen thermally aged for 173 h at 700 °C, was averaged over the entire exposed surface area. In view of the increased susceptibility of thermally aged Ni-Cr-Mo alloys to intergranular corrosion, the increased

current density observed in the DOE test may be the result of preferential dissolution at grain boundaries rather than an overall increase in the corrosion rate. Such preferential attack, mainly confined to the grain boundary regions, would result in a true enhancement factor much greater than the proposed upper bound of 2.5.

### 3.2 CENTER FOR NUCLEAR WASTE REGULATORY ANALYSES INVESTIGATIONS

To evaluate the performance predictions reported by the DOE for the waste package outer barrier, uniform corrosion under passive dissolution conditions and localized corrosion in the form of crevice corrosion were investigated using mill-annealed, thermally treated, and welded specimens of Alloy 22. Electrochemical techniques were used in these investigations. The approach developed for long-term performance prediction, including the use of empirically derived parameters for assessing localized corrosion and the modeling of the passive dissolution behavior, is described.

#### 3.2.1 Passive Corrosion of Alloy 22

##### 3.2.1.1 As-Received Material

The chemical compositions of the Alloy 22 heats used in this investigation are shown in table 3-1. Prior to the start of a test, all specimens were polished to a 600-grit finish, cleaned ultrasonically in detergent, rinsed in deionized water, ultrasonically cleaned in acetone, and dried. Passive dissolution rates were measured in solutions containing 0.028 to 4.0 M NaCl under potentiostatic polarization in order to determine the effect of chloride concentration. Tests were conducted in a 2-L glass cell with a polytetrafluoroethylene (PTFE) lid. The cells were fitted with a water-cooled Allihn-type condenser and a water trap to minimize solution loss at elevated temperatures and air intrusion. An SCE was used as a reference electrode in all experiments. The SCE was connected to the solution through a water-cooled Luggin probe with a porous silica tip so that the reference electrode could be maintained at room temperature. A platinum flag was used as a counter electrode. All solutions were deaerated with high-purity nitrogen (99.999 percent) for at least 24 h prior to the start of the tests to obtain accurate anodic current density measurements at potentials ranging from -200 to 800 mV<sub>SCE</sub>. Specimens were held potentiostatically for a period of 48 h while the anodic current density was recorded. The resolution of the current measurement was determined to be  $1.25 \times 10^{-10}$  A/cm<sup>2</sup>. At the conclusion of the test, the specimens were reweighed and examined microscopically for signs of corrosion.

**Table 3-1. Chemical composition (in weight percent) of the heats of Alloys 22 and 622 filler metal**

Heat	Ni	Cr	Mo	W	Fe	Co	Si	Mn	V	P	S	C
Alloy 22 2277-8-3175	57.8	21.40	13.60	3.00	3.80	0.09	0.030	0.12	0.15	0.008	0.002	0.004
Alloy 22 2277-8-3235	56.5	21.40	13.47	2.87	3.94	1.31	0.023	0.24	0.17	0.008	0.001	0.003
622 Filler XX1045BG11	58.5	20.73	14.13	3.15	3.05	0.09	0.060	0.24	0.01	0.007	0.001	0.006

Corrosion rates were calculated based on Faraday's law and according to ASTM G102 (American Society for Testing and Materials, 1999c) using Eq. (3-3):

$$Cr = \frac{Ki_{\text{corr}}EW}{\rho} \quad (3-3)$$

where  $i_{\text{corr}}$  is the passive corrosion current density in  $A/cm^2$ ,  $EW$  is the equivalent weight,  $K$  is a conversion factor ( $3,270 \text{ mm}\cdot\text{g}\cdot\text{A}^{-1}\cdot\text{cm}^{-1}\cdot\text{yr}^{-1}$ ),  $\rho$  is the density in  $g/cm^3$  and  $CR$  is in  $mm/yr$ . For Alloy 22,  $\rho$  is  $8.69 \text{ g/cm}^3$ . Assuming congruent dissolution of the major alloying elements as  $Ni^{2+}$ ,  $Cr^{3+}$ ,  $Mo^{3+}$ ,  $Fe^{2+}$ , and  $W^{4+}$  within the potential range of  $-200$  to  $400 \text{ mV}_{\text{SCE}}$ , the  $EW$  for Alloy 22 is  $26.04 \text{ g/equivalent}$  (American Society for Testing and Materials, 1999c).

Soluble corrosion products formed during passive dissolution were analyzed using capillary electrophoresis (CE). In CE, ionic speciation is achieved based on differences in the ionic migration time of the species present in the unknown solution under an applied electric field, in this case  $20 \text{ kV}$ . Species are then detected as they pass an ultraviolet lamp/detector assembly. Quantitation is performed by comparison of peak areas to those measured on samples of known concentration. Samples were loaded into the capillary using hydrostatic sampling for  $30 \text{ s}$  at a height of  $10 \text{ cm}$ . This sampling method roughly amounts to a sampling volume of  $37 \text{ nL}$  using a  $75\text{-}\mu\text{m}$  inner diameter capillary. All oxyanions ( $CrO_4^{2-}$ ,  $MoO_4^{2-}$ ,  $WO_4^{2-}$ ) were detected directly using a  $214\text{-nm}$  lamp and the method described by Kelly et al. (1996) in which the capillary electrolyte consisted of deionized water with  $1.5 \text{ mM Na}_2\text{SO}_4$ ,  $2.5 \text{ mM}$  osmotic flow modifier Anion BT, and pH adjusted to  $10.5$  using  $NaOH$ . All cations ( $K^+$ ,  $Na^+$ ,  $Cr^{3+}$ ,  $Ni^{2+}$ ) were analyzed using the method described by Krol et al. (2000) using indirect detection at  $254 \text{ nm}$  and a capillary electrolyte consisting of deionized water with  $6 \text{ mM}$  benzimidazole,  $2.5 \text{ mM}$  tartaric acid, and  $2 \text{ mM}$  18-crown-6-ether. All samples were analyzed at  $25 \text{ }^\circ\text{C}$  with a nominal minimum detection limit of  $\sim 70$  to  $100 \text{ ppb}$  for all species of interest. Tests were conducted in  $220$  to  $250 \text{ mL}$  of deaerated  $0.028 \text{ M KCl}$  solutions. Initial analyses of test solutions using CE were performed using small specimens with an area of  $8 \text{ cm}^2$ . Subsequent tests were performed using a specimen with a surface area of  $72 \text{ cm}^2$ . Specimens were held potentiostatically for a period of  $330 \text{ h}$  in a test cell equipped with provisions for extracting small samples of solution for analyses.

The results of passive current density measurements obtained after  $48 \text{ h}$  under potentiostatic conditions are shown in figure 3-7. At potentials of  $200 \text{ mV}_{\text{SCE}}$  or less, the passive current was in the range of  $6 \times 10^{-9}$  to  $3 \times 10^{-8} \text{ A/cm}^2$  and was relatively independent of the chloride concentration and solution pH in the range of  $2.7$  to  $8.0$ . In tests conducted at potentials above  $400 \text{ mV}_{\text{SCE}}$ , the onset of transpassive dissolution was observed. At  $\text{pH } 0.7$ , the passive current densities increased to approximately  $7 \times 10^{-8} \text{ A/cm}^2$  at  $200 \text{ mV}_{\text{SCE}}$ . The increase in the anodic current density observed at  $\text{pH } 0.7$  at an applied potential of  $200$  to  $600 \text{ mV}_{\text{SCE}}$  may be the result of enhanced oxide film dissolution in this highly acidic solution. Temperature, on the other hand, had a significant effect on the passive corrosion rate in dilute chloride solutions (figure 3-8). The passive corrosion rate increased by a factor of  $10$  when the temperature of the  $0.028 \text{ M}$  chloride solution ( $\text{pH } 8.0$ ) was increased from  $20$  to  $95 \text{ }^\circ\text{C}$ . However, practically no temperature effect was noted in  $4 \text{ M}$  chloride. Increasing temperature also decreased the potential range at which the passive film was stable. At  $20 \text{ }^\circ\text{C}$ , passive behavior was observed at potentials just above  $400 \text{ mV}$  whereas transpassive behavior was observed at these potentials when the solution temperature was increased to  $95 \text{ }^\circ\text{C}$ .

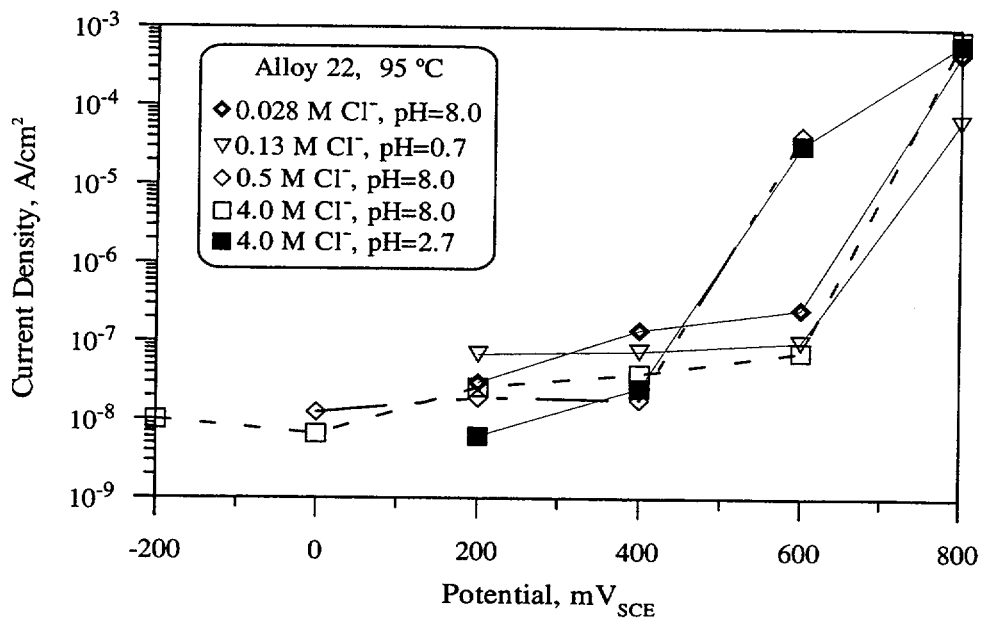


Figure 3-7. Steady-state anodic current densities for Alloy 22 in Cl<sup>-</sup> solutions at 95 °C

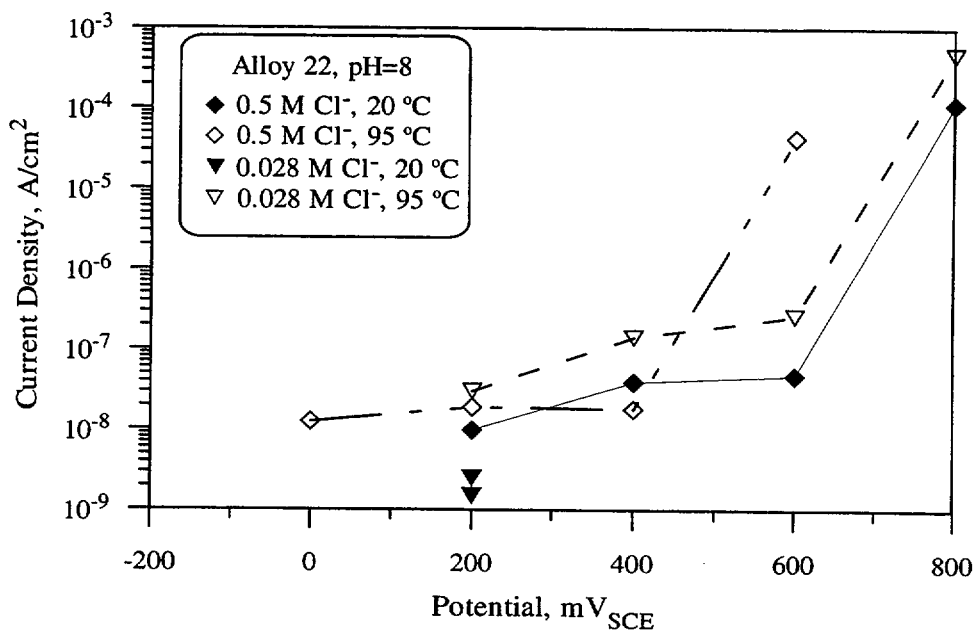
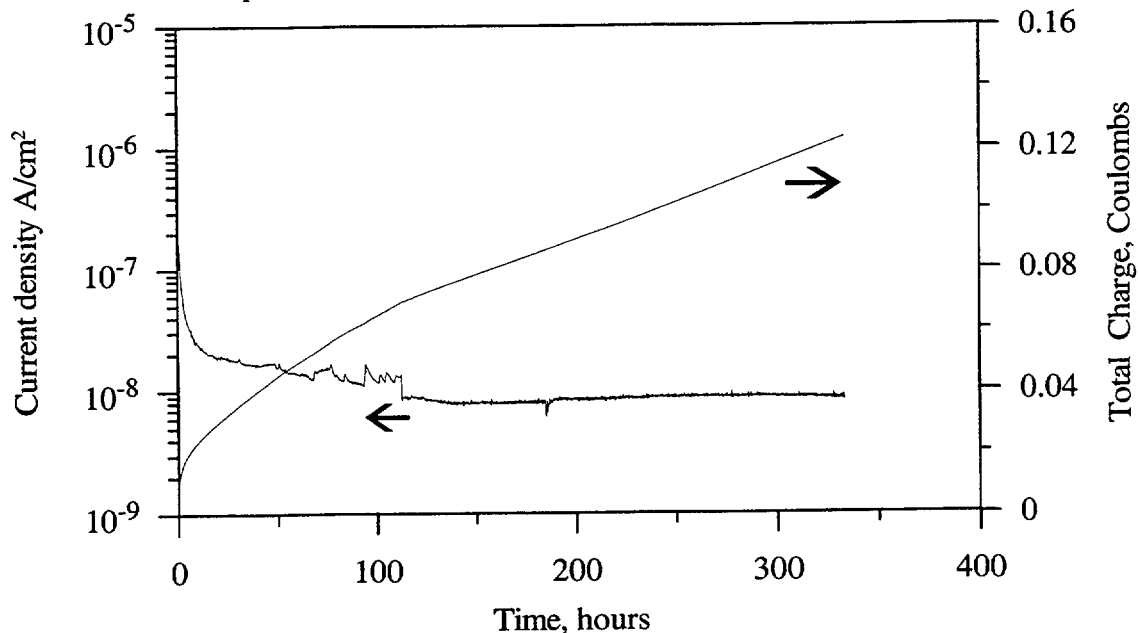


Figure 3-8. Effect of temperature on steady-state anodic current densities for Alloy 22

Initial analyses of solutions using CE were performed using a small test specimen (8 cm<sup>2</sup>) immersed in 220 mL of solution. The specimen was potentiostatically polarized at 100 mV<sub>SCE</sub> for 300 h. After 280 h, the passive current density was in the range of  $8.4 \times 10^{-9}$  to  $9.0 \times 10^{-9}$  A/cm<sup>2</sup> (figure 3-9). Integrating the current density with time resulted in a calculated charge density of 0.015 C/cm<sup>2</sup> for the duration of the test. Assuming stoichiometric dissolution, the total metal ion concentration as a result of Alloy 22 corrosion should be 147 ppb at the conclusion of the test, with 84 ppb Ni and 32 ppb Cr. Analyses of the solution using CE did not detect any species expected to result from passive dissolution.

The current density and total charge as a function of time for the transpassive dissolution of Alloy 22 are shown in figure 3-10. Measured concentrations of Cr(VI), Mo(VI), W(VI) (analyzed as oxyanions CrO<sub>4</sub><sup>2-</sup>, MoO<sub>4</sub><sup>2-</sup>, WO<sub>4</sub><sup>2-</sup>), and Ni<sup>2+</sup> in solution as a function of time are shown in figure 3-11. The calculated charge in coulombs necessary to achieve the combined concentrations of these species is shown in figure 3-12. It is apparent that the charge measured by integrating the current density as a function of time (figure 3-10) is more than three times that calculated based on the concentrations of the metal cations and oxyanions. In addition, the concentration of Ni<sup>2+</sup>, after an initial increase, actually decreases with time. These discrepancies indicate that removal of corrosion products from the solution is occurring throughout the test. Examination of the cell after the conclusion of the test revealed the deposition of a Ni-rich precipitate on the Pt counter electrode and a deposit layer rich in Mo, W, Cr, and Fe on the Alloy 22 specimen. Although the chemical composition of the deposits, determined using scanning electron microscopy with energy dispersive spectroscopy analyses, are shown in table 3-2, quantitative analyses of these deposits were not yet performed.

The geometry of the test specimen was changed to increase the surface area to solution volume ratio. The larger specimen had a surface area of 72 cm<sup>2</sup> and was tested under passive conditions at a potential of 0 mV<sub>SCE</sub> in 0.028 M Cl<sup>-</sup> at 95 °C. In spite of the increased surface area, no cations or oxyanions expected to occur as a result of the passive dissolution of Alloy 22 were observed after 660 h of testing where a total



**Figure 3-9. Anodic current density and total charge as a function of time measured on Alloy 22 at 100 mV<sub>SCE</sub> in 0.028 M chloride solution at 95 °C**

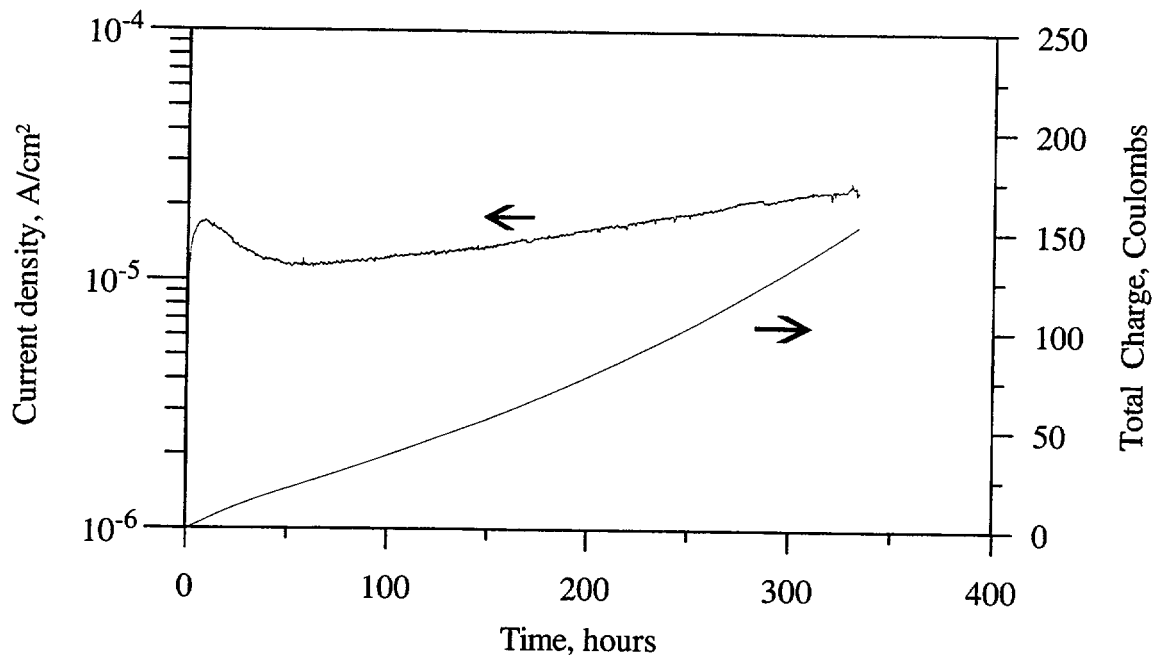


Figure 3-10. Anodic current density and total charge as a function of time measured on Alloy 22 at 500 mV<sub>SCE</sub> in 0.028 M chloride solution at 95 °C

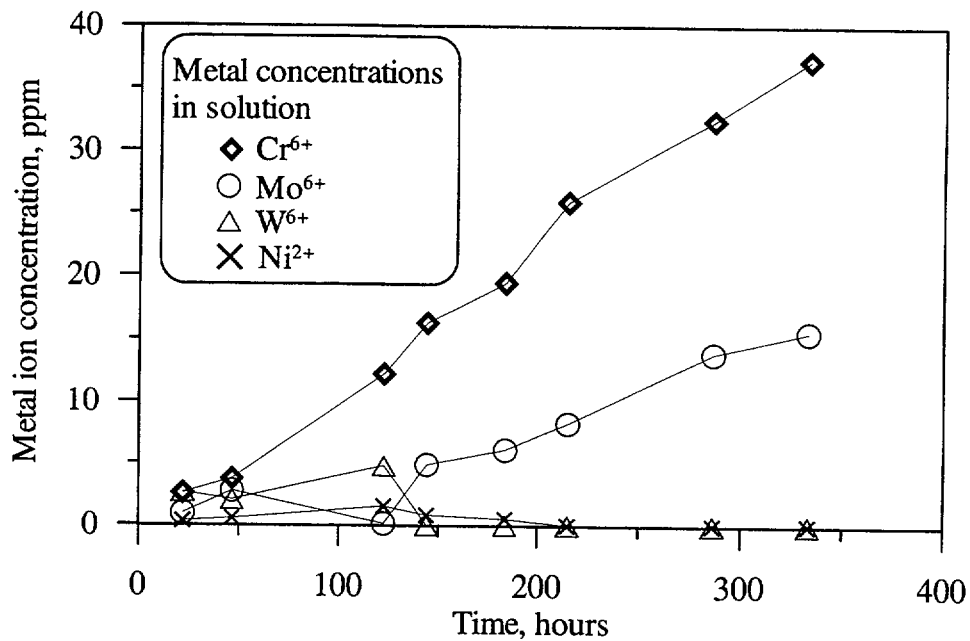


Figure 3-11. Metal ion concentrations measured using capillary electrophoresis from the anodic dissolution of Alloy 22 at 500 mV<sub>SCE</sub> in 0.028 M chloride at 95 °C

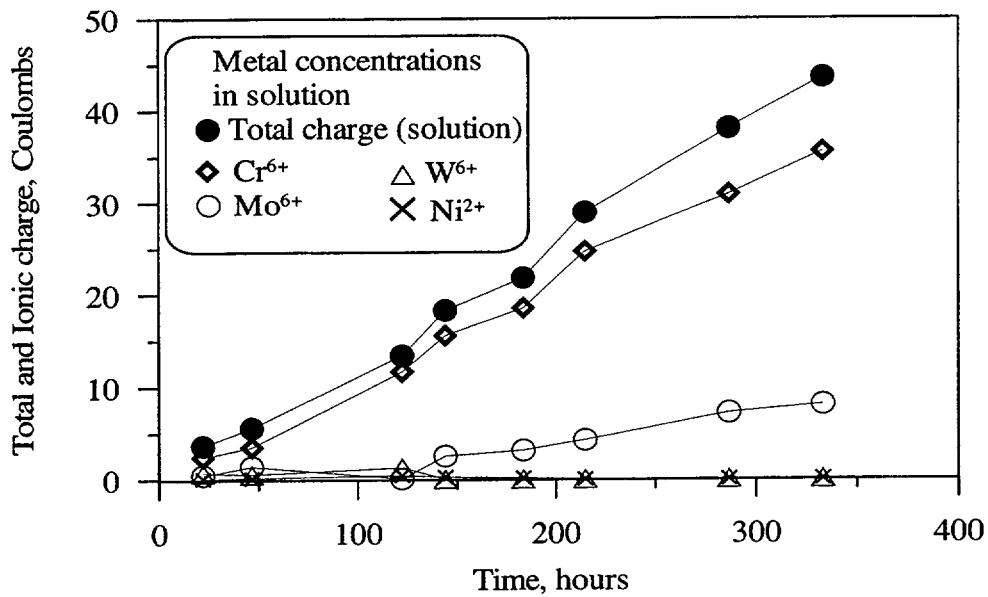


Figure 3-12. Charge in coulombs for metal ions calculated from the measured solution concentrations. Total charge is the sum of the charge based on solution concentrations.

Table 3-2. Chemical analyses of test solutions and corrosion products

Element	Base Alloy Weight Percent	Deposit on Specimen, Weight Percent	Deposit on Pt Electrode, Weight Percent	In solution, Weight Percent
Ni	56.0	6.7	55.0	—
Cr	21.4	22.8	3.9	69.9
Mo	13.6	7.0	4.7	29.1
Fe	3.8	21.3	—	—
W	3.0	18.7	—	—
O	—	21.4	24.3	—

charge of 1.82 coulombs ( $2.53 \times 10^{-2} \text{ C/cm}^2$ ) was recorded corresponding to a total metal concentration of 2,230 ppb if no precipitation or redeposition of the cations and oxyanions occurred.

The passive dissolution rate of Ni-Cr-Mo-Fe alloys can be determined by several methods. It is conceptually possible to measure the passive dissolution rate by monitoring the weight loss of a specimen exposed to a representative environment. Practically, such measurements are difficult and subject to large measurement errors in relatively short-term tests. Growth of the oxide film may result in a net weight gain that could falsely indicate low corrosion rates or even negative values. The deposition of dissolved species can also cause artificially low corrosion rates. Measurement of metal ion concentrations in the electrolyte solutions after exposure can be used to calculate the passive corrosion rates (Kirchheim et al., 1989) with a resolution of  $2 \times 10^{-8} \text{ A/cm}^2$ . Passive dissolution rates can also be obtained using electrochemical methods with a greater resolution of  $1.25 \times 10^{-10} \text{ A/cm}^2$ . Potentiostatic polarization yields steady-state corrosion rates but requires instrumentation with adequate resolution. There are also several disadvantages to the technique, including the need to deaerate the system thoroughly to avoid interference with the oxygen reduction reaction that may reduce the measured anodic current to values lower than the true dissolution current under passive conditions. The application of a potential may also alter the composition and thickness of the oxide layer.

The potentiostatic test results from this study with specimens that did not have creviced surfaces have indicated the passive dissolution of Alloy 22 is low and similar to those reported for Fe-Cr alloys (Kirchheim et al., 1989). A strong temperature effect was also observed in dilute chloride solutions. The passive corrosion rate in 0.028 M chloride at 95 °C was 10 times higher than that measured at 20 °C. At present, it is unclear if this apparent temperature effect in the 0.028 M chloride solution is a result of a higher passive dissolution rate at the elevated temperature or an artifact of the higher oxygen solubility at the lower temperature. The low passive corrosion rates ( $<0.001 \text{ mm/yr}$ ) measured here suggest that if localized corrosion is not initiated and the corrosion potential ( $E_{\text{corr}}$ ) of the waste package is less than 400 mV<sub>SCE</sub>, the lifetime of the 20-mm thick Alloy 22 containers may be extended to over 20,000 yr. Improved modeling and mechanistic understanding of passive dissolution are necessary to evaluate the validity of these long-term predictions. At higher potentials where transpassive dissolutions were observed, failure may occur in a few thousand years. Transpassive dissolution at high potentials, rather than the initiation of localized corrosion, suggests that Alloy 22 is resistant to pitting corrosion in NaCl solutions. However, these very high potentials seem to be difficult to attain even under the most severe oxidizing conditions.

In a recent DOE report (Civilian Radioactive Waste Management System Management and Operating Contractor, 2001b), it is suggested that the activation energy for passive dissolution of Alloy 22 is in the range of 32 to 36 kJ/mole. The corrosion rate data obtained from the Long Term Corrosion Test Facility, which is assumed to be valid for 60 °C, was combined with an activation energy dependence calculated using alternative data sets to arrive at a temperature dependent passive dissolution rate for Alloy 22. The main effect the activation energy calculation performed by DOE, is that the corrosion rate is reduced at lower temperatures. Because lower temperatures are expected as the heat generated by the radioactive waste decays, the reduced corrosion rate at lower temperatures may increase the lifetime of the waste packages. It should be noted however, that the different data sets obtained using different test methods and solutions were used to determine the corrosion rate and the temperature dependence of the corrosion rate. The DOE data obtained from specimens exposed in the Long-Term Corrosion Test Facility did not show that the corrosion rate was a function of temperature. In addition, the data used by DOE to determine the temperature dependence of the corrosion rate are limited to short term tests and conditions that may not yield accurate measurements of corrosion rates. For example, the activation energy of 36 kJ/mole was calculated

from current density data obtained under potentiodynamic conditions in solutions that were not deaerated. Accurate measurements of passive current density are not possible under these conditions. The data used to calculate an activation energy of 32 kJ/mole was obtained in acidic solutions under potentiostatic conditions with the potential maintained at 350 mV versus a Ag/AgCl reference electrode (or approximately 305 mV<sub>SCE</sub>). The conditions used in these tests may be very near the conditions for the onset of transpassive dissolution, particularly at higher temperatures and result in a larger activation energy. A reliable determination of both the passive dissolution rate and the temperature dependence of the passive corrosion rate should be performed using data obtained under identical experimental conditions.

### 3.2.1.2 Passive Corrosion of Welded Material

Potentiostatic anodic current density was also measured as a function of potential on welded Alloy 22 specimens. These specimens have a significantly larger surface area compared to the cylindrical specimen used for the majority of the passive corrosion tests. Approximately one-fourth of the total exposed specimen surface area (20 cm<sup>2</sup>) was weldment. All corners and edges were rounded prior to testing to prevent preferential attack in these areas. The results of anodic dissolution rate measurements of the welded specimen are shown in figure 3-13. At potentials less than 600 mV<sub>SCE</sub>, the anodic current density for the welded specimens was in the range of 2 × 10<sup>-8</sup> to 4 × 10<sup>-8</sup> A/cm<sup>2</sup> and quite similar to the anodic current density measured for the base alloy. The anodic current density of the welded specimen tested in 4 M chloride adjusted to pH 2.7 is slightly greater than that measured in the alkaline solutions. At 600 mV<sub>SCE</sub>, the anodic current density of specimens tested in solutions adjusted to pH 2.7 and 11.0 increases substantially and, at 800 mV<sub>SCE</sub>, the anodic current density measured in all solutions was greater than 10<sup>-4</sup> A/cm<sup>2</sup>. Posttest examination of the specimen revealed preferential attack in the weld region that exposed the weld microstructure; however, no intergranular corrosion was observed.

### 3.2.1.3 Modeling of Alloy 22 Passive Dissolution

This subsection is to summarize effort on modeling the passive dissolution of Alloy 22. If localized corrosion is not initiated and the corrosion potential of Alloy 22 is lower than 400 mV<sub>SCE</sub>, the lifetime of the

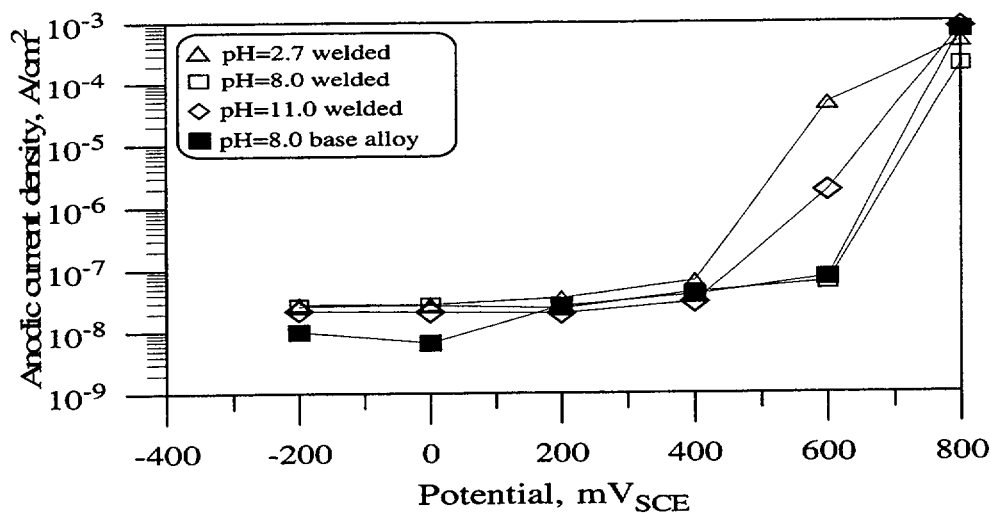
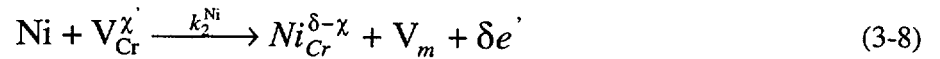
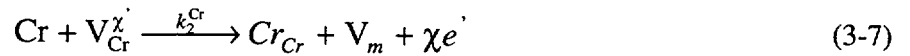
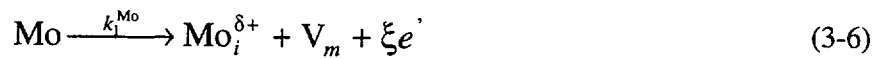
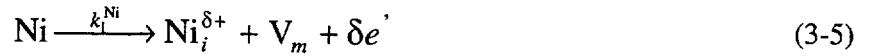


Figure 3-13. Steady-state passive dissolution rate for welded and as-received Alloy 22

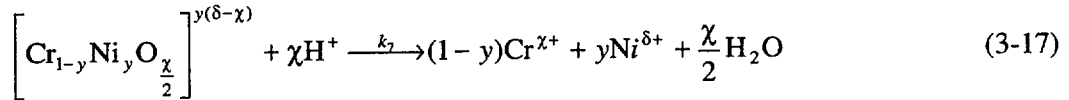
alloy is generally estimated from the potentiostatic measurements of the passive current density and the application of Faraday's law (Dunn et al., 2000c; American Society for Testing and Materials, 1999c). For example, the life of a 2-cm-thick wall of Alloy 22 under steady passive dissolution is estimated to be on the order of tens of thousands of years (Pensado and Mohanty, 2001). This estimate, relevant to the performance of high-level waste containers in the proposed geologic repository at Yucca Mountain, relies on two hypotheses: stoichiometric and homogeneous dissolution. In this paper, "homogeneous dissolution" means dissolution phenomena that does not result in the creation of defects in the bulk of the alloy. These two hypotheses are analyzed with the support of a mechanistic model based on the point defect model (Macdonald, 1992; Zhang and Macdonald, 1998).

The model is intended to describe the passive dissolution of Ni-Cr-Mo alloys. The passive dissolution of Alloy 22 is assumed to be controlled by the formation of a protective Cr<sub>2</sub>O<sub>3</sub>-rich film on the metal surface, based on observations by Boudin et al. (1994) for other Ni-Cr alloys in which the Cr content is greater than 12 wt %. The conduction mechanism through the Cr<sub>2</sub>O<sub>3</sub> film is assumed to be mainly by interstitial cations or oxygen vacancies or by both carriers. The Cr<sub>2</sub>O<sub>3</sub> film, lacking relevant proportions of Mo, is assumed to contain Cr, Ni, and Mo as interstitial defects, Ni as a substitutional defect, and oxygen and Cr vacancies. The hypothesis that the film does not include Mo in relevant proportions is supported by Auger electron spectroscopy experimental studies on alloys such C4 (a Ni-Cr-Mo alloy) (Lorang et al., 1990) and other alloy types (Lumsden and Staehle, 1976). It is possible that Mo exists as a substitutional defect in the film. Because the contribution of Mo to the passive current density in Alloy 22 is small compared to the contributions of Ni and Cr and because of the negligible content of Mo in the oxide, the conduction mode through the film assumed for Mo is not significant with respect to model computations of passive dissolution.

At the metal/film interface, it is postulated that the following reactions describe the dissolution process:



At the film/solution interface, the reactions envisioned to occur are



The symbols  $\chi$ ,  $\delta$ , and  $\xi$  denote oxidation states of Cr, Ni, and Mo in the oxide film. Substitutional Ni in the chromium oxide lattice is represented as  $\text{Ni}_{\text{Cr}}^{\delta-\chi}$ . Cr, Ni, and Mo interstitials in the oxide are symbolized as  $\text{Cr}_i^{\chi+}$ ,  $\text{Ni}_i^{\delta+}$ , and  $\text{Mo}_i^{\xi+}$ .  $\text{V}_o^{2*}$  and  $\text{V}_{\text{Cr}}^{\chi'}$  denote oxygen and cation vacancies in the alloy, respectively. Finally,  $\text{V}_m$  represents the metal vacancies in the bulk of the alloy (produced by the injection of a cation from the alloy into the film oxide) and  $e'$ , the electrons released by the charge transfer reactions. The rate constants are symbolized by  $k$  with a subscript and superscript.

The symbol  $y$  represents the fraction of Ni cations at the film/solution interface that is,

$$y = \frac{[\text{Ni}]}{[\text{Ni}] + [\text{Cr}]} \quad (3-18)$$

where the concentrations,  $[X]$ , are computed at the film/solution interface. The implicit assumption is that the incorporation of substitutional Ni into the chromium oxide film does not induce a significant volume change.

By invoking a detailed charge balance at the metal/film interface, an expression for the current density can be derived

$$I \approx F[\chi a_{\text{Cr}}(k_1^{\text{Cr}} + k_3^{\text{Cr}}) + \delta a_{\text{Ni}}(k_1^{\text{Ni}} + k_3^{\text{Ni}}) + \xi a_{\text{Mo}} k_1^{\text{Mo}}] \quad (3-19)$$

The current density,  $I$ , is a linear combination of  $a_{Cr}$ ,  $a_{Ni}$ , and  $a_{Mo}$  (the alloy atomic fractions at the metal/film interface). It can be proved, in the context of the point defect model and invoking steady-state constraints, that the passive current density is independent of the applied potential if and only if the rate of charge transport of cation vacancies through the oxide film is negligible with respect to the rate of interstitial and oxygen vacancy transport through the oxide, a result already accounted for in Eq. (3-19). Equation (3-19) is consistent with experimental results, indicating that the passive current density for Alloy 22 is independent of the applied potential, over a wide range (up to the potential for transpassive dissolution) and also independent of environmental conditions such as pH and chloride concentration (Dunn et al., 1999b, 2000c). The passive current density seems dependent on the temperature, but only at low chloride concentrations (Dunn et al., 2000c).

Based on the observation that the passive current density decreases with increasing Cr content in Ni-Cr alloys, it can be concluded that

$$k_1^{Cr} + k_3^{Cr} < k_1^{Ni} + k_3^{Ni} \quad (3-20)$$

Equation (3-20) implies that in the relatively short-term, preferential dissolution of Ni with respect to Cr occurs through the Cr-rich passive film, as reported by Cavanaugh et al. (1983). As a result of constraints in estimated values of rate constants for the elementary reactions associated with the creation of interstitials (Cr, Ni, and Mo) and substitutionals (Cr and Ni) at the metal/film interface, it is concluded that charge transport through the passive film is mainly due to interstitial species. Note that interstitial conduction is associated with the injection of vacancies at the metal-scale interface. This conclusion of vacancy injection is consistent with studies of Ni-Cr alloys of both high and low chromium content (Shida et al., 1981; Stott et al., 1981; Douglass, 1968) and nickel (Hales and Hill, 1972) oxidized in air at high temperatures ( $>1000^\circ\text{C}$ ). The hypothesis of homogeneous dissolution requires additional evaluation given the possible existence of vacancies in the alloy.

Preliminary mass-balance computations on the effect of vacancies in the alloy lifetime have been reported elsewhere.<sup>5,6</sup> In these computations, it has been argued that, for a plate composed of Alloy 22 with one surface exposed to the electrolyte, vacancies accumulate in the bulk of the alloy with negligible change of the plate thickness in time (i.e., the alloy evolves into a porous structure). Setting as a failure criterion the establishment of a maximum porosity, such as 50 percent,<sup>7</sup> results in shorter lifetimes than those predicted with the hypotheses of stoichiometric and homogeneous dissolution. The formation of porous structures is common place in dealloying of binary alloys composed of a reactive element (e.g., Mg, Al, Mn, Zn) and one more noble element (e.g., Ag, Au, Cu, Ni) and polarized at a potential above a critical potential such that the

---

<sup>5</sup>Pensado, O., D.S. Dunn, and G.A. Cragnolino. Modeling of the passive film on nickel-chromium-molybdenum alloys. *Presentation to Symposium on Corrosion of Metals and Alloys*. April 24–28, 2000. San Francisco, CA. 2000.

<sup>6</sup>Cragnolino, G.A., D.S. Dunn, Y.-M. Pan, and O. Pensado. Corrosion processes affecting the performance of Alloy 22 as a high-level radioactive waste container material. *Scientific Basis for Nuclear Waste Management XXIV, Sydney, Australia, August 27–31, 2000*. Warrendale, PA: Materials Research Society. 2000. In Press.

<sup>7</sup>Other authors have followed a similar approach to define material failure setting 50 percent as an arbitrary threshold value. For example, Raj and Ashby (1975), in their diffusion-controlled cavity growth model, postulate that mechanical failure for a material subject to creep occurs when the grain boundaries contain 50-percent vacancies.

reactive component actively dissolves, but not the noble component (Min and Li, 1994; Sieradzky et al., 1989). Also, injection of vacancies at the metal-scale interface and subsequent condensation of vacancies has been proposed as the mechanism for void formation in Ni-Cr alloys (Shida et al., 1981; Douglass, 1968) and in nickel (Hales and Hill, 1972) oxidized in air at high temperatures. Other authors have also suggested that dissolution via the injection of vacancies results in volume preservation of a metal subject to oxidation, unless vacancies annihilate at vacancy sinks such as dislocations or grain boundaries (Hales and Hill, 1972). Nonetheless, it is difficult to defend the notion of the evolution of Alloy 22 into a porous structure at repository service conditions given the extremely low vacancy diffusivities expected at temperatures of the order of 100 °C.

The model presented in Eqs. (3-11) to (3-17), plus the predominant interstitial conduction through the oxide film is consistent with other studies (Shida et al., 1981) suggesting that injection of vacancies into the alloy and condensation of these vacancies lead to the formation of voids at grain inclusions, grain boundaries, and at the alloy-scale interface, at least in experiments performed at high temperatures (>1,000 °C). At lower temperatures (<100 °C) computations accounting for finite vacancy diffusivities indicate that vacancies tend to accumulate at the metal/film interface. This accumulation could potentially lead to film spalling, similar to the mechanism proposed by Macdonald (1992) for the onset of localized corrosion. In Macdonald's model, cation vacancies accumulate at the metal/film interface, causing the oxide film to detach from the metal. Studies in other systems (e.g. iron) also support the notion that loss of scale adhesion can be caused by vacancy condensation at the metal-film interface (Dunnington et al., 1952; Tylecote and Mitchell, 1960). It is acknowledged, however, that dislocations in the metal, high angle grain boundaries, pre-existing voids, and suitable regions at the metal-scale interface could perform as vacancy sinks (Shida et al. 1981; Evans, 1988). Evans (1988) has qualitatively outlined the conditions under which vacancy condensation is not expected to occur by comparing the number of vacancies to the number of sinks in the system.

The following heuristic model is proposed to account for film spalling using the bounding case in which the existence of sinks in the system is disregarded. A finite difference approach using a procedure in Mathematica is implemented to track vacancy transport, which requires partitioning of the alloy plate thickness into  $N$  subdivisions as indicated in figure 3-14. A vacancy concentration fraction,  $P$ , is defined as

$$P = \frac{c_v}{c_{Ni} + c_{Cr} + c_{Mo} + c_v} \quad (3-21)$$

where  $c_j$  are concentrations (mol/cm<sup>3</sup>) computed in the first cell in figure 3-14 (i.e., between  $x_0$  and  $x_1$ ), and the subscripts  $v$ , Ni, Cr, and Mo represent vacancies, nickel, chromium, and molybdenum, respectively. After  $P$  exceeds a critical value,  $P_{max}$ , film spalling is assumed to occur, probably followed by active dissolution of the alloy. In the heuristic model, when  $P$  exceeds  $P_{max}$  the metal/film interface is advanced to the position  $x_1$ . The time at which the thickness of the alloy slab is zero is defined as the failure time of the alloy.

In the transport model, vacancy diffusion is coupled to the diffusion of the solid-state components. Displacement of an atom into a vacancy is accompanied by a virtual displacement of the vacancy to the site previously occupied by the atom. The vacancy mechanism is well established as the dominant mechanism of diffusion in alloys (Shewmon, 1963). The effective diffusion coefficient for vacancies may be several orders

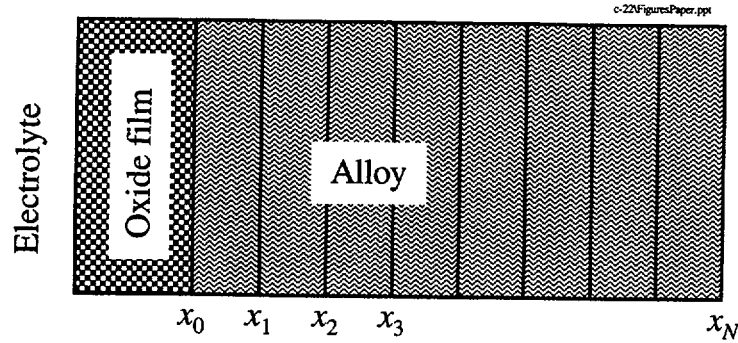


**Figure 3-14.** After the fraction of vacancies between  $x_0$  and  $x_1$  exceeds a maximum threshold value,  $P_{\max}$ , the new metal/film interface is defined to be located at  $x_1$ . This process is repeated until the corrosion front penetrates the whole alloy thickness.

of magnitude (perhaps up to 10) faster than the diffusion coefficient of the solid-state components. At the temperatures of interest ( $\sim 100^\circ\text{C}$ ), the diffusion coefficient of the solid-state components is very small. For example, extrapolating to  $100^\circ\text{C}$ , the expressions for diffusion of Cr in Fe-Ni-Cr alloys by Chen et al. (1989) result in diffusion coefficients ranging from  $10^{-42}$  to  $10^{-40}$   $\text{cm}^2/\text{s}$ . Cr diffusion coefficients for Ni-Cr-Mo alloys are expected to be a similar order of magnitude. Thus, effective vacancy diffusivities may be of the order of  $10^{-30}$   $\text{cm}^2/\text{s}$  at  $100^\circ\text{C}$ . Detailed computations indicate that with such small diffusivities, vacancies tend to accumulate at the metal/oxide interface.

Results from the estimates of the alloy lifetime are reported in figure 3-15. The initial thickness of the alloy is 2 cm. The lifetime was computed as a function of the critical vacancy concentration fraction,  $P_{\max}$ . An initial passive current density of  $5.4 \times 10^{-8}$   $\text{A}/\text{cm}^2$  was selected as input to the model. Note that the passive current density in Eq. (3-19) depends on the alloy composition at the metal/oxide interface; thus, it decreases as vacancies accumulate at this interface. Lifetimes in figure 3-15 are independent of the selected diffusion coefficients (provided that they are less than  $10^{-20}$   $\text{cm}^2/\text{s}$ ), and of the temporal and spatial steps in the finite difference computations. The heuristic model could be improved by accounting for the penetration extent of the corrosion front after active dissolution. As a first approximation, this is accounted for by the uncertainty in the model parameter  $P_{\max}$ . The heuristic model also does not account for the possible existence of vacancy sinks at the metal/oxide interface and at grain boundaries, as suggested by Evans (1988). Vacancy sinks could delay the establishment of a critical vacancy concentration fraction. In any circumstance, the existence of the vacancies (with or without sinks) may alter the cohesion of the oxide to the alloy.

Equation (3-3) relates the passive current density,  $i_{\text{corr}}$  ( $\text{A}/\text{m}^2$ ), to the corrosion rate,  $CR$  ( $\text{m}/\text{s}$ ), which can also be expressed as

$$CR = \frac{i_o}{F\rho \sum_j \frac{z_j f_j}{W_j}} \quad (3-22)$$

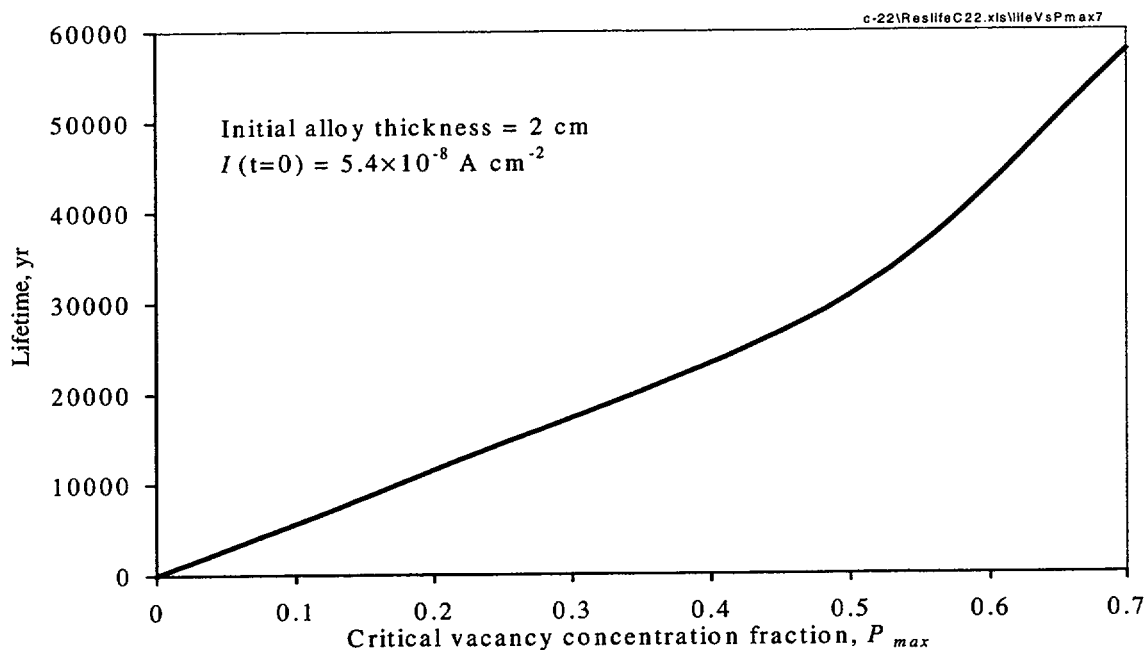


**Figure 3-15. Lifetime of an Alloy 22 plate (with an initial thickness of 2 cm) versus the critical vacancy concentration fraction,  $P_{max}$**

where the index,  $j$ , accounts for the predominant alloy components (Ni, Cr, and Mo for Alloy 22);  $F$  is Faraday's constant ( $9.64867 \times 10^4$  C/mol);  $\rho$ , the alloy density ( $\text{kg/m}^3$ );  $z_j$ , the oxidation state of the ionic species  $j$ ;  $f_j$ , the weight fraction of the alloy component  $j$ ; and  $W_j$ , the weight per gram equivalent of element  $j$  ( $\text{kg/mol}$ ). Substitution of  $\rho = 8,690 \text{ kg/m}^3$  (density of Alloy 22);  $z_{\text{Ni,Cr,Mo}} = 2, 3, 6$ , and the weight fractions for Ni, Cr, and Mo [roughly equal to 0.58, 0.21, and 0.14, respectively (Dunn et al., 1999b)] into Eq. (3-22), results in a corrosion rate of  $5 \times 10^{-4} \text{ mm/yr}$  for a current density of  $5.4 \times 10^{-8} \text{ A/cm}^2$ . Under this slow corrosion rate, an alloy plate 2 cm thick would fail in 40,000 yr. The failure time of 40,000 yr corresponds to  $P_{max} \sim 0.6$  in figure 3-15. Values of  $P_{max}$  less than 0.6 are not unrealistic, implying shorter lifetimes than those predicted with Eq. (3-22). Interestingly, the mean lifetime obtained by uniformly sampling  $P_{max}$  in the range 0–0.99 equals 46,000 yr. CNWRA analyses suggest shorter failure times than those predicted using the simplistic calculation based on Faraday's law are possible. The validity of the model has not been confirmed at this time. Validation will be required to determine if the model provides a realistic assessment of waste package failure times.

It is acknowledged that the ideas presented above require experimental verification. Unfortunately, the slow rate of the dissolution process renders verification experiments quite challenging. Accelerated tests at higher temperatures could be attempted, bearing in mind that thermodynamic and transport processes at higher temperatures are different. Of particular importance is the verification of the formation of vacancies in the bulk of the alloy. These vacancies could lead to the decohesion of the film oxide from the alloy substrate. Incorporation of vacancy sinks into the model will yield extended times to failure. Thus, it is also relevant to establish if vacancies are stable or quickly annihilate at sinks.

One implication of the model is that if the vacancy diffusivity is small (with the consequent accumulation of vacancies at the metal/film interface and negligible vacancy concentration in the bulk of the alloy), then, in the long-term average, alloy dissolution is stoichiometric. In the short term, nonstoichiometric dissolution may be observed such as in studies by Cavanaugh et al. (1983). However, the model indicates that the nonstoichiometric process cannot be steadily maintained as that would require rapid solid-state transport of the preferentially dissolving component. It must be acknowledged that the model does not account for enhanced transport along grain boundaries, or a change in morphology of the dissolving surface (possibly occurring after spalling of the passive film), increasing the reactive surface area. Long-term nonstoichiometric dissolution is feasible with these considerations. If long-term experiments indicate noncongruent dissolution, this factor could be an indication of fast penetrating paths of the corrosion front or a change in the reactive surface area, as homogeneous and uniform dissolution cannot sustain nonstoichiometric dissolution in the long-term.

### 3.2.2 Localized Corrosion

Alloy 22 is susceptible to localized corrosion in the form of crevice corrosion within certain ranges of  $\text{Cl}^-$  concentration and temperature as are other Ni-Cr-Mo alloys such as Alloys 825 and 625 (Dunn et al., 1999a). Repassivation potential measurements were conducted to determine the minimum potential for the initiation and propagation of crevice corrosion (Dunn et al., 2000a). Chemical compositions of the two heats of Alloy 22 used in these measurements, as well as the composition of the Alloy 622 filler rod used for welded specimens, are provided in table 3-1. The geometry and dimensions of the specimens used in the various tests are reported elsewhere (Dunn et al., 1999b). Flat specimens in the as-received mill annealed and as-welded conditions fitted with two PTFE crevice-forming washers. Cyclic potentiodynamic polarization (CPP) tests were conducted in glass cells and in PTFE-lined autoclaves to measure the repassivation potential for crevice corrosion ( $E_{\text{rrev}}$ ) using a potential scan rate of 0.167 mV/s. The welded specimens were machined from 12.7-mm-thick heat 2277-8-3235 plate and welded along the crevice area using the tungsten inert gas procedure with argon as the shielding gas. The weld was performed using a double V-notch as the joint geometry and Alloy 622 (heat XX1045BG11) as the filler rod, using 8 passes per side (16 passes total).

The minimum  $\text{Cl}^-$  concentration and the potential required for crevice corrosion to be initiated at a given temperature (e.g., 95 °C) are both higher for Alloy 22 than for the other alloys (figure 3-16). Recent data for Alloy 22 tested in glass cells in 4.0 M chloride, obtained using a modified test technique that limits the maximum applied potential to avoid transpassive dissolution, are in agreement with data obtained in autoclaves. By avoiding transpassive dissolution, localized corrosion was consistently initiated. In previous tests that allowed the applied potential to reach high values and promote transpassive dissolution (Cragolino et al., 1999), the initiation of localized corrosion in glass cells was not consistently initiated. At lower chloride concentrations, such as 0.5 and 1.0 M chloride, localized corrosion was not consistently initiated in tests conducted in either autoclaves or glass cells. A plot of  $E_{\text{rrev}}$  for the as-received mill annealed Alloy 22 as a function of temperature is shown in figure 3-17. A significant decrease in the  $E_{\text{rrev}}$  values (allowing for a data scattering of  $\pm 100$  mV) can be observed for the three  $\text{Cl}^-$  concentrations with a temperature increase from 80–105 °C, followed by a leveling off at higher temperatures. It should be noted that no crevice corrosion was observed in the 0.5 M  $\text{Cl}^-$  solution at 80 or 95 °C. When the  $E_{\text{rrev}}$  values (using only those that represent a low bound) are replotted as a function of the logarithm of the  $\text{Cl}^-$  concentration (figure 3-18), a linear dependence is satisfied up to 150 °C, according to the following expression

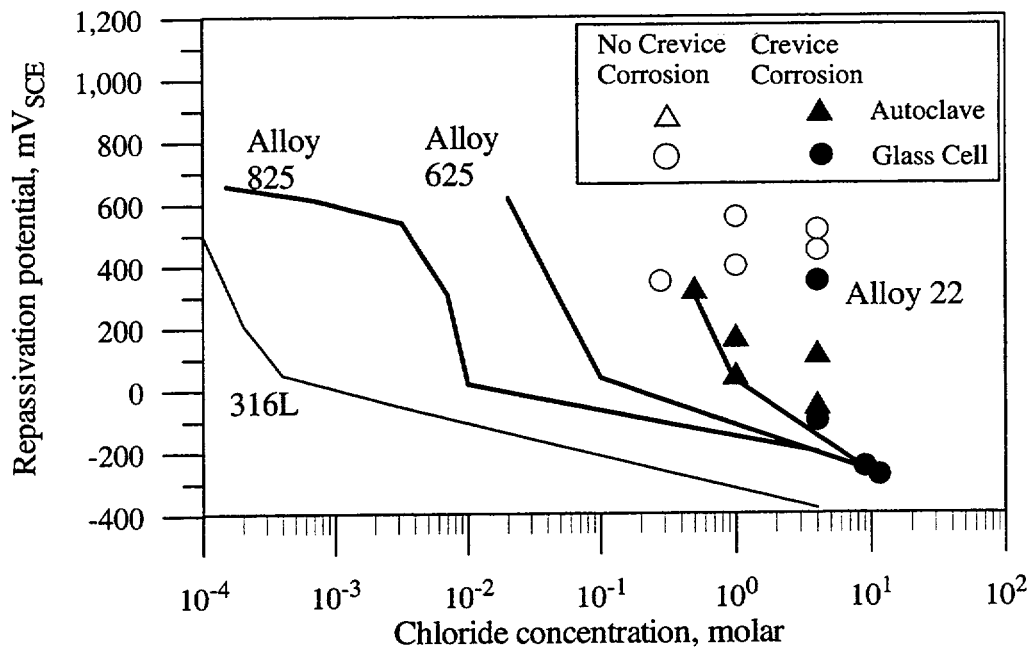


Figure 3-16. Repassivation potentials as a function of chloride at 95 °C for Alloys 825, 625, and 22 as well as Type 316L stainless steel

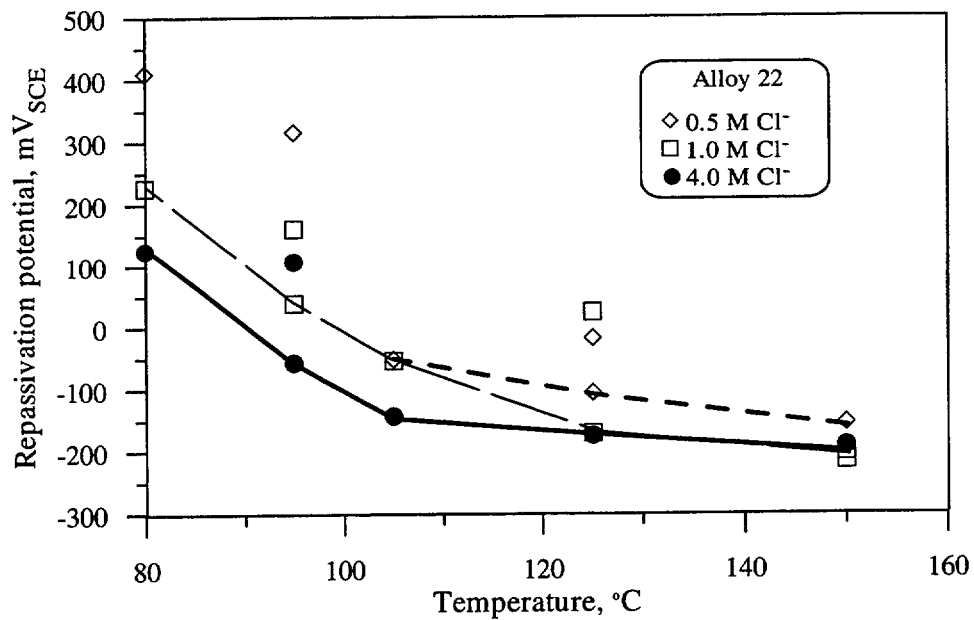
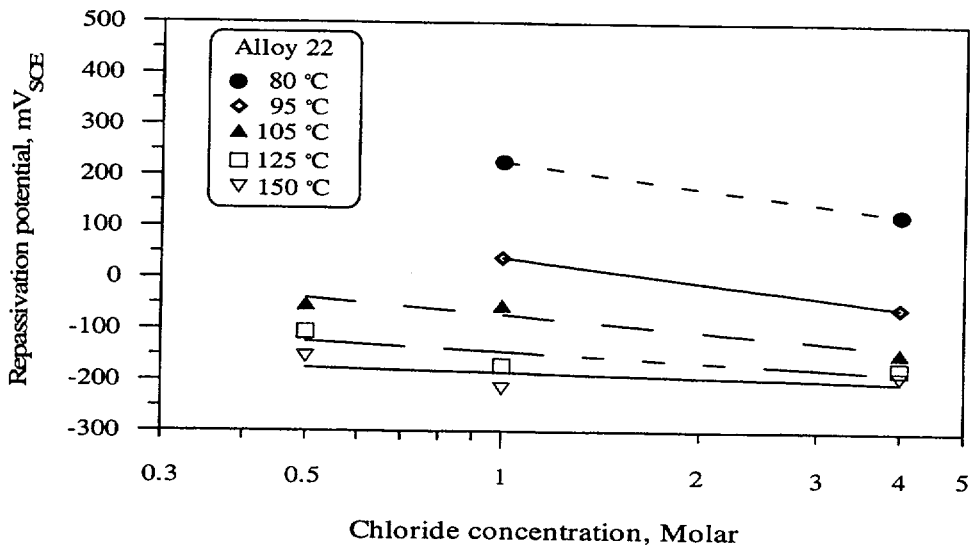


Figure 3-17. Effect of temperature on the repassivation potential for crevice corrosion of Alloy 22 in Cl<sup>-</sup> solutions



**Figure 3-18. Repassivation potential for crevice corrosion of Alloy 22 as a function of Cl<sup>-</sup> concentration at various temperatures**

$$E_{\text{rcrev}} = E_{\text{rcrev}}^0(T) + B(T) \log[\text{Cl}^-] \quad (3-23)$$

where both  $E_{\text{rcrev}}^0$  and  $B$  are parameters that, within the 80 to 105 °C temperature range using the data shown in figure 3-8, can be expressed through a data regression [note that coefficients have been modified with respect to those in Dunn et al. (2000c)] as Eq. (3-24)

$$E_{\text{rcrev}}^0(T) = 1,300 - 13.1T; \quad B(T) = -362.7 + 2.3T \quad (3-24)$$

where  $T$  is the temperature in °C and  $E_{\text{rcrev}}$  is in mV<sub>SCE</sub>. It is apparent from Eq. (3-24) that  $E_{\text{rcrev}}$  is strongly dependent on temperature around the boiling point of water at atmospheric pressure and the dependence on Cl<sup>-</sup> concentration decreases with increasing temperature.

The  $E_{\text{rcrev}}$  for welded specimens was measured using the same test methods described for the as-received mill annealed alloy. A comparison of the  $E_{\text{rcrev}}$  for the welded material to the as-received millannealed alloy, shown in figure 3-19, suggests that the effect of welding on  $E_{\text{rcrev}}$  appears to be negligible at both 95 and 125 °C.

### 3.2.2.1 Effect of Thermal Aging on Localized Corrosion

The effect of thermal aging on the  $E_{\text{rcrev}}$  was determined using Alloy 22 heat 2277-8-3175 (table 3-2) using chloride concentrations ranging from 0.5 to 4.0 M. All tests were conducted in glass cells with the solution temperature maintained at 95 °C. Specimens were thermally aged at 870 °C for times ranging from 5 min to 240 h. Note that aging time represents the time the specimens were exposed in the furnace at 870 °C rather than the time at temperature. This distinction is particularly important for aging times less than 30 min because the time for the specimens to reach temperature after placement in the furnace is close to 3 min.

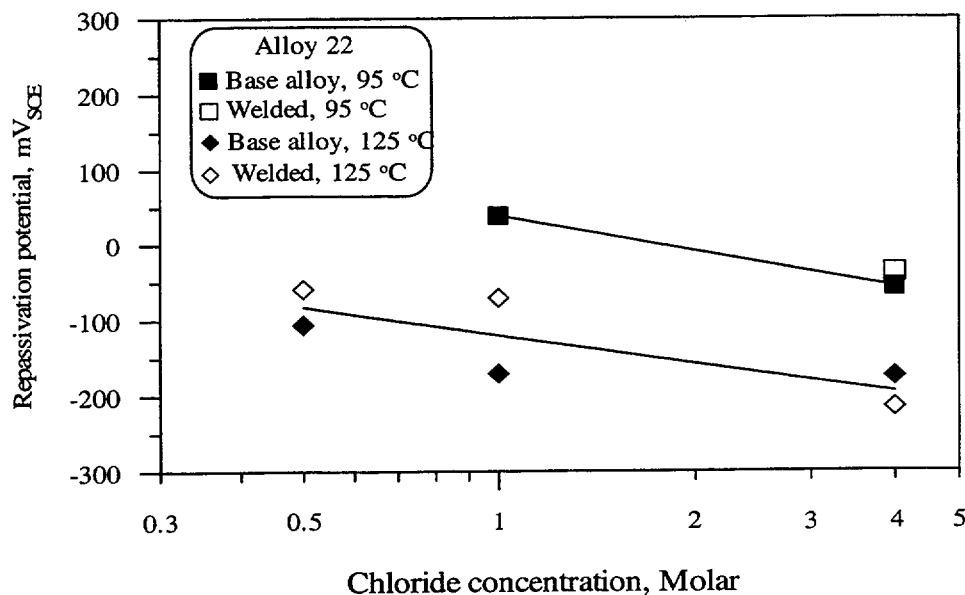


**Figure 3-19. Repassivation potential for crevice corrosion of base metal and welded Alloy 22 in Cl<sup>-</sup> solutions**

Figure 3-20 shows the comparison of  $E_{\text{rcrev}}$  values for the as-received mill annealed Alloy 22 (zero thermal aging time) to the as-welded and to thermally aged specimens. The  $E_{\text{rcrev}}$  for the base alloy in the 4.0 M chloride solution was measured to be  $-98 \text{ mV}_{\text{SCE}}$ , whereas  $E_{\text{rcrev}}$  values ranging from  $-230$  to  $-260 \text{ mV}_{\text{SCE}}$  were measured on specimens thermally aged for 5 to 30 min. Examination of the specimens revealed intergranular corrosion in the crevice regions. As the aging time increased, the number of intergranular corrosion sites and the severity of attack increased. From the results shown in figure 3-20, it is apparent the  $E_{\text{rcrev}}$  is significantly reduced by thermal aging; however, beyond 5 min aging at  $870 \text{ }^{\circ}\text{C}$ ,  $E_{\text{rcrev}}$  does not appear to be a function of aging time. Previous results (Dunn et al., 2000d) for specimens aged at  $870 \text{ }^{\circ}\text{C}$  showed that Alloy 22 specimens exhibited a significant decrease of  $E_{\text{rcrev}}$  measured in 4.0 M NaCl solution at  $95 \text{ }^{\circ}\text{C}$ , as a result of a thermal treatment for 30 min. No further decrease of  $E_{\text{rcrev}}$  was observed when the heat treatment time was increased to 24 h but the effect of thermal aging for times less than 30 min was not studied.

### 3.2.3 Center for Nuclear Waste Regulatory Analyses Approach to Performance Prediction

The performance of the Alloy 22 waste package outer barrier is evaluated considering the passive corrosion rate, the susceptibility of the alloy to localized corrosion, and the localized corrosion propagation rate. Passive corrosion of the Alloy 22 outer barrier occurs when  $E_{\text{corr}}$  is less than  $E_{\text{rcrev}}$ . The passive corrosion rate is considered to be independent of both temperature and chloride concentration. Two passive corrosion rates have been used in performance simulations conducted with TPA code Version 3.2 on the basis of preliminary experimental work on Alloy 22. With the low passive current density value of  $6 \times 10^{-8} \text{ A/cm}^2$ , the corresponding Alloy 22 corrosion rate is  $6 \times 10^{-4} \text{ mm/yr}$ , whereas high passive current density of  $2 \times 10^{-7} \text{ A/cm}^2$  results in passive corrosion rate of  $2 \times 10^{-3} \text{ mm/yr}$ . Without localized corrosion, the failure time for a

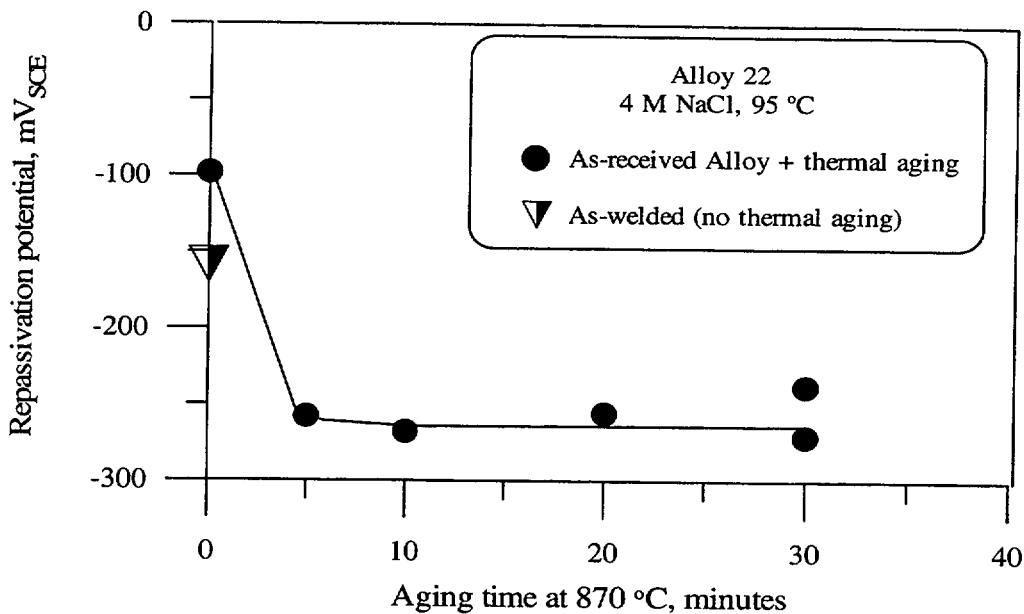


**Figure 3-20. Effect of thermal aging at 870 °C on the repassivation potential of Alloy 22**

20-mm-thick Alloy 22 waste package outer barrier is approximately 34,000 yr with the low passive dissolution rate and 10,000 yr with the high passive dissolution rate.

The conditions for localized corrosion initiation are defined by a comparison of  $E_{\text{corr}}$  with  $E_{\text{rcrev}}$ . Values of  $E_{\text{corr}}$  are calculated as the potential at which the passive corrosion rate of the alloy (anodic reaction) is equal to the rate of oxygen and water reductions (cathodic reaction). Values of  $E_{\text{rcrev}}$  are determined from laboratory tests and expressed as an equation, such as Eq. (3-23) in which  $E_{\text{rcrev}}$  is dependent on temperature and chloride concentration. Both temperature and chloride concentration are independently calculated in the TPA code. For conditions in which the  $E_{\text{corr}}$  is greater than the  $E_{\text{rcrev}}$ , localized corrosion is assumed to occur without an initiation time (i.e., localized corrosion is instantly initiated). The localized corrosion propagation rate is assumed to be  $2 \times 10^{-4}$  m/yr (0.2 mm/yr). The penetration rate of localized corrosion is based on a low active dissolution current density of  $2 \times 10^{-5}$  A/cm<sup>2</sup>. The propagation rate used in the TPA code has been shown (Cragolino et al., 1999) to be close to the slowest localized corrosion propagation rates measured in either laboratory or in-service exposures. If the  $E_{\text{corr}}$  decreases or the  $E_{\text{rcrev}}$  increases such that  $E_{\text{corr}}$  is lower than the  $E_{\text{rcrev}}$ , localized corrosion is considered to repassivate, and the corrosion rate of the Alloy 22 waste package outer barrier is determined by the passive corrosion rate.

The output of the TPA code indicates that localized corrosion is never initiated for the Alloy 22 waste package outer barrier because the value for  $E_{\text{corr}}$  never exceeds the value for  $E_{\text{rcrev}}$ . As a result, the lifetime of the Alloy 22 waste package outer barrier is determined by the passive dissolution rate.

## 4 GENERAL AND LOCALIZED CORROSION OF THE DRIP SHIELD

The safety strategy adopted by the DOE for the proposed HLW repository at Yucca Mountain relies on several key attributes for the unsaturated repository system, one of which is the integrity of the drip shield to divert incoming water away from the waste packages (Civilian Radioactive Waste Management System Management and Operating Contractor, 2000a). The primary materials considered by DOE for construction of the drip shield are Pd-bearing Ti alloys, such as Ti Grade 7<sup>1</sup> (UNS R52400) and Ti Grade 16<sup>2</sup> (no UNS designation). Ti-Pd alloys are  $\alpha$  Ti alloys that have similar mechanical properties to commercial purity Ti, but exhibit considerably better corrosion resistance than commercial purity Ti in many aqueous environments (Schutz, 1995; Donachie, 1988).

Ti alloys are known to exhibit excellent corrosion resistance under many conditions as a result of the spontaneous formation of a protective TiO<sub>2</sub> passive film. Because of this corrosion resistance, Ti alloys have been used in a wide variety of applications ranging from flue gas scrubbers to desalination plants. As a result, the effects of many environmental variables on the corrosion behavior of Ti alloys have been evaluated. In general, the pH of the environment has not been found to strongly influence the corrosion behavior of Ti alloys except in highly acidic media [ $< \text{pH } 1$  (Pourbaix, 1974; Kelly, 1979)]. Studies examining the passive corrosion rate of Ti alloys (Brossia and Cragnolino, 2000, 2001a; Kolman and Scully, 1996) as well as localized corrosion susceptibility (Brossia and Cragnolino, 2000, 2001a; Koizumi and Furuya, 1973) have shown little influence of bulk environment pH. Chloride, as is the case for most engineering alloys that rely on a passive film for improved corrosion resistance, is known to lead to localized corrosion of Ti alloys. Historically speaking, however, Ti alloys usually exhibit crevice corrosion more readily than pitting corrosion (Schutz, 1995) but will still experience pitting corrosion at sufficiently high potentials. Increases in temperature in many cases can result in an overall increase in the observed dissolution rate and are also known to reduce the critical potentials ( $E_{\text{bd}}$  and  $E_{\text{tp}}$ ) for localized corrosion (Posey and Bohlman, 1967). Perhaps the most dramatic effect on the corrosion behavior of Ti alloys is observed in the presence of fluoride. This effect is generally attributed to the observation that fluoride complexes with Ti to form  $\text{TiF}_6^{2-}$  and that this complexant is more thermodynamically stable than the TiO<sub>2</sub> passive film. Kelsall and Robbins (1990) reported the Gibb's free energy ( $\Delta G^\circ$ ) for  $\text{TiF}_6^{2-}$  to be  $-2,118 \text{ kJ/mol}$  in contrast to  $-884.5$  and  $-889.5$  for the anatase and rutile forms of TiO<sub>2</sub>.

Despite some efforts to understand the effects of environmental variables on the corrosion behavior of Ti alloys, little is known concerning the corrosion behavior of Pd-bearing Ti alloys under the conditions that may be encountered in the proposed Yucca Mountain repository. As a consequence, the DOE has undertaken an experimental program to examine the corrosion of these materials with the eventual goal of predicting the long-term performance of a drip shield as part of the overall repository safety case. To aid in evaluating the safety case DOE may put forth in any license application, CNWRA has been engaged in a limited scope experimental effort to also understand the effects of various key environmental variables on the corrosion of Ti-Pd alloys. This chapter discusses the investigations conducted by DOE thus far and reviews recent activities at the CNWRA.

---

<sup>1</sup>Nominal Composition (maximum weight percent): 0.03 N, 0.10 C, 0.015 H, 0.30 Fe, 0.25 O, 0.12–0.25 Pd, bal. Ti.

<sup>2</sup>Nominal Composition (maximum weight percent): 0.03 N, 0.10 C, 0.015 H, 0.30 Fe, 0.25 O, 0.05 Pd, bal. Ti.

## 4.1 U.S. DEPARTMENT OF ENERGY INVESTIGATIONS

Investigations conducted by DOE at Lawrence Livermore National Laboratory (LLNL) have focused on the measurement of corrosion rates and the prediction of localized corrosion. To do this, a series of long-term weight-loss coupon exposures to a variety of environments has been conducted using both noncreviced and creviced specimens. Additionally, some potentiodynamic polarization experiments have also been conducted to determine the open circuit and critical potentials associated with the onset of localized corrosion.

### 4.1.1 Humid-Air Corrosion

Humid-air corrosion is assumed to occur when the RH is greater than the  $RH_{critical}$  (Civilian Radioactive Waste Management System Management and Operating Contractor, 2000m). The  $RH_{critical}$  is based on the deliquescence point (lowest RH at which a saturated solution of the salt can be maintained at a given temperature) for sodium nitrate as discussed in chapters 2 and 3. The DOE model of corrosion of the Ti assumes that the corrosion rate and the distribution of corrosion rates under these conditions are the same as for aqueous corrosion and are independent of time (Civilian Radioactive Waste Management System Management and Operating Contractor, 2000m).

Humid-air corrosion rates were measured at LLNL in the long-term corrosion test facility by exposing weight-loss coupons to the vapor-phase region in the test vessels used for aqueous corrosion testing. The test environments evaluated include simulated acidified water, simulated dilute water, and simulated concentrated water (as defined in chapters 2 and 3) at both 60 and 90 °C (McCright, 1998). The reported vapor-phase corrosion rates after 6 mo exposure were as high as 7.43  $\mu\text{m}/\text{yr}$  in simulated dilute water at 90 °C for Ti Grade 16. This high corrosion rate was later discounted as being an artifact of the post-test cleaning procedure. In contrast, the 1-yr exposure data (where available) show much lower effective corrosion rates (e.g., 4.43  $\mu\text{m}/\text{yr}$  at 6 mo compared to -0.04  $\mu\text{m}/\text{yr}$  after 1 yr in simulated acidified water at 90 °C). It was explained that the 1-yr data were more reliable as the posttest cleaning procedure was modified to correctly clean the specimens without causing excessive damage. Comparison of the 1-yr vapor phase exposures to fully immersed aqueous exposure showed similar results. Interestingly, examination of the 6-mo exposure data consistently showed increased corrosion rates for the vapor phase compared to the fully immersed specimens. No explanation for this observation was given.

### 4.1.2 Aqueous General/Passive Corrosion

Similar to the humid air corrosion rates, the majority of the general passive corrosion rates used by the DOE were measured using weight-loss coupons of Ti Grade 16 exposed at the long-term corrosion test facility. Corrosion rates of specimens exposed in the long-term corrosion test facility were calculated by measuring the weight loss of the specimens after exposures of 6 mo and 1-yr to simulated dilute water, simulated concentrated water, and simulated acidified water, at 60 and 90 °C. The corrosion rates for Ti Grade 16 calculated by weight loss were not observed to be strongly dependent on the temperature or composition of the test solution. Hence, the weight loss data were considered as belonging to the same statistical distribution of corrosion rates.

For specimens that were not fitted with crevice forming washers, the penetration rate, calculated using weight-loss measurements, ranged from ~ -1,700 to 150 nm/yr after 1-yr exposure to the long-term

corrosion test facility simulated waters. The distribution of these corrosion rates is shown in figure 4-1. Creviced specimens, in contrast, had a much tighter distribution and a higher observed maximum corrosion rate, ranging from ~ -350 to 320 nm/yr after 1-yr exposure. Weight gain was observed on nearly half of the Ti Grade 16 weight-loss specimens as a result of the deposition of silicate (assumed to be amorphous SiO<sub>2</sub>) on the surface of the specimens. As a result of uncertainties regarding the SiO<sub>2</sub> and appropriate correction factors to compensate for its presence and removal, data from specimens with weight gains were not used to determine the composite corrosion rate distribution.

When all exposure times and exposure conditions are considered and the negative corrosion rates that were calculated were removed, a range of ~ 5 to 320 nm/yr results (figure 4-2). This composite corrosion rate distribution had a 50<sup>th</sup> percentile at 25 nm/yr and a 90<sup>th</sup> percentile at 100 nm/yr. Thus, approximately 10 percent of the calculated corrosion rates fell in the range 100–320 nm/yr.

### 4.1.3 Microbially Influenced Corrosion

Ti alloys historically have been shown to be essentially immune to microbially influenced corrosion. Typically what has been observed in the case of Ti alloys exposed during laboratory and in-service evaluations is the formation of a biofilm on the metal surface (Schutz, 1991; Little et al., 1992, 1993). Schutz (1991) highlighted that this immunity to microbially influenced corrosion stems from the stability of the TiO<sub>2</sub> passive film in environments containing the typical species present from biogenic activity. This includes the production

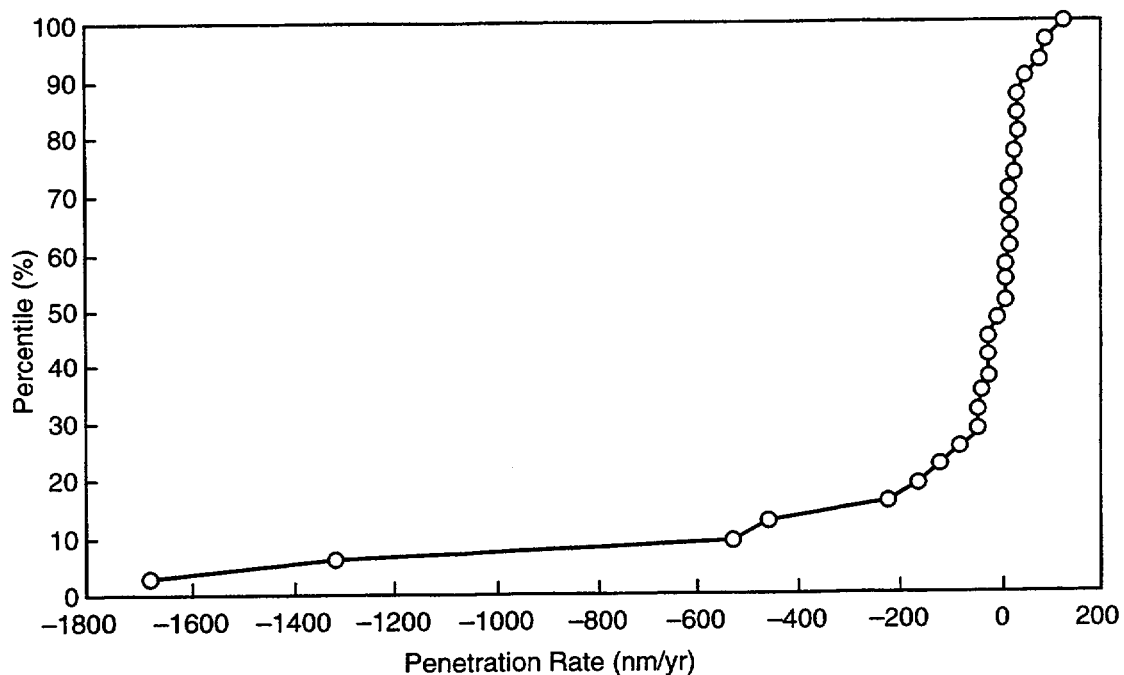


**Figure 4-1. Distribution of corrosion rates calculated by U.S. Department of Energy from weight-loss data generated for Ti Grade 16 after 1-yr exposure at the long-term corrosion test facility (Civilian Radioactive Waste Management System Management and Operating Contractor, 2000m)**

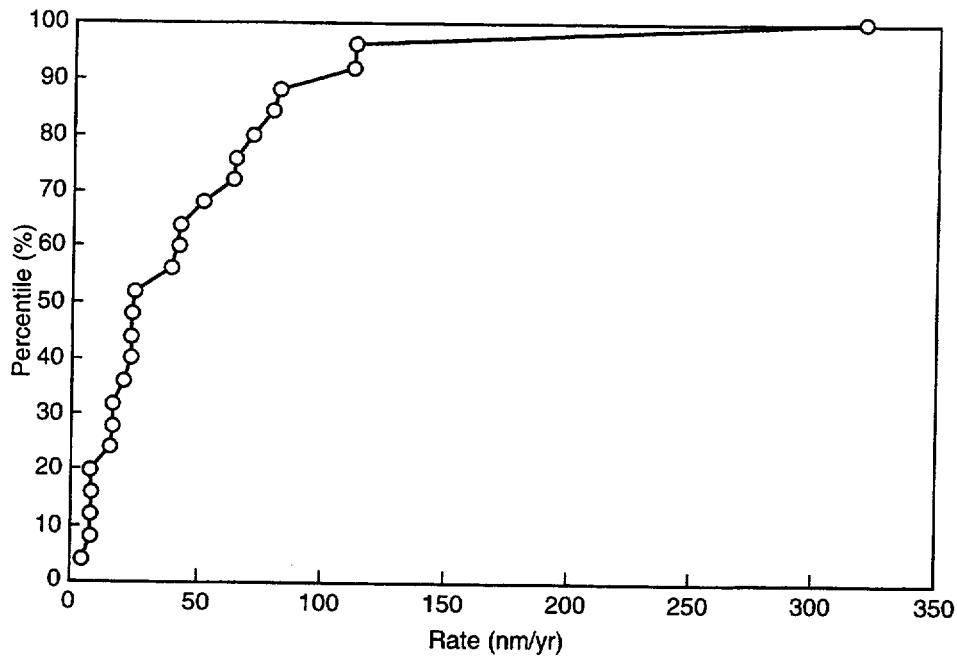


**Figure 4-2. Composite distribution of general corrosion rates for Ti Grade 16 after 1-yr exposure at the long-term corrosion test facility eliminating the negative corrosion rate data (Civilian Radioactive Waste Management System Management and Operating Contractor, 2000m)**

of ammonia, sulfides, hydrogen sulfide, nitrites, ferrous ions, and organo-sulfur compounds that are often produced from anaerobic activity. Production of nitrates, polythionates, thiosulfates, and oxygen from biogenic activity associated with aerobic activity similarly does not significantly increase the corrosion rate of Ti alloys. It has been speculated for transition metals (like Ti) to undergo microbially influenced corrosion, that a partially filled set of d orbitals is necessary to facilitate biogenic redox reactions. For  $Ti^{4+}$  cations, however, there are no d electrons available, and in this configuration, biogenic redox reactions appear to be prevented in natural environments (Brown, 1996).

Recent work conducted by Horn et al. (2001) at LLNL seems to indicate some susceptibility of Ti Grade 7 to microbially influenced corrosion. These workers exposed Ti Grade 7 to *thiobacillus ferrooxidans* (a sulfur-oxidizing bacterium) for 7 mo. They observed an increase in the measured surface roughness for coupons exposed to the bacteria compared to the control samples that were unexposed and those that were only exposed to the sterile thiosulfate-based media. Atomic force microscopy imaging of the specimens revealed this increased RMS roughness to be 361, 409, and 519 nm for the unexposed, sterile media exposed, and bacteria exposed specimens. It was speculated that the differences between this study and the previous works in the literature stem from experiment duration, bacteria nutrient supply, and growth substrates used. It was felt that in the absence of appreciable organic carbon, the bacteria metabolized the thiosulfate present to eventually form atomic sulfur and sulfurous acid. It was speculated that these species could have resulted in increased corrosion of Ti Grade 7. Additional experiments to evaluate this possibility further were discussed by the authors.

#### 4.1.4 Localized Corrosion

DOE evaluated the localized corrosion susceptibility of Ti Grades 7 and 16 using weight-loss coupon exposures (creviced samples) as well as potentiodynamic polarization testing. As discussed previously, creviced weight-loss coupons have been exposed to a variety of J-13 Well water based solutions for considerable time periods. Localized corrosion has not been observed to date at the long-term corrosion test facility using Ti Grade 16 weight-loss coupons, though slightly higher weight-loss calculations were observed for the creviced specimens. It was speculated by DOE that a slightly more aggressive chemistry developed in the occluded region of the crevice, which then led to slightly higher corrosion rates.

A limited set of cyclic potentiodynamic polarization experiments have been conducted to determine the critical potentials for localized corrosion of Ti Grade 7 (Civilian Radioactive Waste Management System Management and Operating Contractor, 2000m). Figure 4-3 shows a CPP curve obtained in simulated saturated water at 120 °C using a (likely) scan rate of 0.167 mV/s. A critical threshold potential was noted ~0.8 V versus Ag/AgCl (0.755 V<sub>SCE</sub>) with subsequent polarization to higher potentials leading to increased currents. Similar results were observed in all solutions tested. Reversal of the potential scan at 2.5 V versus Ag/AgCl (2.455 V<sub>SCE</sub>) did not result in the observance of a positive hysteresis indicating that localized corrosion had taken place. Posttest inspection of the specimen did not reveal the presence of localized corrosion. It was then speculated that the threshold potential observed was associated with the onset of oxygen evolution through the water oxidation reaction. Polarization tests conducted under other conditions (e.g., simulated dilute water, simulated concentrated water, and simulated acidified water at 30, 60, and 90 °C) revealed similar results with no localized corrosion observed during any of the tests.

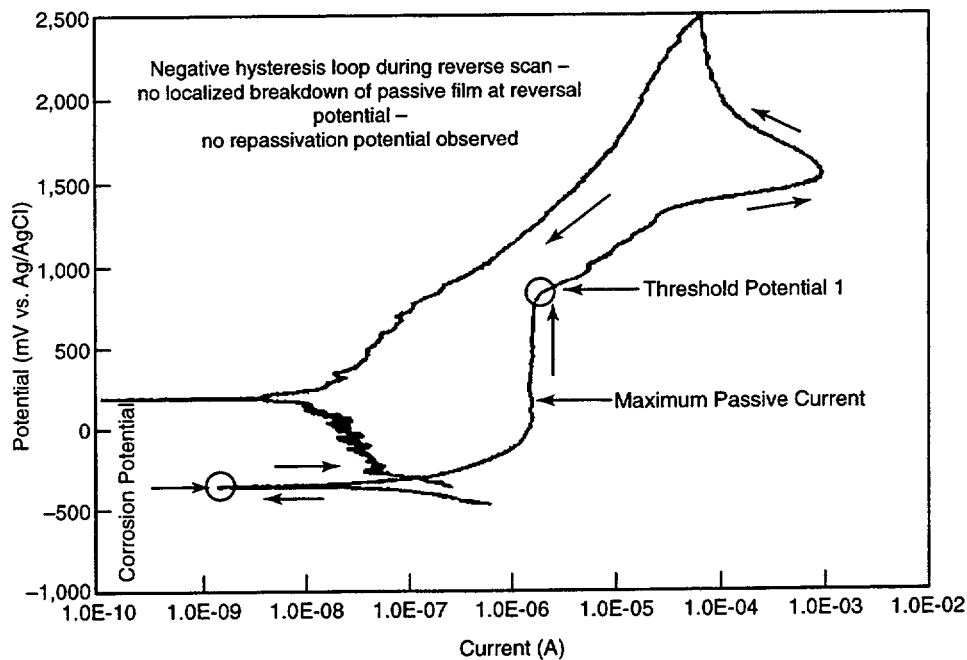


Figure 4-3. Polarization behavior of Ti Grade 7 in simulated concentrated water at 120 °C conducted by the U.S. Department of Energy (Civilian Radioactive Waste Management System Management and Operating Contractor, 2000m)

#### 4.1.5 Evaluation of U.S. Department of Energy Model Abstraction and Predicted Performance

DOE uses the WAPDEG code to predict the performance of the drip shield (Civilian Radioactive Waste Management System Management and Operating Contractor, 2000k). Within WAPDEG, the drip shield is segmented into different patches with the various corrosion model parameters assigned to those patches to model spatial variability in drip shield degradation processes. It has been assumed that 500 patches were sufficient for this modeling purpose (Civilian Radioactive Waste Management System Management and Operating Contractor, 2000i). WAPDEG is an integrated model that incorporates the various degradation processes that may be experienced by the drip shield (e.g., general corrosion, localized corrosion, and hydrogen-induced cracking). In the present report, only the general corrosion and localized corrosion abstracted models will be discussed.

Using the deliquescence point of  $\text{NaNO}_3$  salt as the  $\text{RH}_{\text{crit}}$  for the onset of humid-air corrosion, it has been predicted that the drip shield will undergo general corrosion and will eventually fail because of gradual material loss. The current model assumes that the humid-air corrosion rate is the same as the general aqueous corrosion rate regardless whether water is dripping (Civilian Radioactive Waste Management System Management and Operating Contractor, 2000c). In cases where the drip shield is actively being dripped on, general aqueous corrosion is assumed. The original distribution of corrosion rates used for these corrosion modes that was shown previously in figure 4-2 has been revised to account for possible uncertainties and variabilities as shown in figure 4-4 (Civilian Radioactive Waste Management System Management and Operating Contractor, 2000h). Unlike the case for the waste package outer barrier, no consideration for the possibility of microbially influenced corrosion is given for the drip shield in WAPDEG.

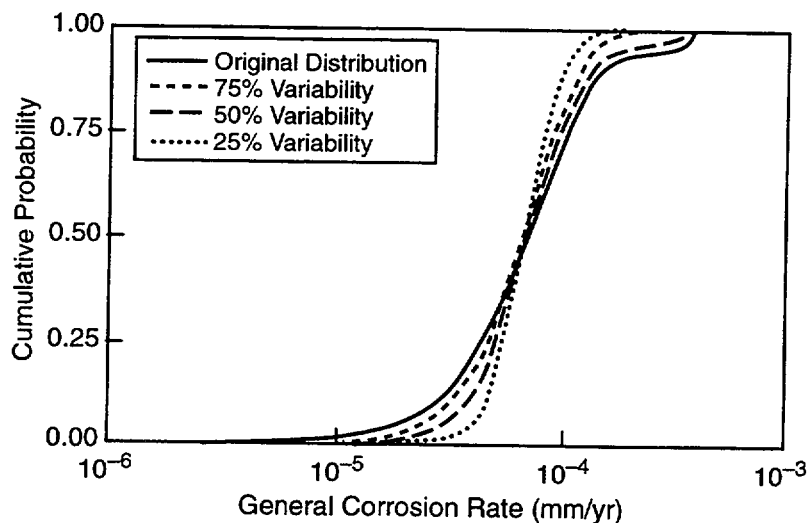
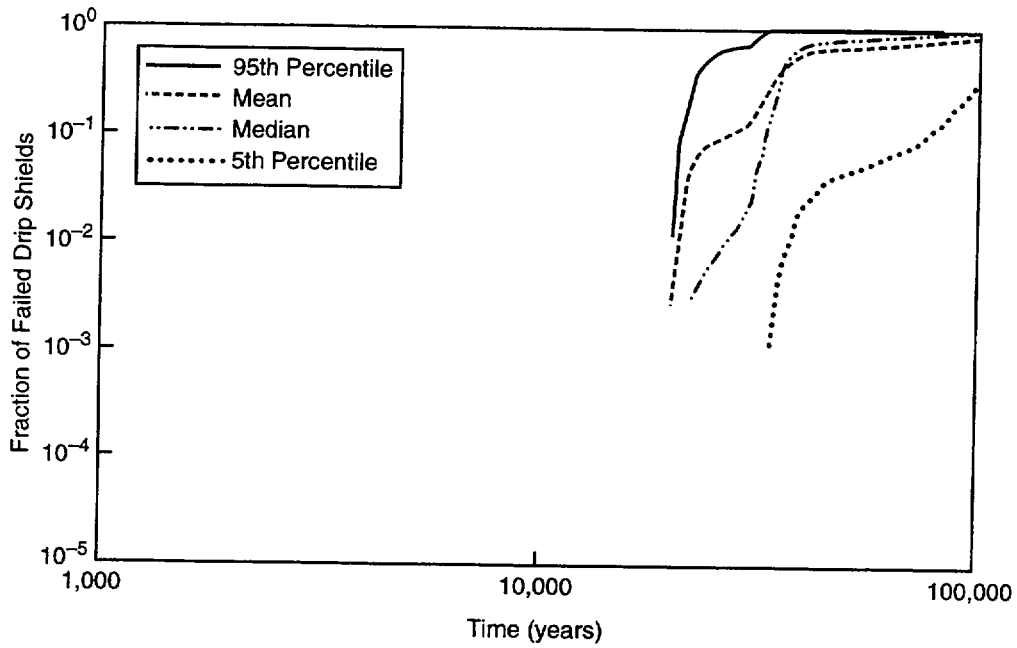


Figure 4-4. Distribution of drip shield corrosion rates illustrating range of values when uncertainties and variability have been included (Civilian Radioactive Waste Management System Management and Operating Contractor, 2000h)

The initiation of localized corrosion of the drip shield is assumed to depend on the local environment on the patches that are experiencing active dripping. This assumption was deemed necessary because the drips provide the only source of the aggressive species (e.g., chloride) required for localized corrosion. Initiation was assumed to occur when the corrosion potential of a given patch exceeded the threshold critical potential for the patch. Localized corrosion will continue as long as this condition is maintained. If the corrosion potential falls below the critical potential or if dripping ceases, localized corrosion of the patch will terminate. Based on the polarization testing conducted at LLNL and the predicted environmental conditions present at the proposed repository, localized corrosion of the drip shield is not predicted to occur (i.e., the corrosion potential is always less than the critical potential). Though this approach has merit, the parameters utilized for the threshold potential are associated with the onset of oxygen evolution on the metal surface and not with a corrosion process (neither localized corrosion nor transpassive dissolution). The use of the potential at which oxygen evolution occurs as the threshold potential for localized corrosion is incorrect and misleading. Furthermore, no long-term potentiostatic tests have been conducted at lower potentials than this to establish if, in fact, localized corrosion of Ti Grade 7 (or Ti Grade 16) does not occur within the range of thermodynamic stability of water. Additionally, no examination of the corrosion behavior of Ti Grade 24 that will be used as the drip shield structural members has been reported. Ti Grade 24, basically Ti Grade 5 (Ti-6Al-4V) with 0.05 Pd added for improved corrosion resistance, is a newly developed material with little to no industrial experience and essentially no published information on its corrosion behavior. If Ti Grade 24 is, for example, more susceptible to localized corrosion than Ti Grade 7, early failure of the structural members of the drip shield may occur. This could then result in an increased probability of drip shield failure caused by rock fall or other mechanical disruption. DOE has agreed to either provide additional data or will provide additional technical bases for the data and assumptions already available in these areas.

Because localized corrosion is not predicted to occur, the only failure mechanism that leads to failure of the drip shield (excluding hydrogen induced cracking) is general corrosion. Using the distribution of corrosion rates shown in figure 4-2, the basecase failure distribution shown in figure 4-5 was generated. For comparison, enhanced drip shield and degraded drip shield simulations are also shown in figure 4-5. The enhanced drip shield represents setting the drip shield corrosion parameters to their 5<sup>th</sup> percentile values, whereas the degraded case represents setting the drip shield corrosion parameters to their 95<sup>th</sup> percentile values. Clearly, it is evident that the predicted drip shield performance is highly sensitive to the nominal parameter values used. Interestingly, though, examination of the predicted mean dose rate for these cases reveals little effect of drip shield performance (figure 4-6). This observation was explained as resulting from the dominance of the waste package performance in restricting the dose (Civilian Radioactive Waste Management System Management and Operating Contractor, 2000f); for any effect of early drip shield failure to be observed in the predicted dose, the waste package would also have to fail. Though this is intuitive (i.e., the waste package has to fail prior to radionuclide release), it seems logical that some change in the waste package failure times should also occur and thereby influence the predicted dose. Based on the DOE analysis, the drip shield is predicted to last well beyond the 10,000-yr regulatory compliance period with the first failures occurring in the 20,000-yr time frame. There is some concern with respect to this prediction, which is centered mainly on the methods utilized to determine the passive corrosion rate using weight-loss methods. With such highly corrosion resistant materials as Ti, the amount of specimen weight lost during exposure to relatively benign solutions is so small that it is difficult to measure and easily complicated by other factors such as silica deposition and variations in cleaning procedures. The DOE has commented on these effects, saying that the measured weight-loss values are near or at the limit of detectability. Because of the limitations inherent in weight-loss measurements for this type of material, other approaches, such as long-term potentiostatic polarization, to measure and monitor the passive current density in a range of environments



**Figure 4-5. Predicted drip shield failure times using WAPDEG for the basecase (mean), and enhanced (5<sup>th</sup> percentile) and degraded (95<sup>th</sup> percentile) drip shield cases (Civilian Radioactive Waste Management System Management and Operating Contractor, 2000h)**

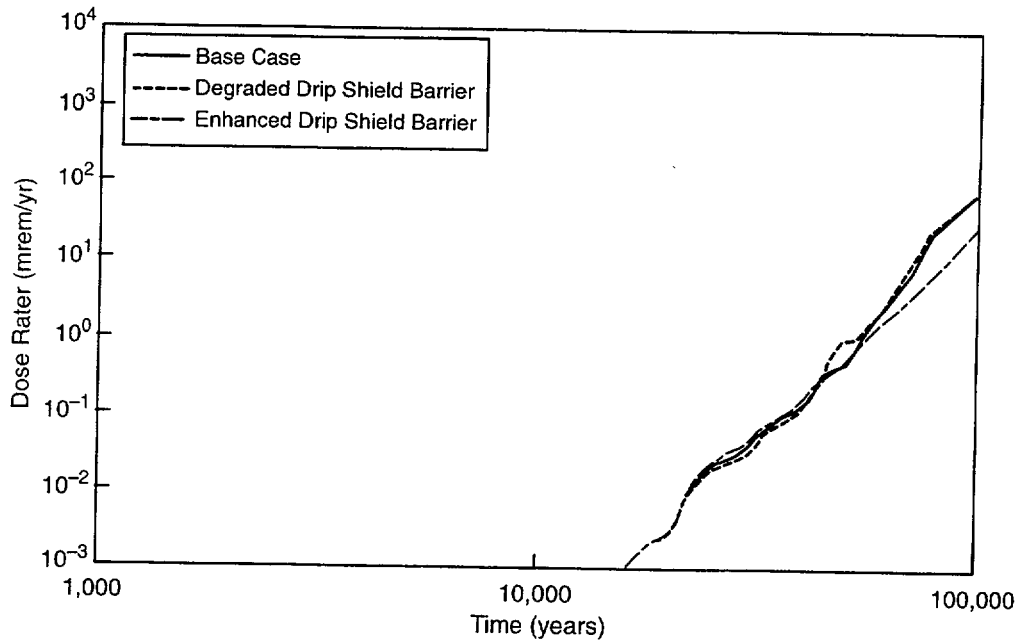


**Figure 4-6. Effect of drip shield case on the predicted dose rate demonstrating little effect of drip shield performance on dose rate consequence (Civilian Radioactive Waste Management System Management and Operating Contractor, 2000h)**

should be conducted. Furthermore, the effects of fluoride and other trace elements (e.g., Pb, Hg) on the corrosion of Ti Grade 7 (and Ti Grade 24) have not been effectively examined in a systematic way to determine if any deleterious results occur.

## 4.2 CENTER FOR NUCLEAR WASTE REGULATORY ANALYSES INVESTIGATIONS

### 4.2.1 Passive and General Corrosion

The general passive corrosion of Ti Grade 7 has been evaluated at the CNWRA using short-term (a few hours) and long-term (several weeks to months) potentiostatic testing. All tests have been conducted using reagent grade sodium salts and acids, deionized (18 M $\Omega$ -cm) water, platinum mesh for counter electrodes, and SCEs for reference electrodes. All tests were conducted under deaerated conditions by purging the solution with N<sub>2</sub> for at least 30 min prior to introduction of the samples and continuous purging throughout the test period. For tests conducted above room temperature but below 100 °C, the specimen was introduced into the test cell only after the test temperature had been reached as well. For tests above 100 °C, a PTFE-lined Type 316L stainless steel autoclave was utilized. In these high-temperature tests, the sample was introduced into the cell, and the solution added and purged with N<sub>2</sub> as the test temperature was approached. After the test temperature had been reached and the temperature was stable, the test was initiated. All samples used were wet polished to 600 grit and ultrasonically cleaned in acetone or methanol prior to testing. The short-term tests revealed that pH, applied potential, and the chloride concentration had little effect on the measured currents (Brossia and Cragolino, 2000, 2001a). Long-term potentiostatic polarization revealed that the initial passive current density was high, but then decreased and eventually reached a steady state after approximately 100 h. Figure 4-7 shows the results from a potentiostatic hold of Ti Grade 7 in deaerated 1 M chloride at 95 °C and an applied potential of 0.0 V<sub>SCE</sub>. After an initial period of relatively rapid dissolution, the current density decreased to nearly constant values approaching current densities below 10<sup>-7</sup> A/cm<sup>2</sup> after 150 h. For comparative purposes, this translates to a corrosion rate of 8.7 × 10<sup>-4</sup> mm/yr or 0.87 μm/yr. Overall, a range of 10<sup>-8</sup> to 4 × 10<sup>-7</sup> A/cm<sup>2</sup> has been observed for steady-state passive current densities of Ti Grade 7 over a pH range of 2.1 to 10.7, a chloride concentration range of 0.1 to 1 M, and an applied potential range of -0.3 to +0.5 V<sub>SCE</sub>. Also shown in figure 4-7 is the range of currents measured during short-term (24-h) tests demonstrating that the steady-state current measured in the long-term test was at least one order of magnitude smaller than the smallest currents measured during short-term testing. This observation highlights the importance of attempting to establish steady-state conditions as closely as possible.

Because little is known about the effect of near-neutral fluoride solutions on the corrosion behavior of Pd-bearing Ti alloys and because fluoride is known to be present in the prevailing groundwater near Yucca Mountain (see chapter 2), a limited study of the effects of fluoride was also undertaken using both potentiodynamic and potentiostatic polarization experiments. The effect of fluoride on the polarization behavior of Ti Grade 7 in 1 M NaCl at 95 °C is shown in figure 4-8. Figure 4-8 shows three polarization curves for noncreviced specimens comparing the anodic behavior observed in 1 M NaCl, 1 M NaF, and 1 M NaF + 1 M NaCl. Ti Grade 7 exhibited a considerably lower open circuit potential in all solutions containing fluoride and a pseudo active/passive transition with a subsequent potential independent current region with current densities considerably higher than those typically encountered during passive dissolution (10<sup>-3</sup> to 10<sup>-1</sup>, as compared to ~ 10<sup>-6</sup> A/cm<sup>2</sup>). It is also interesting to note that in nonacidified fluoride solutions, there existed

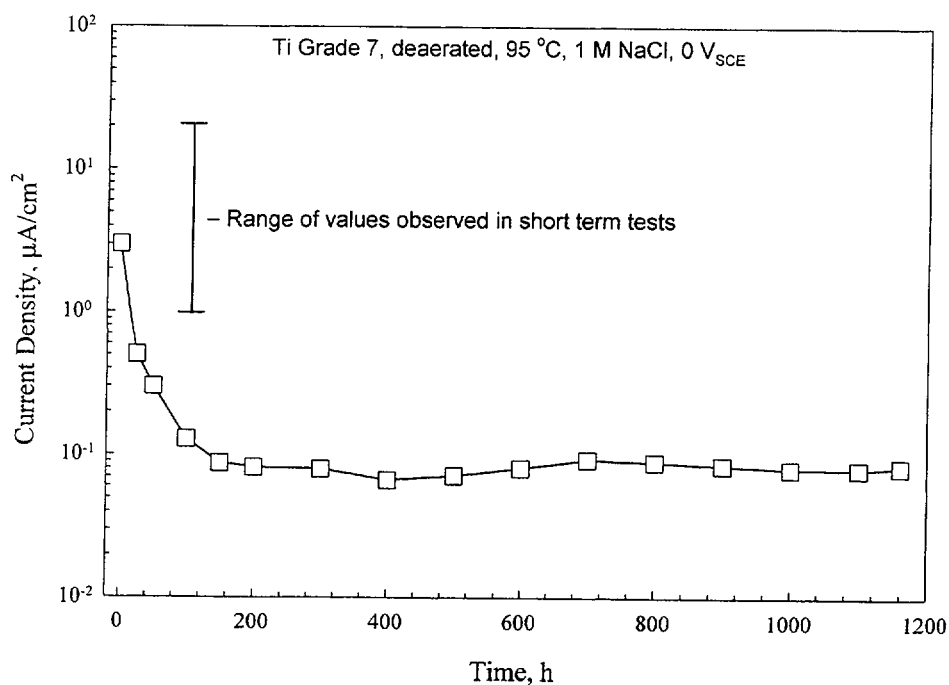


**Figure 4-7.** Long-term passive current measurement for Ti Grade 7 in deaerated, 1M NaCl solution at 95 °C. Also shown are the ranges of passive current densities measured in short-term tests.

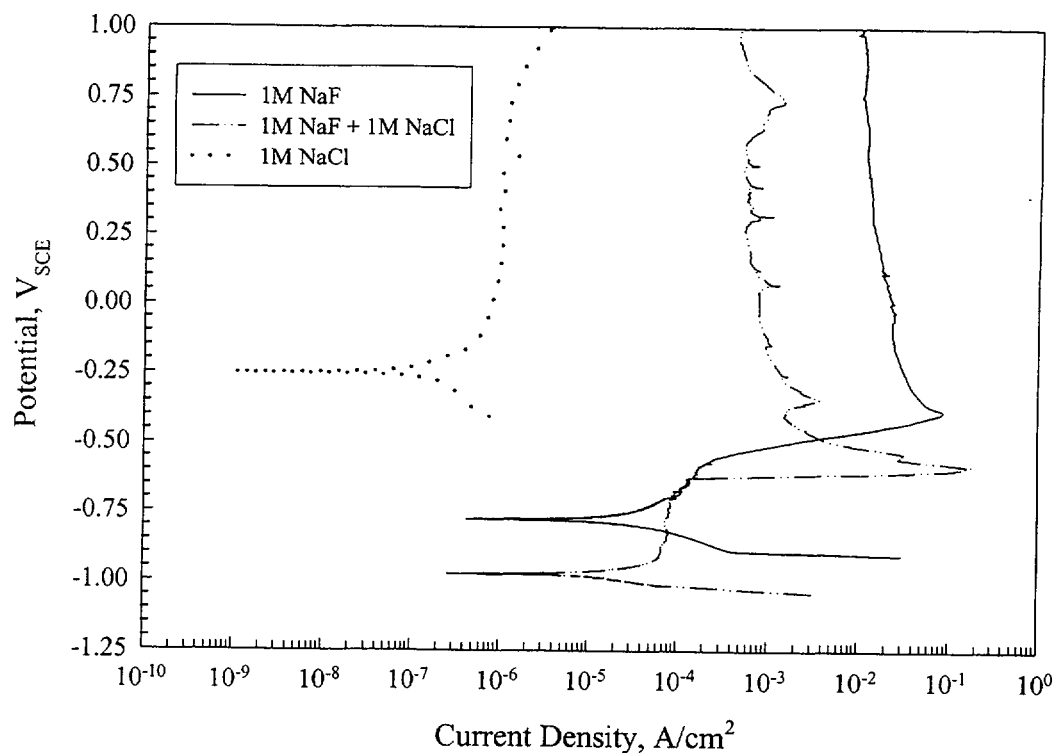


**Figure 4-8.** Effect of fluoride on the anodic polarization behavior of Ti Grade 7 as compared to the polarization behavior in chloride-only solutions. All tests were performed under deaerated conditions at 95 °C and a scan rate of 0.167 mV/s.

a small area of passivity just noble of the open circuit potential, prior to a sharp increase in the current (similar to what is observed during localized corrosion), which then decreased after reaching a critical current density. Post-test examination of the specimens revealed extensive attack, but the attack was generalized in nature. It is possible that these high current densities are limited by transport of  $\text{TiF}_6^{2-}$  through a porous corrosion layer on the surface, similar to the mass transport conditions encountered in electropolishing. Another possibility, which has been proposed in the literature for this apparent mass transport limited dissolution region (Mandry and Rosenblatt, 1972; Levin, 1996; Boere, 1995), is the transport of HF to the metal surface as a rate determining step in the reaction sequence shown in Eq. (4-1). In any event, it is clear that the presence of fluoride above a critical concentration resulted in marked changes in polarization behavior and a significant increase in the current density.



Long-term potentiostatic polarization at  $0 \text{ V}_{\text{SCE}}$  (determined to be an upper bound for the  $E_{\text{corr}}$  in air-saturated solutions) (Brossia and Cragolino, 2001a) revealed that a critical fluoride concentration exists above which a dramatic increase in the measured current is observed. These results are shown in figure 4-9 for Ti Grade 7 exposed in deaerated 1 M NaCl solutions at  $95^\circ\text{C}$ . At very low concentrations ( $10^{-4} \text{ M}$ ), fluoride did not significantly alter the steady-state currents measured. A significant increase in the measured current, however, was noted at  $5 \times 10^{-4} \text{ M}$  fluoride with the current density increasing from  $10^{-8}$  to  $\sim 5 \times 10^{-7} \text{ A/cm}^2$ . Further increases in the fluoride concentration resulted in additional increases in the current density, reaching a plateau of  $4 \times 10^{-5} \text{ A/cm}^2$  at  $10^{-2} \text{ M}$  fluoride. When plotted in a different fashion using the last data point at 453 h as being representative of steady-state, the effect of fluoride concentration on the current is more readily seen (figure 4-10). The presence of fluoride at a concentration of  $10^{-3} \text{ M}$  results in an increase in the current nearly by a factor of 1,000. Similar results have been reported by the State of Nevada for Ti

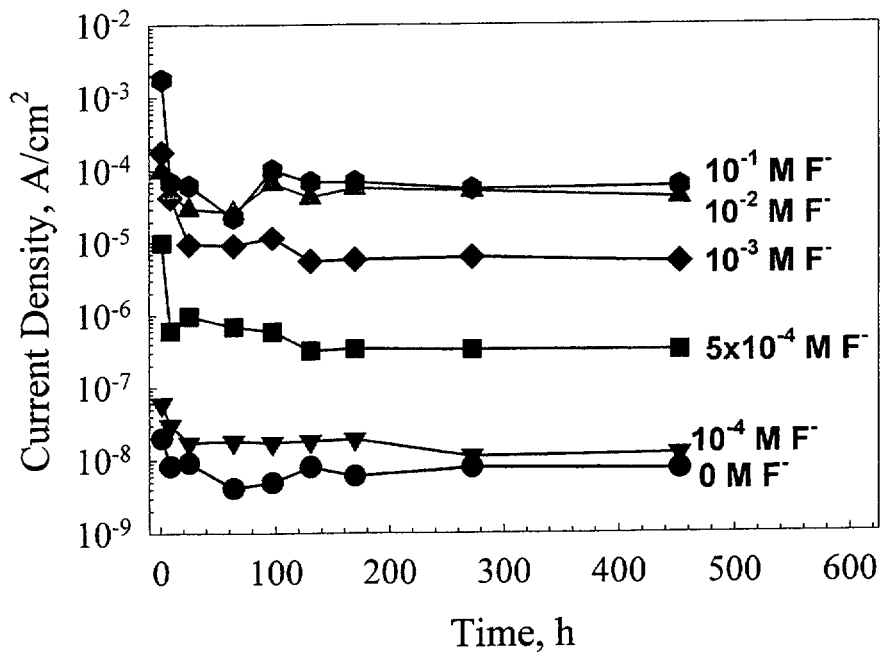
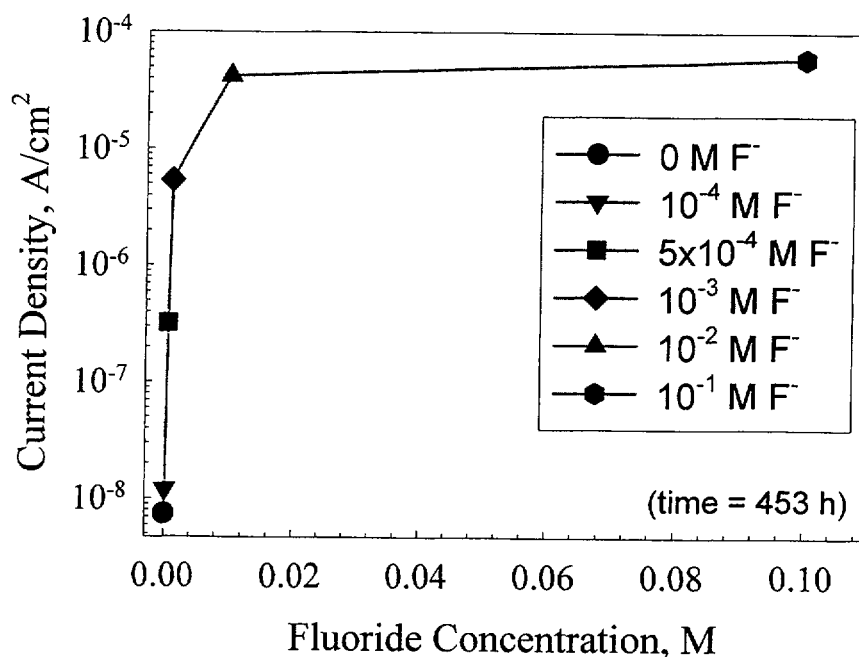


Figure 4-9. Effect of fluoride on the passive current density for Ti Grade 7 over time in a deaerated, 1 M NaCl solution at  $95^\circ\text{C}$  and an applied potential of  $0 \text{ V}_{\text{SCE}}$



**Figure 4-10. Effect of fluoride on the steady-state, passive current density for Ti Grade 7 in deaerated, 1 M NaCl solution at 95 °C and an applied potential of 0 V<sub>SCE</sub>**

Grade 7 in the presence of high fluoride concentrations. For example, it was reported that in simulated 10,000x J-13 Well water with 48,076 ppm (1.36 M) chloride and 14,422 ppm (0.34 M) fluoride that a measured corrosion rate of 19.2  $\mu\text{m}/\text{yr}$  was observed on U-bend specimens and was severe non-uniform some localized corrosion as well.<sup>3</sup>

Results of additional tests examining the effects of other anionic species (e.g., nitrate, sulfate) on the passive current density of Ti Grade 7 in the presence of fluoride are shown in figure 4-11. Clearly, at least at short times, the deleterious effects of fluoride overwhelm any beneficial effects from the presence of either nitrate or sulfate with passive corrosion rates being comparable to tests when neither nitrate or sulfate are present. Interestingly, similar results for dissolution rates also have been observed for commercial purity Ti in the presence of fluoride, indicating that the addition of Pd to Ti (added to improve corrosion resistance) does not substantially improve the performance of Ti in the presence of fluoride (Brossia and Cragolino, 2001b). Thus, the importance of the effect of fluoride on the long-term performance of Ti cannot be underestimated.

#### 4.2.2 Localized Corrosion

The susceptibility of Ti Grade 7 to localized corrosion has been evaluated using potentiodynamic and potentiostatic polarization as a function of chloride concentration, temperature, applied potential, and the presence of weldments. Figure 4-12 shows a typical polarization curve for this material in chloride-only

<sup>3</sup>Pulvirenti, A.L. Results of screening tests on titanium grade 7. *Presentation to the Waste Package Materials Performance Peer Review Panel*. July 24, 2001. Cleveland, OH. 2001.

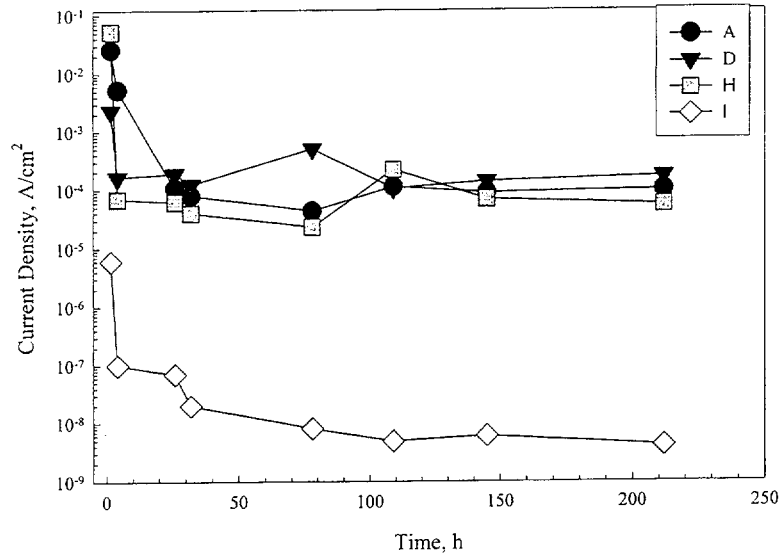


**Figure 4-11. Effect of fluoride on the passive current density of Ti Grade 7 in various deaerated solutions containing chloride, nitrate, and sulfate at 95 °C and an applied potential of 0 V<sub>SCE</sub>. A = 1 M Cl<sup>-</sup>, 0.1 M F<sup>-</sup>, 0.55 M NO<sub>3</sub><sup>-</sup>, 0.92 M SO<sub>4</sub><sup>2-</sup>; D = 3.84 M Cl<sup>-</sup>, 0.07 M F<sup>-</sup>, 2.32 M NO<sub>3</sub><sup>-</sup>, 0.15 M SO<sub>4</sub><sup>2-</sup>; H = 1 M Cl<sup>-</sup>, 0.1 M F<sup>-</sup>, 0.0 M NO<sub>3</sub><sup>-</sup>, 0.0 M SO<sub>4</sub><sup>2-</sup>; I = 1 M Cl<sup>-</sup>, 0.0M F<sup>-</sup>, 0.0 M NO<sub>3</sub><sup>-</sup>, and 0.0 M SO<sub>4</sub><sup>2-</sup>**

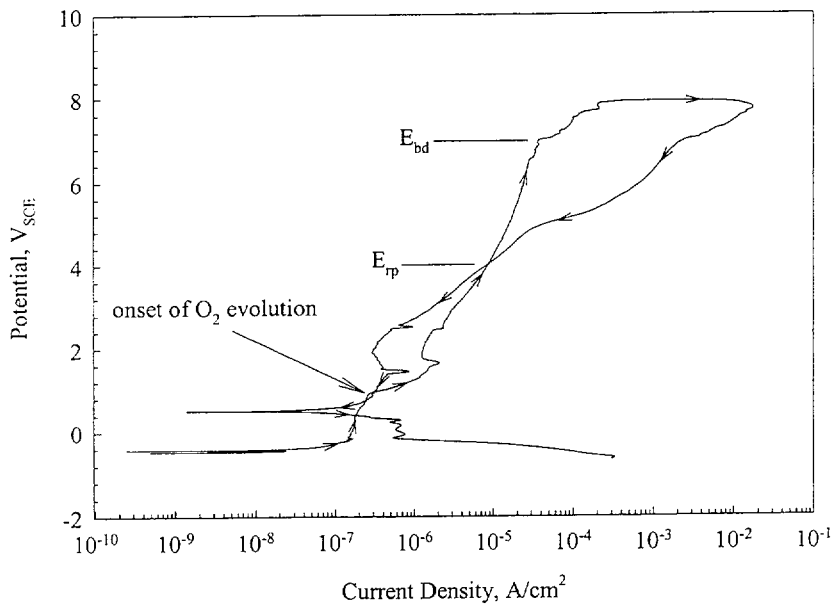


**Figure 4-12. Polarization behavior of Ti Grade 7 in deaerated, 5 M NaCl at 95 °C with a scan rate of 0.167 mV/s**

solutions, with high breakdown ( $E_{bd}$ ) and repassivation ( $E_{rp}$ ) potentials evident. Figure 4-13 summarizes the effects of chloride concentration and weldments on  $E_{bd}$  and  $E_{rp}$  determined from cyclic potentiodynamic polarization experiments performed at 95 °C. The typical attack morphology observed after polarization is shown in figure 4-14. Note the irregular nature of the attack and some evidence of undercutting, resulting from the spread of the attack under the oxide film. Furthermore, under no conditions was attack observed under the crevice former, but rather all attack was observed on the boldly exposed surfaces of the specimens. As a result, the breakdown and repassivation potentials labeled in figure 4-12 as  $E_{bd}$  and  $E_{rp}$  are not crevice and crevice repassivation potentials but are associated with the boldly exposed surface. Though the presence of weldments appeared to be slightly detrimental when examined in the context of the variability (shown by the error bars) of  $E_{bd}$  and  $E_{rp}$ , there is little difference between the wrought and the welded material.

Consequently, Eq. (4-2) was fit to both sets of data (wrought and welded),

$$E_{crit} = E_{crit}^0 - B \log[Cl^-] \quad (4-2)$$

where  $E_{crit}$  is the critical potential (either  $E_{bd}$  or  $E_{rp}$ ),  $E_{crit}^0$  is the critical potential at 1 M chloride concentration, and  $B$  is the slope of the dependence of  $E_{crit}$  on the log of the chloride concentration. For  $E_{bd}$ , the slope was found to be approximately 2.28 V/decade $\cdot[Cl^-]$  with  $E_{bd}^0$  at 7.30 V<sub>SCE</sub> and an  $r^2$  of 0.92. These values are considerably larger than 0.11 V/decade for Ti alloys in bromide (Beck, 1974) solutions and 0.1 V/decade in chloride solutions at 200 °C (Koizumi and Furuya, 1973). It should be noted, though, that the dependence of  $E_{bd}$  on chloride concentration for Pd-bearing Ti alloys has not been previously examined, with the majority of the work similar to this being conducted in other halide solutions. For  $E_{rp}$ , the slope was 0.67 V/decade $\cdot[Cl^-]$  with an  $E_{rp}^0$  of 5.64 V<sub>SCE</sub> and  $r^2$  of 0.84. Slightly better fitting results were obtained for

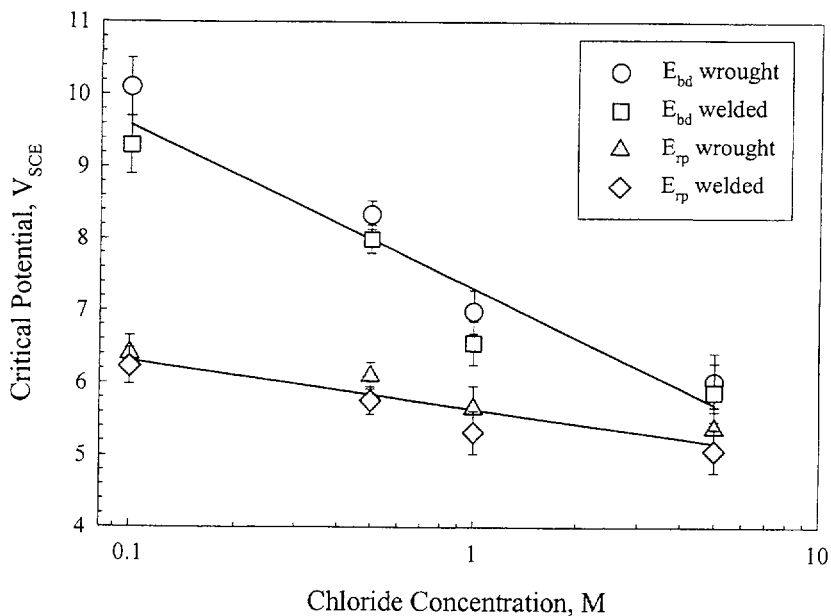


**Figure 4-13. Effect of chloride concentration on the breakdown ( $E_{bd}$ ) and repassivation ( $E_{rp}$ ) potential for wrought and welded Ti Grade 7 in deaerated solutions at 95 °C**

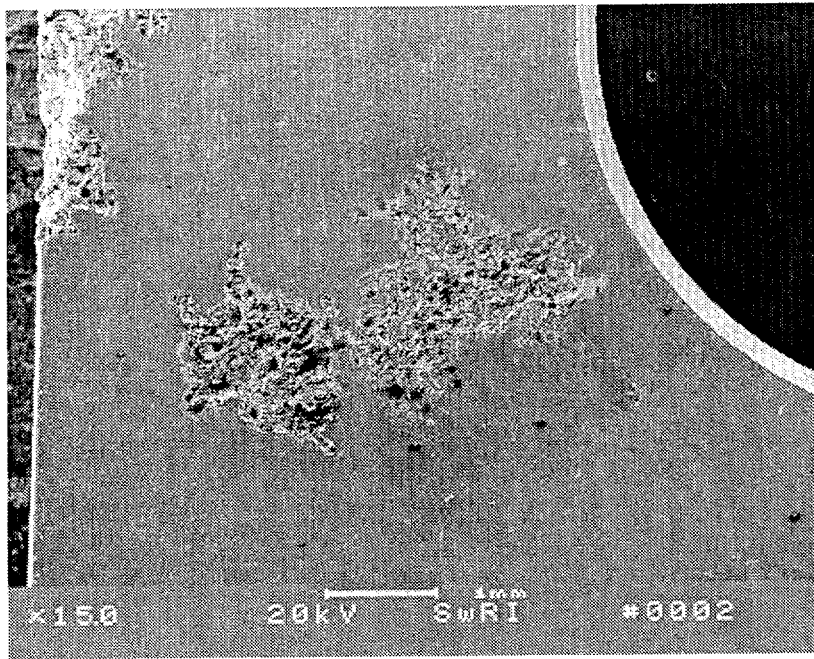


**Figure 4-14. Postpolarization scanning electron micrograph showing corrosion attack**

$E_{rp}$  when the wrought and welded data sets were examined independently ( $r^2$  increased to 0.96 for both  $E_{bd}$  and  $E_{rp}$  for the wrought material); however, because of the overlapping variability ranges for most of the data sets, they were examined as a single set. Even though the critical potentials for the welded and wrought materials were similar, it should be noted that the location of corrosion attack was more extensive at the weldments for welded specimens. The potentials at which localized corrosion is observed are above the potential at which DOE reversed the potential (2.455 V<sub>SCE</sub>) during potentiodynamic polarization testing. Thus, it seems likely that if the DOE had polarized to the higher potentials used here, localized corrosion of Ti Grade 7 would have been observed.

Because the proposed repository will be above boiling for some time and because it has been shown that aqueous films may exist well above 100 °C in the presence of deposited salts by forming saturated solutions, the effect of elevated temperatures on the critical potentials for localized corrosion was also examined. Similar to increasing the chloride concentration, increasing the temperature also resulted in a decrease in the measured critical potentials for Ti Grade 7 ( $E_{rp}$  is shown in figure 4-15) up to a certain critical temperature,  $T_{crit}$ , above which an abrupt decrease in the critical potentials was observed. At temperatures less than  $T_{crit}$ ,  $E_{rp}$  had temperature dependencies ranging from 11 to 14 mV/°C for the wrought and welded specimens. The critical temperatures observed in the present case (between 120 and 140 °C for  $E_{rp}$ ) are similar to the value of approximately 125 °C for  $E_{bd}$  in 1 M chloride reported by Posey and Bohlmann (1967) for Ti Grade 7. It should be noted, however, that Posey and Bohlmann (1967) observed a much stronger temperature dependence for  $E_{bd}$  at temperatures less than  $T_{crit}$  (approximately 70 mV/°C), but similar dependencies at temperatures above  $T_{crit}$ . The source of the differences is unclear, except that Posey and Bohlmann examined the effect of temperature for a wider range than was used in the present study (minimum temperature by Posey and Bohlmann was 25 °C, as opposed to the minimum of 95 °C examined here). At  $T_{crit}$  both  $E_{bd}$  and  $E_{rp}$  decrease significantly, by as much as 2.6 V, similar to that observed by Posey and Bohlmann (1967).

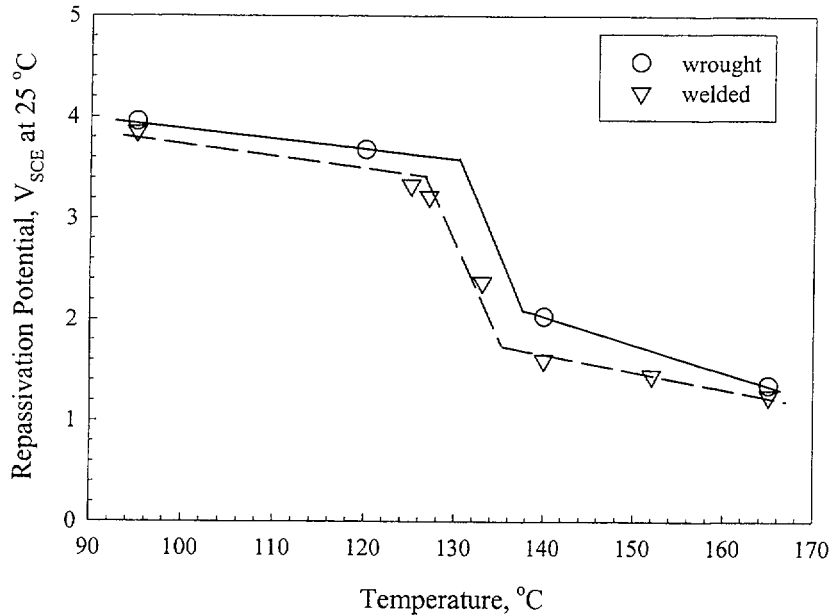


**Figure 4-15. Effect of temperature on the repassivation potential ( $E_r$ ) of wrought and welded Ti Grade 7 in deaerated, 1 M NaCl solutions**

Though not discussed in any detail thus far, the effect of welding on the localized corrosion resistance of Ti Grade 7 appears to be somewhat detrimental, though generally within the data scatter observed. Welded Ti Grade 7 specimens were fabricated using 0.5-in.-thick plates of Ti Grade 7, 0.0625 in.-diameter weld wire, the gas-tungsten arc welding process, a double V groove joint geometry, and 8 to 10 passes per side at a speed of 6–8 in./min. It is thought, however, that if a statistically significant number of experiments were conducted under identical conditions that welded Ti Grade 7 would likely exhibit depressed critical potentials compared to wrought Ti Grade 7. But according to Donachie (1988) and Schutz (1991), Ti weldments should have comparable corrosion resistance to the wrought material because the formation, structure, and thickness of the  $TiO_2$  passive film should be essentially independent of substrate microstructure. In the present case, however, this was not strictly observed, and weldments did seem to act as preferential sites for localized corrosion initiation. At first, one could argue that this observation was a consequence of Pd dilution within the weld bead. The composition of the weldment, though, seems to counter argue this point because the bulk weldment concentration of Pd was comparable to the base metal (~0.14 Pd). The possibility of Pd segregation to interdendritic regions or grain boundaries is another possible reason. When examined using backscattered imaging on the scanning electron microscope, no apparent segregation of Pd is noted (Pd, being heavier than Ti, would show up as a lighter contrast in the image). Rather, a generally uniform image is obtained with a few dark precipitates also being evident as shown in figure 4-16. The composition of the dark precipitates has not been evaluated fully, but because of the contrast differences, these particles must be composed of elements with lower atomic numbers than Ti, and it is speculated that these are perhaps Al/Si oxides. It is possible that the presence of these particles is the cause of the observed decrease in resistance to localized corrosion associated with the weldments, but it is uncertain at this point. It is possible that this decrease is a result of differences in grain structure and shape (figure 4-17). Though grain size and shape have played roles in altering the corrosion resistance of some materials [particularly intergranular corrosion of stainless steels (Sedriks, 1996)], their effects on the corrosion of Ti alloys have never been proven detrimental.

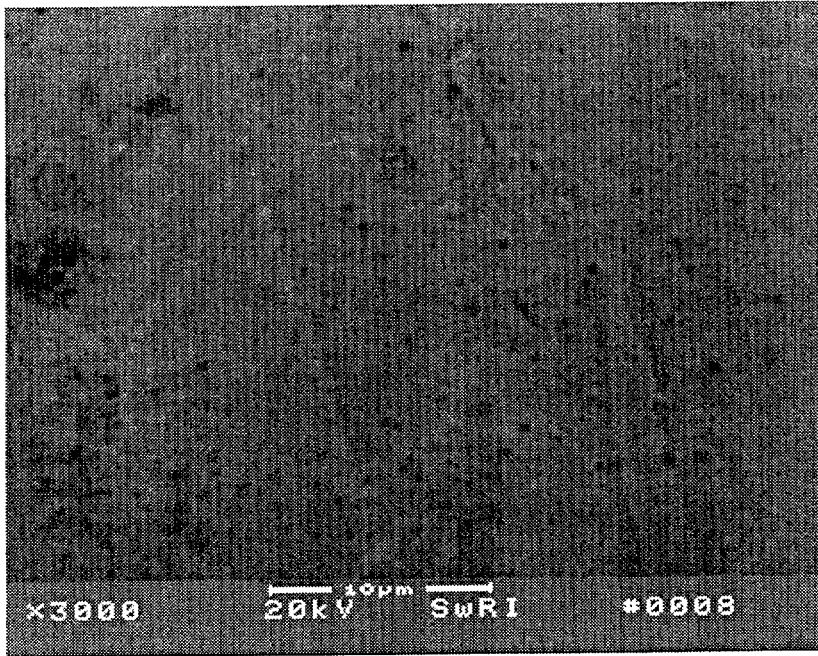


**Figure 4-16. Backscattered scanning electron microscope image of Ti Grade 7 weld microstructure showing a nearly uniform atomic mass distribution indicating that the alloy composition within the weldment is nearly uniform**

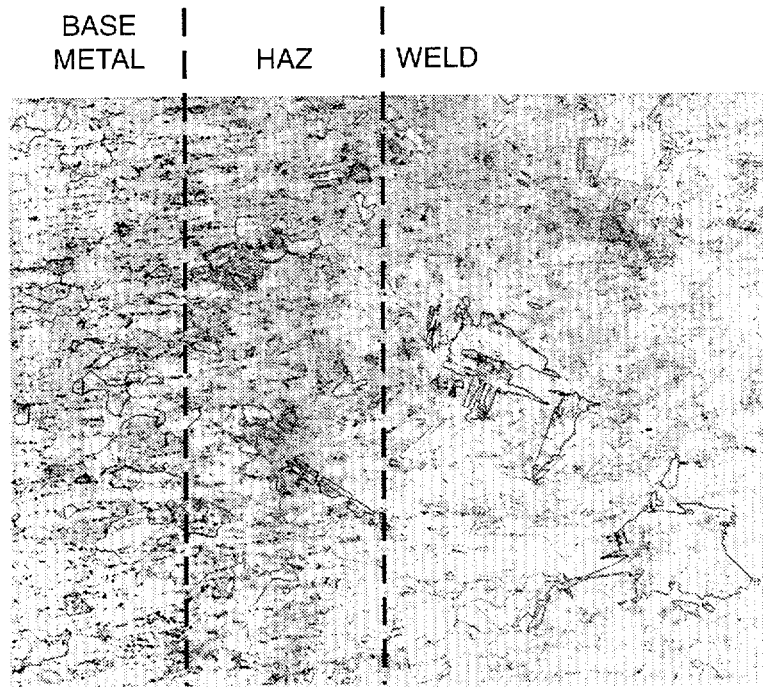


**Figure 4-17. Optical micrograph at 100x showing base metal, heat affected zone, and weldment microstructures for Ti Grade 7**

In all potentiodynamic polarization tests, no corrosion attack was observed under the crevice former. It is thought that this condition arises from differences in the mechanisms associated with pitting and crevice corrosion on Ti. Unlike stainless steels and nickel-based alloys in which crevice corrosion is thought to nucleate via the formation and coalescence of pits inside the crevice, pitting and crevice corrosion on Ti alloys occur via different mechanisms (Beck, 1974). Based on these differences, a theory explaining why no corrosion was observed under the crevice former was generated. For pitting corrosion on Ti, according to Beck (1974), a salt film is needed to produce sufficient ohmic drop for the pit base to undergo active dissolution. At high potentials, the ohmic drop into the creviced area is insufficient for initiation of crevice corrosion (assuming crevice corrosion can occur). That is, with the exterior of the crevice at a high potential, the potential drop into the crevice is still limited to the passive range. For pits to nucleate beneath the crevice former, a salt film will be needed to achieve the required ohmic drop. Beck (1974) was able to demonstrate that the rate-limiting step in the pitting of Ti alloys is diffusion of the halide ion (chloride in this case) to the base of the pit. Because the diffusion distance to the base of a pit outside the crevice is shorter than for a pit inside the crevice, pitting on the noncreviced areas is favored. It is speculated, however, that given sufficient time (e.g., potentiostatic polarization), pits should nucleate inside the crevice as well.

As no crevice corrosion of Ti Grade 7 was observed in the CPP tests and Ti alloys are known to be susceptible to crevice corrosion (McKay, 1984; Ikeda et al., 1990), a series of potentiostatic experiments at  $0 V_{SCE}$  was conducted. Figure 4-18 shows the results of potentiostatic holds in deaerated solutions at  $95^{\circ}C$ . Crevice corrosion initiated on Ti Grade 2 in  $5 M Cl^{-}$  after an induction time of  $\sim 32$  h. This induction time was measured from the start of the experiment to the point at which the current density exceeded  $1 \mu A/cm^2$  and was observed to continue increasing. In this case, corrosion attack under the crevice former was general in nature indicating that crevice corrosion did not initiate as pits that coalesced together. There was no initiation of crevice corrosion on Ti Grade 7 after nearly 1,200 h ( $\sim 7$  wk). Additional long-term (nearly 6 wk) potentiostatic polarization tests at potentials as high as  $1.5 V_{SCE}$  did not result in any observable crevice corrosion of Ti Grade 7 even in high chloride solutions; negligible weight change was measured in all cases.

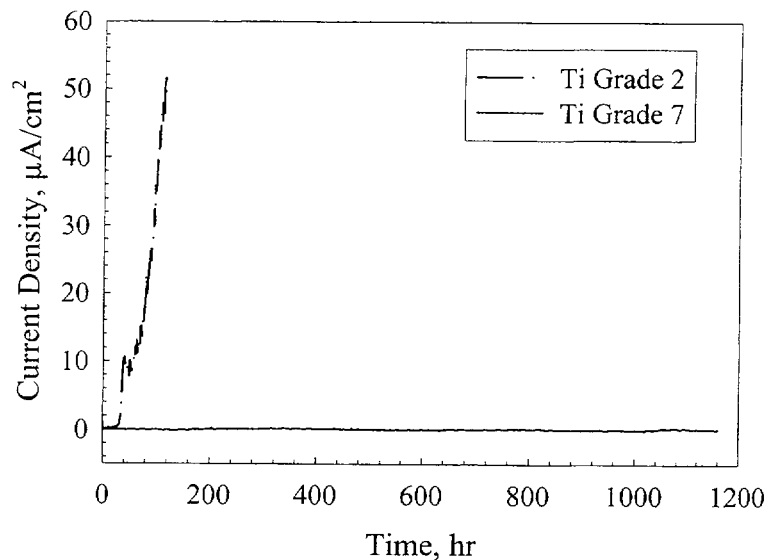


**Figure 4-18. Potentiostatic polarization of creviced Ti Grades 2 and Grade 7 specimens in deaerated, 5 M NaCl at  $95^{\circ}C$  and an applied potential of  $0 V_{SCE}$**

To help explain the resistance of Ti Grade 7 to crevice corrosion compared to Ti Grade 2, the cathodic and anodic polarization behavior of Ti Grades 2 and 7 were examined in a simulated crevice solution (deaerated, 5 M Cl<sup>-</sup>, 0.1 M HCl, 95 °C). Figure 4-19 shows the cathodic polarization curves for Ti Grades 2 and 7, with Ti Grade 7 exhibiting a higher open circuit potential. During cathodic polarization, evolution of gas (assumed to be H<sub>2</sub>) was observed. For both materials, an activation-controlled region was observed that was then followed by a mass transport limited region. The cathodic Tafel slope observed for Ti Grade 2 was -100 mV/decade. Ti Grade 7 exhibited a cathodic Tafel slope of -27 mV/decade at low overpotentials that transitioned to a slope of -138 mV/decade at higher overpotentials. Anodic polarization of Ti Grade 2 (figure 4-20) resulted in the observation of an active/passive transition, with a peak current of nearly 8 × 10<sup>-4</sup> A/cm<sup>2</sup> prior to decreasing to ~ 2 × 10<sup>-5</sup> A/cm<sup>2</sup>. Anodic polarization of Ti Grade 7 exhibited essentially passive behavior at all potentials above the corrosion potential, which is 300 mV higher than that of Ti Grade 2. Furthermore, there was little difference in the observed passive current for either material, but the passive current density did decrease with increasing polarization. Posttest examination of the specimens revealed general corrosion with no evidence of pitting noted.

The Pd addition effectively rendered Ti Grade 7 immune to crevice corrosion, at least for the time periods examined here. Satoh et al. (1987) similarly observed no initiation of crevice corrosion on Ti Grade 7 in boiling 20-percent NaCl solutions at pH 4 after 720 h exposure and in boiling 42-percent MgCl<sub>2</sub> solutions after 240 h. In contrast, commercial purity Ti (similar to Grade 2) was observed to suffer from severe crevice corrosion in 92 and 15 h using identical conditions. Similarly, Schutz and Xiao (1993) did not observe crevice corrosion in Ti Grade 7 after a 30 d exposure in 20 percent NaCl at pH 2 and 260 °C nor in boiling 10-percent FeCl<sub>3</sub> solutions (102 °C). If one assumes that Pd will not influence the anodic dissolution behavior of Ti and will only influence the cathodic reaction kinetics, then one would expect to observe an increase in the open-circuit potential for Ti Grade 7 compared to Ti Grade 2 in a simulated crevice solution. As shown in figures 4-19 and 4-20, this is indeed the case. Note that little difference was observed in the passive region

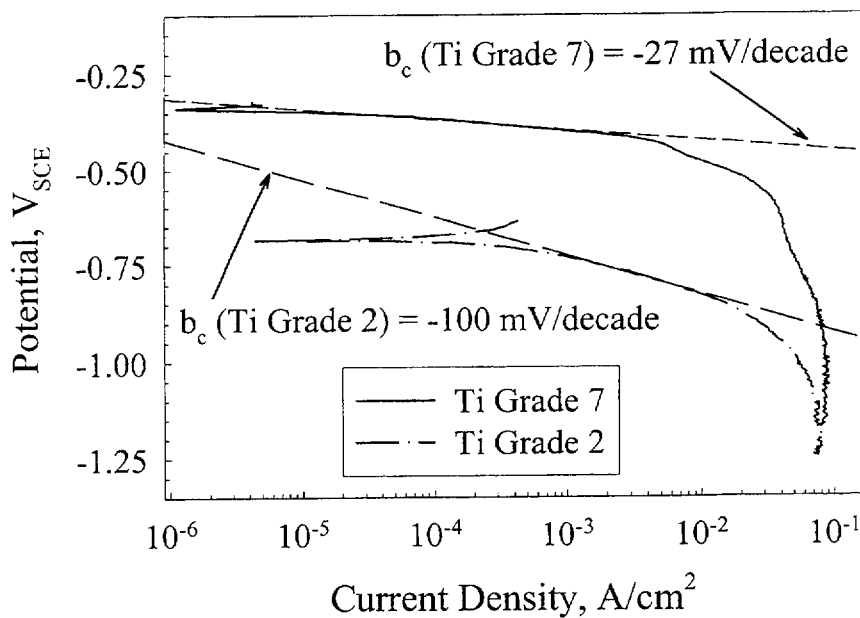


**Figure 4-19. Cathodic polarization of Ti Grades 2 and 7 in a simulated crevice solution of 5 M NaCl, 0.1 M HCl, at 95 °C**

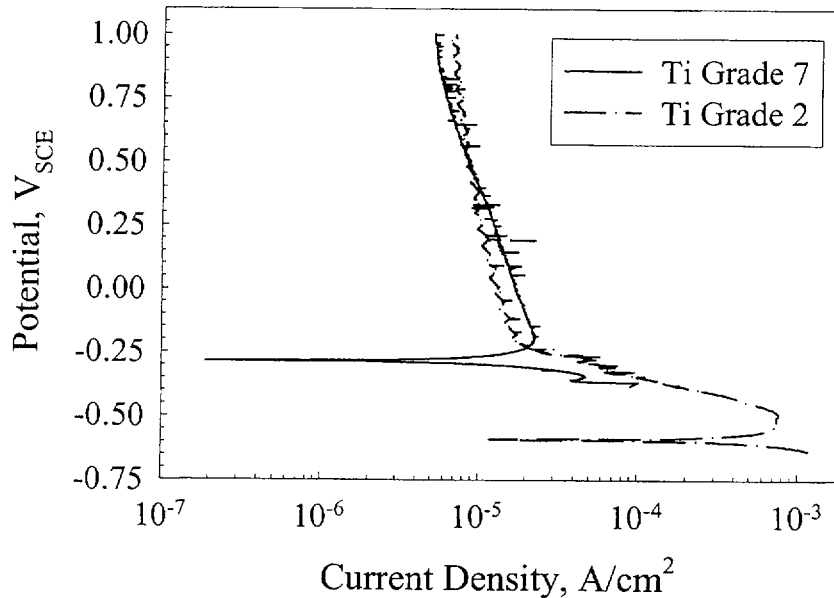


**Figure 4-20. Anodic polarization of Ti Grades 2 and 7 in a simulated crevice solution of 5 M NaCl, 0.1 M HCl, at 95 °C**

of the polarization curves lending credence to the argument that the main role of Pd is through alteration of the cathodic kinetics. This is further brought out by consideration of the cathodic polarization curves for Ti Grades 2 and 7 (figure 4-19). Ti Grade 2 exhibited a cathodic Tafel slope of  $-100$  with Ti Grade 7 exhibiting a cathodic Tafel slope of  $-27$  mV/decade at low overpotentials and  $-138$  mV/decade at high overpotentials. Though a detailed study of the mechanism for the hydrogen evolution reaction (HER) on each material was not conducted,<sup>4</sup> some conclusion can be drawn based on these Tafel slopes and the relationship between the Tafel slope,  $b$ , and the transfer coefficient,  $\alpha$ , shown in Eq. (4-3),

$$b = \frac{2.303RT}{\alpha F} \quad (4-3)$$

where  $R$  is the Universal Gas constant,  $T$  is temperature, and  $F$  is Faraday's constant. First, the HER can be broken into the reaction steps shown in Eqs. (4-4) through (4-6),




---

<sup>4</sup>To conclusively confirm the hydrogen evolution reaction mechanisms, one would still need to know the stoichiometric number (the number of times the rate determining step takes place each time the reaction sequence occurs once), the reaction order [the dependence of reaction rate on  $(\text{H}^+)$ ], and the dependence of H surface coverage on the applied potential.

where these reactions represent the discharge, recombination, and electrodic desorption reaction steps. The values of  $\alpha$  for each of the reaction steps are 0.5, 2.0, and 1.5 at low H coverage ( $\theta_H$ ) (Bockris and Reddy, 1970), resulting in Tafel slopes (at 95 °C) of -146, -36.5, and -48.7 mV/decade. In the present case, the likely rate determining step (rds) on Ti Grade 2 is the discharge reaction step (-100 versus -146 mV/decade). On Ti Grade 7, at low overpotentials, the rds is likely recombination (-27 versus -36.5 mV/decade). At higher overpotentials, it seems likely that the Pd addition to Ti acts in similar fashion to Pt (i.e., as  $\theta_H$  approaches unity, the rds changes to electrodic desorption). At high  $\theta_H$ ,  $\alpha$  for electrodic desorption is 0.5 (Gileadi, 1993), which results in a Tafel slope of -146 in comparison to the -138 mV/decade observed here. This conclusion is in agreement with the mechanisms for HER proposed by Fukuzuka et al. (1980) for Ti Grade 2 (rds = discharge) but does not agree with their mechanism for Ti Grade 7 (rds = electrodic desorption at low  $\theta_H$ ). This difference in reaction mechanisms is likely a result of the difference in environments examined between Fukuzuka et al. (1980) (2 percent HCl at 70 °C) and the present case. Thus, it appears that Pd acts to increase  $i_0$  and decreases the cathodic Tafel slope (e.g., lower overpotential needed to achieve similar reaction rates) for HER such that the cathodic reaction line no longer intercepts the anodic dissolution line below the active/passive transition but intersects in the passive range. The consequence then is that ohmic drop in the crevice on Ti Grade 2 puts a portion of the crevice in the active nose, and rapid dissolution occurs. In Ti Grade 7, an ohmic drop into the crevice does not significantly increase the dissolution rate, and eventually the interior of the crevice will be cathodic and generate H<sub>2</sub> gas or will lead to increased concentrations of H<sub>abs</sub> in the metal lattice. If Pd accumulates on the metal surface as dissolution proceeds as has been reported (Okazaki et al., 1997; Shida and Kitayama, 1988; Shimogori et al., 1976), the cathodic reaction kinetics could be further enhanced (e.g.,  $i_0$  may increase further) resulting in an additional increase in the open circuit potential and thereby causing the disappearance of the slight active/passive transition observed in the present case.

### 4.2.3 Center for Nuclear Waste Regulatory Analyses Model Abstraction and Predicted Performance

The current model for drip shield performance in the TPA code is highly abstracted and strictly limited to a distribution of failure times. The distribution of failure times ranges from 2,700 to 20,400 yr using a log-normal distribution. This range was arrived at using an anticipated range of steady-state general corrosion current densities of between  $8.5 \times 10^{-8}$  and  $6.4 \times 10^{-7}$  A/cm<sup>2</sup> based on early long-term potentiostatic testing. The current version of the TPA code does not consider the possibility of localized corrosion of the drip shield nor does it account for the possibility of enhanced corrosion from fluoride. Current plans include attempts to account for fluoride effects.

Though there is no model for truly predicting the performance of the drip shield in the TPA code, some simulations replacing waste package parameters with drip shield parameters have been conducted. Using the relationships between chloride concentration, temperature and the repassivation potential as well as planned drip shield thickness and passive corrosion rates, the drip shield is predicted to fail by general thinning and not by localized corrosion (neglecting the possibility for hydrogen induced cracking). This stems from the prediction that at all chloride concentrations and temperatures anticipated that the corrosion potential will always be below the repassivation potential. This result is intuitive on examination of the data generated for Ti Grade 7 with repassivation potentials well above 1 V<sub>SCE</sub>, even at high temperatures and high chloride concentrations.

## 5 FUTURE WORK

Though considerable progress has been made in evaluating the DOE data and model predictions using CNWRA experimental efforts and predictions, some questions still remain and should be evaluated. Recent work by consultants for the State of Nevada<sup>1</sup> demonstrated that the presence of trace impurities (e.g., lead, mercury, arsenic) can have a dramatic effect on the corrosion resistance of Alloy 22. The conditions studied, particularly the temperature and pressure, however, are well outside the range of anticipated conditions for the repository. Thus, examination of the possible detrimental effects of these impurities on Alloy 22 in more realistic conditions is warranted. It should also be noted that the effects of these impurities on the corrosion behavior of Ti Grade 7 (and Ti alloys in general) are unknown and should be evaluated. Further examination of the possible inhibitory effects of other anionic species (e.g., sulfate, nitrate) present in the local groundwater chemistry should be conducted. This examination is particularly important because these species may inhibit the occurrence of localized corrosion of Alloy 22 (as suggested by DOE). Other areas to be examined further include the effect of temperature on the passive corrosion rate of Alloy 22, the possibility of microbially influenced corrosion of Ti Grade 7, and the preferential dissolution of key alloying elements in Alloy 22 that may lead to passive oxide spalling and perhaps increased susceptibility to localized corrosion.

By conducting this work, the NRC and CNWRA will be in a better position to effectively evaluate the safety case presented by the DOE in any license application for Yucca Mountain. These activities will also enhance the technical credibility of the NRC and CNWRA, will improve the models and parameters used in the NRC/CNWRA TPA code, and will also help identify issues based on risk information that DOE should focus on prior to any license application.

---

<sup>1</sup>Barkatt, A., and J.A. Gorman. Tests to explore specific aspects of the corrosion resistance of C-22. *Presentation to Nuclear Waste Technical Review Board*. August 1, 2000. Carson City, NV. 2000.

## 6 SUMMARY AND CONCLUSIONS

DOE is responsible for developing a safety case for the proposed HLW repository at Yucca Mountain. However, various uncertainties exist in the current information provided by DOE. These uncertainties include the potential environments to which the waste package and drip shield may be exposed, the effects and concentrations of trace impurities that may be present, the effects of microbial activity and thermal aging on the component materials, and the estimated general corrosion rates. To resolve these uncertainties, DOE and NRC have reached an agreement whereby the DOE has committed to provide additional information in the form of technical justifications and/or additional measurements.

The environment in the emplacement drifts may have a significant effect on the long term performance of the engineered barriers. Environmental characteristics that have been identified as important to long-term engineered barrier performance include temperature, chemistry of deliquescent salts, groundwater composition, concentration of trace elements in the host rock and groundwater, and the evaporative concentration of dissolved salts. Groundwater at Yucca Mountain has been classified into two types (i) saturated zone water and perched water in the unsaturated zone, and (ii) unsaturated zone pore water. The compositions of the saturated zone and perched waters are dominated by rock/mineral interaction and are sodium bicarbonate based waters. Samples of unsaturated zone water has been extracted from bore holes. Because of the uncertainties associated with the extraction of the pore waters from relatively dry rocks at Yucca Mountain, the characteristics of pore waters are not yet fully understood. Both the groundwater and host rock in the Yucca Mountain region has been shown to have measurable concentrations of trace elements, such as lead and mercury. These trace elements may promote localized corrosion and stress corrosion cracking.

Hygroscopic salts may be deposited onto the surfaces of engineered barrier system components by evaporation of groundwaters that contacts the engineered barrier system components, or from dust or aerosols entrained in the drift air. Analysis has shown that the mutual deliquescence relative humidity of a salt mixture is lower than the deliquescence point of any of its pure components. Based on the deliquescence point of the NaCl-NaNO<sub>3</sub>-KNO<sub>3</sub> system and the presence of the highly hygroscopic salts such as CaCl<sub>2</sub> and MgCl<sub>2</sub>, the minimum deliquescence point may be close to 20 percent. With such a low deliquescence point, the engineered barrier system components, if in contact with salt deposits, would be subject to aqueous corrosion during the entire emplacement period.

Evidence exists that the effect of bacteria on the average bulk environment is small, but this conclusion cannot be extrapolated to local environmental effects. Arguments based on low microbial activity because of limited nutrients, water, energy, or other components of the metabolic process do not represent how localized impacts can be distributed in the repository, drift, or over a waste package surface. To adequately characterize the effects of microbial activity on the environment, the distribution of components or effects, including development of biofilms, needs to be considered. The effects of localized impacts such as biofilm development, colloid formation, and the production of inorganic acids, methane, organic byproducts, carbon dioxide, and other chemical species that could change the longevity of materials and the transport of radionuclides from the near field have not been investigated by the DOE. In addition, utilization of repository construction and structural materials should be considered as nutrient and energy sources.

The DOE prediction of waste package lifetimes is based on uniform corrosion rates in the absence of localized corrosion. Data used by the DOE for the uniform corrosion rates are confounded by the deposition of silica on the test specimens and limited by the relatively poor sensitivity of weight loss measurements. Susceptibility of Alloy 22 to localized corrosion was determined to be negligible based on a comparison of corrosion potentials to critical potential for the initiation of localized corrosion which did not include the critical potential for crevice corrosion even though this is the most likely localized corrosion mode for the waste packages. Phase instability as a result of thermal aging and microbially influenced corrosion are considered as processes that would accelerate the uniform corrosion rate rather than increase the susceptibility of the alloy to localized corrosion. In work conducted at the CNWRA, the performance of the Alloy 22 waste package outer barrier has been shown to be dependent on the both composition of the environment and fabrication processes. Passive uniform corrosion rates measured under potentiostatic conditions are less than  $10^{-3}$  mm/yr suggesting that in the absence of conditions necessary for pit initiation and propagation of localized corrosion, the lifetime of the proposed 20 mm thick waste packages will be greater than the 10,000-yr regulatory compliance period. It should be noted however that the base alloy in the as-received condition is susceptible to localized corrosion in chloride solutions above a critical concentration that can be reached under anticipated repository conditions. Fabrication processes such as welding and local thermal aging as a result of the proposed induction annealing stress mitigation process can significantly alter the long term performance of the alloy. Thermal aging tests have shown a significant decrease in the localized corrosion resistance. DOE has agreed to evaluate this further and provide additional information after testing of mock-ups.

The DOE is currently predicting drip shield lifetimes to be greater than the 10,000-yr compliance period. This is based on the observation that localized corrosion of Ti Grade 7 is difficult to initiate and thus the primary mode of corrosion failure for the drip shield (excluding hydrogen-induced cracking that will be addressed in a subsequent report) is uniform general corrosion. The corrosion rates utilized by the DOE in predicting performance are derived from weight loss measurements. Unfortunately, weight loss measurements on highly corrosion resistant materials exposed to relatively benign solutions typically are not sensitive measures of the corrosion rate (i.e., the amount of weight lost is too small to effectively and accurately measure). In work conducted by the CNWRA, it is clear that pitting corrosion of Ti Grade 7 is an unlikely failure mode for the drip shield as pitting was only observed at potentials well outside the thermodynamic stability region for aqueous solutions. The possibility of crevice corrosion occurring on Ti Grade 7 at lower potentials has been investigated but thus far no initiation has been observed. In contrast to the DOE, the CNWRA has utilized long-term potentiostatic polarization testing to monitor the passive current density in order to gain a better understanding of the possible effects of environment on dissolution rates. Of note, it is clear that the presence of fluoride, even at relatively low concentrations, led to a considerable increase in the dissolution rate of Ti Grade 7. The effects of this increase on the predicted performance of the drip shield should be evaluated further by the DOE (as agreed to DOE/NRC technical exchanges).

Based on the work presented in this report, it is clear that there exist a number of uncertainties in the current information that has been provided by the DOE to date in the area of waste package and drip shield performance. These include the potential environments to which these materials may be exposed, the effects and concentrations of trace impurities that may be present, the effects of microbial activity and thermal aging on the materials, and the general corrosion rates that have been calculated. Because of these uncertainties, a number of agreements between the NRC and the DOE have been arranged such that DOE has committed to provide additional information in the form of technical justifications and/or additional measurements using the same or alternative methods. The experimental efforts of the CNWRA to examine some of these concerns has assisted in resolving issues as well as to identify and elucidate what some of these concerns are.

Additionally, the results generated from the CNWRA experimental efforts are utilized in the NRC/CNWRA TSPA code to predict the performance of the proposed Yucca Mountain repository. The experimental efforts have demonstrated that enhanced concentration of various deleterious species can occur through evaporative processes and thus a wide range of possible environments may be encountered in the repository over time. Alloy 22 has been found to be resistant to localized corrosion in the wrought condition at relatively low chloride concentrations, however thermal aging and welding tend to make the material more susceptible to localized corrosion. It has also been shown that the passive corrosion rate of Alloy 22 is relatively insensitive to environmental conditions but the effect of temperature needs further examination. Ti Grade 7 has been observed to be essentially immune to pitting corrosion except at extremely high potentials (well above those that would reasonably be expected in the repository). Long-term polarization at lower potentials has also revealed that Ti Grade 7 is highly resistant to crevice corrosion, though it is uncertain if crevice corrosion might initiate at longer times (perhaps years are needed). Ti Grade 7 owes this high resistance to localized corrosion to the addition of Pd. Pd additions, however, did not mitigate the effects of fluoride which was shown to dramatically increase the passive corrosion rate by several orders of magnitude even at relatively low concentrations.

## 7 REFERENCES

- American Society for Testing and Materials. Standard practice for preparing, cleaning, and evaluating corrosion test specimens: G1–90. *Annual Book of ASTM Standards. Volume 03.02: Wear and Erosion—Metal Corrosion*. West Conshohocken, PA: American Society for Testing and Materials. 1997.
- American Society for Testing and Materials. Standard reference test method for making potentiostatic and potentiodynamic anodic polarization measurements: G5. *Annual Book of ASTM Standards. Volume 03.02: Wear and Erosion—Metal Corrosion*. West Conshohocken, PA: American Society for Testing and Materials. 1999a.
- American Society for Testing and Materials. Standard test method for conducting cyclic potentiodynamic polarization measurements for localized corrosion susceptibility of iron-, nickel-, or cobalt-based alloys: G61–86. *Annual Book of ASTM Standards. Volume 03.02: Wear and Erosion—Metal Corrosion*. West Conshohocken, PA: American Society for Testing and Materials: 237–241. 1999b.
- American Society for Testing and Materials. Standard practice for calculation of corrosion rates and related information from electrochemical measurements: G102–89. *Annual Book of ASTM Standards. Volume 03.02: Wear and Erosion—Metal Corrosion*. West Conshohocken, PA: American Society for Testing and Materials: 416–422. 1999c.
- American Society for Testing and Materials. Standard test method for pitting and crevice corrosion resistance of stainless steels and related alloys by use of ferric chloride solution: G48–00. *Annual Book of ASTM Standards*. West Conshohocken, PA: American Society for Testing and Materials. 2000.
- Amy, P., and A. Haldeman. *The Microbiology of the Terrestrial Deep Subsurface*. Boca Raton, FL: CRC Lewis Publishers. 1997.
- Apps, J.A. Hydrochemical analysis. *The Site-Scale Unsaturated Zone Model of Yucca Mountain, Nevada for the Viability Assessment*. G.S. Bodvarsson, T.M. Bandurraga, and Y.S. Wu, eds. LBNL–40376. UC–814. Berkeley, CA: Lawrence Berkeley National Laboratory. 1997.
- Banfield, J.F., and K.H. Nealson. Geomicrobiology: Interactions between microbes and minerals. *Reviews in Mineralogy* 35. 1997.
- Beck, T.R. A review: Pitting attack of titanium alloys. *Localized Corrosion*. Houston, TX: NACE International: NACE–3: 644. 1974.
- Bickford, D.F., and R.A. Corbett. Material selection for the defense waste processing facility. *Corrosion of Nickel-Base Alloys*. Metals Park, OH: American Society for Metals: 59–67. 1985.
- Bockris, J.O.M., and A.K.N. Reddy. *Modern Electrochemistry*. New York: Plenum Press. 1970.

- Boere G. Influence of fluoride on titanium in an acidic environment measured by polarization resistance technique. *Journal of Applied Biomaterials* 6: 283–288. 1995.
- Boudin, S., J.L. Vignes, G. Lorang, M. Da Cunha Belo, G. Blondiaux, S.M. Mikhailov, J.P. Jacobs, and H.H. Brongersma. Analytical and electrochemical study of passive films formed on nickel-chromium alloys: Influence of the chromium bulk concentration. *Surface and Interface Analysis* 22: 462–466. 1994.
- Brennenstuhl, A.M., P.E. Doherty, P.J. King, and T.G. Dunstall. The effects of biofouling on the corrosion of nickel heat exchanger alloys at Ontario Hydro. *Microbially Influenced Corrosion and Biodeterioration*. N.J. Dowling, M.W. Mittlemen, and J.C. Danko, eds. Knoxville, TN: The University of Tennessee: 25–31. 1990.
- Brossia, C.S., and G.A. Cragolino. Effects of environmental, electrochemical, and metallurgical variables on the passive and localized dissolution of Ti grade 7. *Proceedings of the Corrosion 2000 Conference*. Paper No. 211. Houston, TX: NACE International. 2000.
- Brossia, C.S., and G.A. Cragolino. Effects of environmental and metallurgical conditions on the passive and localized dissolution of Ti-0.15Pd. *Corrosion* 57: 768–776. 2001a.
- Brossia, C.S., and G.A. Cragolino. Effect of palladium on the localized and passive dissolution of titanium. *Proceedings of the Corrosion 2001 Conference*. Paper No. 01127. Houston, TX: NACE International. 2001b.
- Brossia, C.S., D.S. Dunn, O.C. Moghissi, and N. Sridhar. *Assessment of Methodologies to Confirm Container Performance Model Predictions*. CNWRA 2000-06. San Antonio, TX: Center for Nuclear Waste Regulatory Analyses. 2000.
- Brown, D.A. *Introduction to Microbiology Relevant to the Canadian Nuclear Fuel Waste Management Program—A Literature Review*. AECL TR-581. COG-92-337. Pinawa, Manitoba: Atomic Energy Canada Limited. 1996.
- Browning, L., W.M. Murphy, B.W. Leslie, and W.L. Dam. Thermodynamic interpretations of chemical analyses of unsaturated zone water from Yucca Mountain, Nevada. *Scientific Basis for Nuclear Waste Management XXIII*. R.W. Smith and D.W. Shoesmith, eds. Symposium Proceedings 608. Pittsburgh, PA: Materials Research Society: 237–242. 2000.
- Carlos, B.A., D.L. Bish, and S.J. Chipera. *Manganese-Oxide Minerals in Fractures of the Crater Flat Tuff in Drill Core USW G-4, Yucca Mountain, Nevada*. LA-11787. Los Alamos, NM: Los Alamos National Laboratory. 1990.
- Carlos, B.A., S.J. Chipera, D.L. Bish, and S.J. Craven. Fracture lining oxide minerals in silicic tuff, Yucca Mountain, Nevada, U.S.A. *Chemical Geology* 107: 47–69. 1993.

- Carlos, B.A., S.J. Chipera, and D.L. Bish. *Distribution and Chemistry of Fracture-Lining Minerals at Yucca Mountain, Nevada*. LA-12977-MS. Los Alamos, NM: Los Alamos National Laboratory. 1995.
- Castor, S.B., J.V. Tingley, and H.F. Bonham, Jr. Pyritic ash-flow tuff, Yucca Mountain, Nevada. *Economic Geology* 89: 401-407. 1994.
- Cavanaugh, M.A., J.A. Kargol, J. Nickerson, and N.F. Fiore. The anodic dissolution of a Ni-base superalloy. *Advances in Localized Corrosion*. Houston, TX: NACE International: NACE-9: 144-59. 1983.
- Chen, T.-F., Y. Iijima, K.-I. Hirano, and K. Yamauchi. Diffusion of chromium in nickel-base Ni-Cr-Fe Alloys. *Journal of Nuclear Materials* 169: 285-290. 1989.
- Cieslak, M.J., T.J. Headley, and A.D. Romig, Jr. The welding metallurgy of Hastelloy alloys C-4, C-22, and C-276. *Metallurgical Transactions* 17A: 2,035-2,047. 1986.
- Civilian Radioactive Waste Management System Management and Operating Contractor. *Geochemistry: Book 3—Section 6 of Yucca Mountain Site Description*. B00000000-01717-5700-00019. Revision 00. Las Vegas, NV: Civilian Radioactive Waste Management System Management and Operating Contractor. 1998.
- Civilian Radioactive Waste Management System Management and Operating Contractor. *Evaporation of J-13 Water: Laboratory Experiments and Geochemical Modeling*. PA-EBS-99405. Las Vegas, NV: Civilian Radioactive Waste Management System Management and Operating Contractor. 1999.
- Civilian Radioactive Waste Management System Management and Operating Contractor. *Repository Safety Strategy: Plan to Prepare the Postclosure Safety Case to Support Yucca Mountain Site Recommendation and Licensing Considerations*. TDR-WIS/RL-000001. Revision 3. Las Vegas, NV: Civilian Radioactive Waste Management System Management and Operating Contractor. 2000a.
- Civilian Radioactive Waste Management System Management and Operating Contractor. *Multiscale Thermohydrologic Model*. ANL-EBS-MD-000049. Revision 00. Las Vegas NV: Civilian Radioactive Waste Management System Management and Operating Contractor. 2000b.
- Civilian Radioactive Waste Management System Management and Operating Contractor. *Environment on the Surfaces of the Drip Shield and Waste Package Outer Barrier*. ANL-EBS-MD-000001, Revision 00. ICN 01. Las Vegas NV: Civilian Radioactive Waste Management System Management and Operating Contractor. 2000c.
- Civilian Radioactive Waste Management System Management and Operating Contractor. *In-Drift Microbial Communities*. ANL-EBS-MD-000038, Revision 00. ICN 01. Las Vegas, NV: Civilian Radioactive Waste Management System Management and Operating Contractor. 2000d.

- Civilian Radioactive Waste Management System Management and Operating Contractor. *General Corrosion and Localized Corrosion of Waste Package Outer Barrier*. ANL-EBS-MD-000003. Revision 00. Las Vegas, NV: Civilian Radioactive Waste Management System Management and Operating Contractor. 2000e.
- Civilian Radioactive Waste Management System Management and Operating Contractor. *Waste Package Degradation Process Model Report*. TDR-WDS-MD-000002, Revision 00. ICN 01. Las Vegas, NV: Civilian Radioactive Waste Management System Management and Operating Contractor. 2000f.
- Civilian Radioactive Waste Management System Management and Operating Contractor. *Aging and Phase Stability of Waste Package Outer Barrier*. ANL-EBS-MD-000002. Revision 00. Las Vegas, NV: Civilian Radioactive Waste Management System Management and Operating Contractor. 2000g.
- Civilian Radioactive Waste Management System Management and Operating Contractor. *Total System Performance Assessment for the Site Recommendation*. TDR-WIS-PA-000001, Revision 00. ICN 01. Las Vegas, NV: Civilian Radioactive Waste Management System Management and Operating Contractor. 2000h.
- Civilian Radioactive Waste Management System Management and Operating Contractor. *Abstraction of Models for Pitting and Crevice Corrosion of Drip Shield and Waste Package Outer Barrier*. ANL-EBS-PA-000003. Revision 00. Las Vegas, NV: Civilian Radioactive Waste Management System Management and Operating Contractor. 2000i.
- Civilian Radioactive Waste Management System Management and Operating Contractor. *Total System Performance Assessment (TSPA) Model for the Site Recommendation*. MDL-WIS-PA-000002. Revision 00. Las Vegas, NV: Civilian Radioactive Waste Management System Management and Operating Contractor. 2000j.
- Civilian Radioactive Waste Management System Management and Operating Contractor. *WAPDEG: Analysis of Waste Package and Drip Shield Degradation*. ANL-EBS-PA-000001. Revision 00. Las Vegas, NV: Office of Civilian Radioactive Waste Management System Management and Operating Contractor. 2000k.
- Civilian Radioactive Waste Management System Management and Operating Contractor. *Engineered Barrier System: Physical and Chemical Environment Model*. ANL-EBS-MD-000033. Revision 01. Las Vegas, NV: Office of Civilian Radioactive Waste Management System Management and Operating Contractor. 2000l.
- Civilian Radioactive Waste Management System Management and Operating Contractor. *General Corrosion and Localized Corrosion of the Drip Shield*. ANL-EBS-MD-000004. Revision 00. Las Vegas, NV: Office of Civilian Radioactive Waste Management System Management and Operating Contractor. 2000m.

- Civilian Radioactive Waste Management System Management and Operating Contractor. *In-Drift Precipitate/Salts Analysis*. ANL-EBS-MD-000045, Revision 00. ICN 02. Las Vegas, NV: Office of Civilian Radioactive Waste Management System Management and Operating Contractor. 2001a.
- Civilian Radioactive Waste Management System Management and Operating Contractor. *FY01 Supplemental Science and Performance Analysis. Volume 1: Scientific Bases and Analyses*. TDR-MGR-MD-000007, Revision 00, ICN 01. Las Vegas, NV: Office of Civilian Radioactive Waste Management System Management and Operating Contractor. 2001b.
- Costerton, J.W., Z. Lewandowski, D.E. Caldwell, D.R. Korber, and H.M. Lappin-Scott. Microbial biofilms. *Annual Review of Microbiology* 49: 711–746. 1995.
- Cragolino, G.A., D.S. Dunn, C.S. Brossia, V. Jain, and K. Chan. *Assessment of Performance Issues Related to Alternate EBS Materials and Design Options*. CNWRA 99-003. San Antonio, TX: Center for Nuclear Waste Regulatory Analyses. 1999.
- Donachie, M.J. *Titanium: A Technical Guide*. Materials Park, OH: ASM International. 1988.
- Drever, J.I. *The Geochemistry of Natural Waters*. 2<sup>nd</sup> Edition. Englewood Cliffs: NJ: Prentice Hall Press. 1988.
- Douglas, D.L. The oxidation mechanism of dilute Ni-Cr alloys. *Corrosion Science* 8: 665–678. 1968.
- Dunn, D.S., G.A. Cragolino, and N. Sridhar. Methodologies for predicting the performance of Ni-Cr-Mo alloys proposed for high-level nuclear waste containers. *Scientific Basis for Nuclear Waste Management XXII*. D.J. Wronkiewicz and J.H. Lee, eds. Symposium Proceedings 556. Pittsburgh, PA: Materials Research Society: 879–886. 1999a.
- Dunn, D.S., Y.-M. Pan, and G.A. Cragolino. *Effects of Environmental Factors on the Aqueous Corrosion of High-Level Radioactive Waste Containers—Experimental Results and Models*. CNWRA 99-004. San Antonio, TX: Center for Nuclear Waste Regulatory Analyses. 1999b.
- Dunn, D.S., G.A. Cragolino, and N. Sridhar. An electrochemical approach to predicting long-term localized corrosion of corrosion-resistant high-level waste container materials. *Corrosion* 56(1): 90–104. 2000a.
- Dunn, D.S., Y.-M. Pan, and G.A. Cragolino. Stress corrosion cracking, passive, and localized corrosion of alloy 22 high-level radioactive waste containers. *Proceedings of the Corrosion 2000 Conference*. Paper No. 206. Houston, TX: NACE International. 2000b.
- Dunn, D.S., G.A. Cragolino, and N. Sridhar. Passive dissolution and localized corrosion of Alloy 22 high-level waste container weldments. *Scientific Basis for Nuclear Waste Management XXIII*. R.W. Smith and D.W. Shoesmith, eds. Symposium Proceedings 608. Pittsburgh, PA: Materials Research Society. 89–94. 2000c.

- Dunnington, B.W., F.H. Beck, and M.G. Fontana. The mechanism of scale formation on iron at high temperature. *Corrosion* 8: 2t. 1952.
- Evans, H.E. Cavity formation and metallurgical changes induced by growth of oxide scale. *Materials Science and Technology* 4: 1,089–1,098. 1988.
- Fehlner, F.P. Low-temperature oxidation. *The Role of Vitreous Oxides*. New York: John Wiley and Sons. 1986.
- Fukuzuka, T., K. Shimogori, and H. Satoh. Role of palladium in hydrogen absorption of Ti-Pd alloy. Titanium science and technology. *Proceedings of the 4<sup>th</sup> International Conference on Titanium*. Kyoto, Japan: AIME: 3: 2,695–2,703. 1980.
- Ge, Z., A. S. Wexler, and M.V. Johnston. Multicomponent aerosol crystallization. *Journal of Colloid and Interface Science* 183: 68–77. 1996.
- Ge, Z., A.S. Wexler, and M.V. Johnston. Deliquescence behaviour of multicomponent aerosols. *Journal of Physical Chemistry A* 102: 173–180. 1998.
- Geesey, G. *Review of the Potential for Microbially Influenced Corrosion of High-Level Nuclear Waste Containers*. CNWRA 93-014. San Antonio, TX: Center for Nuclear Waste Regulatory Analyses. 1993.
- Geesey, G., and G.A. Cragolino. A review of the potential for microbially influenced corrosion of high-level nuclear waste containers in an unsaturated repository site. *1995 International Conference on Microbially Influenced Corrosion*. Paper No. 76. Houston, TX: NACE International. 1995.
- Gileadi, E. *Electrode Kinetics for Chemists, Chemical Engineers, and Materials Scientists*. New York: VCH Publishers. 1993.
- Hales, R., and A.C. Hill. The role of metal lattice vacancies in the high temperature oxidation of nickel. *Corrosion Science* 12: 843–853. 1972.
- Hardie, L.A., and H.P. Eugster. The evolution of closed-basin brines. *Mineral. Soc. Am. Spec.* 3: 273–290. 1970.
- Harrar, J.E., R.D. McCright, and A. Goldberg. *Field Electrochemical Measurements of Corrosion Characteristics of Materials in Hypersaline Geothermal Brine*. UCRL-52376. Livermore, CA: Lawrence Livermore National Laboratory. 1977.
- Harrar, J.E., R.D. McCright, and A. Goldberg. Corrosion characteristics of materials in hypersaline geothermal brine. *SAMPE Quarterly* 10(1): 1–15. 1978.
- Harrar, J. E., J.F. Carley, W.F. Isherwood, and E. Raber. *Report to the Committee to Review the Use of J-13 Well Water in Nevada Nuclear Waste Storage Investigations*. UCRL-ID-21867. Livermore, CA: Lawrence Livermore National Laboratory. 1990.

- Heubner, U.L., E. Altpeter, M.B. Rockel, and E. Wallis. Electrochemical behavior and its relation to composition and sensitization of NiCrMo alloys in ASTM G-28 solution. *Corrosion* 45(3): 249–259. 1989.
- Hoffmann, T. Welding of nickel alloys and high-alloy special stainless steels. *Nickel Alloys*. U. Huebner, ed. New York: Marcel Dekker Publishers: 100–128. 1998.
- Horn, J., S. Martin, B. Masterson, and T. Lian. Biochemical contributions to corrosion of carbon steel and Alloy 22 in a continual flow system. *Proceedings of the CORROSION '99 Conference*. Paper No. 162. Houston, TX: NACE International. 1999.
- Horn, J., S. Martin, A. Rivera, P. Bedrossian, and T. Lian. Potential biogenic corrosion of Alloy 22, a candidate waste packaging material, under simulated repository conditions. *Proceedings of the Corrosion 2000 Conference*. Paper No. 387. Houston, TX: NACE International. 2000.
- Horn, J., S. Martin, and B. Masterson. Evidence of biogenic corrosion of titanium after exposure to a continuous culture of thiobacillus ferrooxidans grown in thiosulfate medium. *Proceedings of the Corrosion 2001 Conference*. Paper No. 01259. Houston, TX: NACE International. 2001.
- Ikeda, B.M., M.G. Bailey, D.C. Cann, and D.W. Shoesmith. Effect of iron content and microstructure on the crevice corrosion of grade-2 titanium under nuclear waste vault conditions. *Advances in Localized Corrosion*. Houston, TX: NACE International: NACE-9: 439–444. 1990.
- Kelly, E.J. Anodic dissolution and passivation of titanium in acidic media, III: Chloride solutions. *Journal of the Electrochemical Society* 126: 2,064–2,075. 1979.
- Kelly, R.G., C.S. Brossia, K.R. Cooper, J. Krol. Analyses of disparate levels of anions of relevance to corrosion processes. *Journal of Chromatography A* 739: 191–198. 1996.
- Kelsall, G.H., and D.J. Robbins. Thermodynamics of Ti-H<sub>2</sub>O-F(-Fe) systems at 298 K. *Journal of Electroanalytical Chemistry* 283: 135–157. 1990.
- Kerrisk J.F. Groundwater Chemistry at Yucca Mountain, Nevada. Vicinity Report LA-10929-MS. Los Alamos, NM: Los Alamos National Laboratory. 1987.
- Kirchheim, R., B. Heine, H. Fischmeister, S. Hofmann, H. Knote, and U. Stoltz. The passivity of iron-chromium alloys. *Corrosion Science* 30(7): 899–917. 1989.
- Klöwer, J. Nickel alloys and high-alloy special stainless steel in thermal waste treatment. *Nickel Alloys*. U. Huebner, ed. New York: Marcel Dekker Publishers: 235–259. 1998.
- Koizumi, T., and S. Furuya. Pitting corrosion of titanium in high temperature halide solutions. *Titanium Science and Technology* 4: 2,383–2,393. 1973.

- Kolman, D.G., and J.R. Scully. On the repassivation behavior of high-purity titanium and selected  $\alpha$ ,  $\beta$ , and  $\beta+\alpha$  titanium alloys in aqueous chloride solutions. *Journal of the Electrochemical Society* 143: 1,847–1,860. 1996.
- Krol, J., M. Benvenuti, and J. Romano. *Ion Analysis Methods for IC and CIA® and Practical Aspects of Capillary Ion Analysis Theory*. Milford, MA: Waters Corporation. 2000.
- Levin, V.A. Corrosive synergism of chlorine and hydrogen fluoride in a titanium-hydrochloric acid system. *Zashchita Metallov* 32: 143. 1996.
- Lian, T., S. Martin, D. Jones, A. Rivera, and J. Horn. Corrosion of candidate container materials by Yucca Mountain bacteria. *Proceedings of the CORROSION '99 Conference*. Paper No. 476. Houston, TX: NACE International. 1999a.
- Lian, T., D. Jones, S. Martin, and J. Horn. A quantitative assessment of microbiological contributions to corrosion of candidate nuclear waste package materials. *Scientific Basis for Nuclear Waste Management XXII*. D.J. Wronkiewicz and J.H. Lee, eds. Pittsburgh, PA: Materials Research Society: 1,175–1,182. 1999b.
- Little, B., P. Wagner, and F. Mansfeld. Microbiologically influenced corrosion of metals and alloys. *International Materials Review* 36: 253–272. 1991.
- Little, B.J., P.A. Wagner, and R.I. Ray. An experimental evaluation of titanium's resistance to microbiologically influenced corrosion. *Proceedings of the CORROSION '92 Conference*. Paper No. 173. Houston, TX: NACE International. 1992.
- Little, B.J., P.A. Wagner, and R.I. Ray. An evaluation of titanium exposed to thermophilic and marine biofilms. *Proceedings of the Corrosion '93 Conference*. Paper No. 308. Houston, TX: NACE International. 1993.
- Little, B.J., P.A. Wagner, and Z. Lewandowski. Spatial relationships between bacteria and mineral surfaces. *Geomicrobiology: Interactions Between Microbes and Minerals*. J.F. Banfield and K.H. Nealson, eds. Symposium Proceedings 35. Washington, DC: Mineralogical Society of America: 123–159. 1997.
- Lorang, G., N. Jallerat, K. Vu Quang, and J.-P. Langeron. AES depth profiling of passive overlayers formed on nickel alloys. *Surface and Interface Analysis* 16: 325–330. 1990.
- Lumsden, J.B., and R.W. Staehle. Composition of protective films formed on iron and stainless steels. *Surface Analysis Techniques for Metallurgical Applications: A Symposium*. Philadelphia, PA: American Society for Testing and Materials: 39–51. 1976.
- Macdonald, D.D. The point defect model for the passive state. *Journal of Electrochemical Society* 139: 3,434–3,449. 1992.

- Mandry, M.J., and G. Rosenblatt. The effect of fluoride ion on the anodic behavior of titanium in sulfuric acid. *Journal of the Electrochemical Society* 119: 29. 1972.
- McCright, R.D. *Engineered Materials Characterization, Corrosion Data, and Modeling—Update for the Viability Assessment*. UCRL-ID-119564. Volume 3. Revision 1.1. Livermore, CA: Lawrence Livermore National Laboratory. 1998.
- McKay, P. *Corrosion Chemistry within Pits, Crevices, and Cracks*. A. Turnbull, ed. London: Her Majesty's Stationary Office. 1984.
- Min, U.-S., and J.C.M. Li. The microstructure and dealloying kinetics of a Cu-Mn alloy. *Journal of Material Resources* 9: 2,878–2,883. 1994.
- Okazaki, Y., K. Kyo, Y. Ito, and T. Tateishi. Effects of Mo and Pd on corrosion resistance of V-free titanium alloys for medical implants. *Materials Transactions* 38: 344. 1997.
- Pandis, S.N., A.S. Wexler, and J.H. Seinfeld. *Journal of Physical Chemistry* 99: 9,646. 1995.
- Pedersen, K., and F. Karlsson, *Investigations of Subterranean Microorganisms: Their Importance for Performance Assessment of Radioactive Waste Disposal*. SKB 95-10. Stockholm, Sweden: Swedish Nuclear Fuel and Waste Management Company. 1995,
- Pensado, O., and S. Mohanty. Prediction of waste package life for high-level radioactive waste disposal at Yucca Mountain. *Scientific Basis for Nuclear Waste Management XXIII*. D. Shoesmith and R. Smith, eds. Pittsburgh, PA: Materials Research Society: 147–152. 2001.
- Perfect, D.L., C.C. Faunt, W.C. Steinkampf, and A.K. Turner. *Hydrochemical Data Base for the Death Valley Region, California and Nevada*. U.S. Geological Survey Open-File Report 94-305. 1995.
- Pitonzo, B., P. Castro, P. Amy, D. Bergman, and D. Jones. Microbially-influenced corrosion capability of Yucca Mountain bacterial isolates. *High-Level Radioactive Waste Management: Proceedings of the Seventh Annual International Conference, Las Vegas, Nevada, April 29–May 3, 1996*. La Grange Park, IL: American Nuclear Society. 1996.
- Posey, F.A., and E.G. Bohlmann. Pitting of titanium alloys in saline waters. *Desalination* 3: 269–279. 1967.
- Pourbaix, M. *Atlas of Electrochemical Equilibria in Aqueous Solutions*. Houston, TX: NACE International. 1974.
- Raj, R., and M.F. Ashby. Intergranular fracture at elevated temperature. *Acta Metallurgica* 23: 653–666. 1975.
- Rosenberg, N.D., K.G. Knauss, and M.F. Dibley. *Evaporation of Topopah Spring Tuff Pore Water*. UCRL-ID-135765. Livermore, CA: Lawrence Livermore National Laboratory. 1999.

- Rosenberg N. D., G.E. Gdowski, and K.G. Knauss. Evaporative chemical evolution of natural waters at Yucca Mountain, Nevada. *Applied Geochemistry* 16: 1,231–1,240. 2001.
- Satoh, H., K. Shimogori, and F. Kamikubo. The crevice corrosion resistance of some titanium materials: A review of the beneficial effects of palladium. *Platinum Metals Review* 31: 115. 1987.
- Schutz, R.W. A case for titanium's resistance to microbiologically influenced corrosion. *Materials Performance* 1: 58–61. 1991.
- Schutz, R.W. Titanium. *Corrosion Tests and Standards, Application and Interpretation*. Philadelphia, PA: American Society for Testing and Materials: 493–506. 1995.
- Schutz, R.W., and M. Xiao. Corrosion control for low-cost reliability. *Proceedings of the 12<sup>th</sup> International Corrosion Congress Conference*. Houston, TX: NACE International: 1,213–1,225. 1993.
- Sedriks, A.J. *Corrosion of Stainless Steels*. New York: Wiley-Interscience Publishers. 1996.
- Shewmon, P.G. *Diffusion in Solids*. New York: McGraw-Hill Company. 1963.
- Shida, Y., G.C. Wood, F.H. Stott, D.P. Whittle, and B.D. Bastow. Intergranular oxidation and internal void formation in Ni-40% Cr alloys. *Corrosion Science* 21(8): 581–597. 1981.
- Shida, Y., and S. Kitayama. Effect of Pd addition on the crevice corrosion resistance of Ti. *Proceedings of the 6<sup>th</sup> World Conference on Titanium*. Paris, France: 1,729–1,733. 1988.
- Shimogori, K., H. Sato, H. Tomari, and A. Ooki. Development of new crevice corrosion resistant Ti alloys. *Titanium and Titanium Alloys*. Volume 2. J.C. Williams and A.F. Belov, eds. New York: Plenum Press Publishers. 1976.
- Sieradzky, K., R.R. Coderman, K. Shukla, and R.C. Newman. Computer simulations of corrosion: selective dissolution of binary alloys. *Philosophical Magazine* 159: 713–746. 1989.
- Smailos, E. Corrosion of high-level waste packaging materials in disposal relevant brines. *Nuclear Technology* 104: 343–350. 1993.
- Sridhar, N. Effect of alloying elements on localized corrosion resistance of nickel-base alloys. *Advances in Localized Corrosion*. H. Isaacs, U. Bertocci, J. Kruger, and S. Smialowska, eds. Houston, TX: NACE International: 263–269. 1990.
- Stot, F.H., G.C. Wood, Y. Shida, W.P. Whittle, and B.D. Bastow. The development of internal and intergranular oxides in nickel-chromium-aluminum alloys at high temperature. *Corrosion Science* 21(8): 599–624. 1981.
- Tang, I.N. Phase transformation and growth of aerosol particles composed of mixed salts. *Journal of Aerosol Science* 7: 361–371. 1976.

- Tang, I.N. *In Generation of Aerosols and Facilities for Exposure Experiments*. K. Willeke, ed. Ann Arbor, MI: Ann Arbor Science Publishers. 1980.
- Tang, I.N., H.R. Munkelwitz, and J.G. Davis. Aerosol growth studies-IV: Phase transformation of mixed salt aerosols in a moist atmosphere. *Journal of Aerosol Science* 9: 505-511. 1978.
- Tylecote, R.F., and T.E. Mitchell. Marker movements in the oxidation of iron and some other metals. *Journal of Iron Steel Institute*. 196: 445. 1960.
- U.S. Nuclear Regulatory Commission. *Issue Resolution Status Report, Key Technical Issue: Container Life and Source Term*. Revision 3b. Washington, DC: U.S. Nuclear Regulatory Commission. 2001.
- Vogt, R., and B.J. Finlayson-Pitts. *Journal of Physical Chemistry* 98: 3,747. 1994.
- Weast, R.C., and M.J. Astle, eds. *CRC Handbook of Chemistry and Physics: A Ready Reference Book of Chemical and Physical Data*. 62<sup>nd</sup> Edition. Boca Raton, FL: CRC Press. 1981.
- Weiss, S.I., D.C. Noble, and L.T. Larson. Task 3: Evaluation of mineral resource potential, caldera geology, and volcano-tectonic framework at and near Yucca Mountain. Part II: Major and trace-element geochemical data. *Evaluation of the Geologic Relations and Seismotectonic Stability of the Yucca Mountain Area Nevada Nuclear Waste Site Investigation (NNWSI)*. Progress Report. Reno, NV: University of Nevada, Center for Neotectonic Studies Mackay School of Mines. 1994.
- White, A.F., H.C. Claassen, and L.V. Benson. *The Effect of Dissolution of Volcanic Glass on the Water Chemistry in a Tuffaceous Aquifer*. U.S. Geological Survey Open-File Report 1535-Q. 1980.
- Wolery, T.J. *A Software Package for Geochemical Modeling of Aqueous Systems*. UCRL-MA-110662-Pt.3. Livermore, CA: Lawrence Livermore National Laboratory. 1992.
- Yang, I.C., G.W. Rattray, and P. Yu. *Interpretation of Chemical and Isotopic Data from Boreholes in the Unsaturated Zone at Yucca Mountain, Nevada*. U.S. Geological Survey WRIR 96-4058. 1996.
- Yang, I.C., P. Yu, G.W. Rattray, J.S. Ferarese, and R.N. Ryan. *Hydrochemical Investigations in Characterizing the Unsaturated Zone at Yucca Mountain, Nevada*. U.S. Geological Survey WRIR 98-4132. 1998.
- Zhang, L., and D.D. Macdonald. Segregation of alloying elements in passive systems-II: Numerical simulation. *Electrochimica Acta* 43: 2,673-2,685. 1998.

**APPENDIX A**  
**TABULATED CORROSION DATA**

## APPENDIX A

**Table A-1. Repassivation potential measurements for Alloy 22**

Material	Chloride Concentration, M	Temperature, °C	pH	Repassivation Potential, mV <sub>SCE</sub>
Wrought	0.5	105	8	-52
Wrought	0.5	125	8	-106
Wrought	0.5	125	8	-18
Wrought	0.5	150	8	-155
Wrought	1.0	80	8	227
Wrought	1.0	95	8	161
Wrought	1.0	95	8	39
Wrought	1.0	105	8	-54
Wrought	1.0	125	8	-171
Wrought	1.0	125	8	24
Wrought	1.0	150	8	-216
Wrought	1.0	150	8	-202
Wrought	4.0	80	8	125
Wrought	4.0	95	8	-57
Wrought	4.0	95	8	107
Wrought	4.0	95	8	-98
Wrought	4.0	105	8	-143
Wrought	4.0	125	8	-175
Wrought	4.0	150	8	-192
Welded	0.005	95	6	271
Welded	0.05	95	6	129
Welded	0.1	95	6	214
Welded	0.5	95	8	-10

**Table A-1. Repassivation potential measurements for Alloy 22 (cont'd)**

<b>Material</b>	<b>Chloride Concentration, M</b>	<b>Temperature, °C</b>	<b>pH</b>	<b>Repassivation Potential, mV<sub>SCE</sub></b>
Welded	0.5	125	8	-59
Welded	1.0	125	8	-71
Welded	4.0	95	8	-38
Welded	4.0	95	8	-159
Welded	4.0	125	8	-216
Welded	4.0	150	8	-195
5 min @ 870 °C	0.01	95	6	351
5 min @ 870 °C	0.05	95	6	198
5 min @ 870 °C	0.1	95	6	15
5 min @ 870 °C	0.5	95	6	-123
5 min @ 870 °C	1.0	95	6	-233
5 min @ 870 °C	4.0	95	6	-258
10 min @ 870 °C	0.5	95	6	-39
10 min @ 870 °C	1.0	95	6	-143
10 min @ 870 °C	4.0	95	6	-268
20 min @ 870 °C	0.5	95	6	-66
20 min @ 870 °C	1.0	95	6	-210
20 min @ 870 °C	4.0	95	6	-256
30 min @ 870 °C	0.5	95	6	-76
30 min @ 870 °C	1.0	95	6	-89
30 min @ 870 °C	4.0	95	6	-238
30 min @ 870 °C	4.0	95	6	-271
60 min @ 870 °C	0.01	95	6	305
2 hr @ 870 °C	0.01	95	6	350
4 hr @ 870 °C	4.0	95	6	-252

**Table A-1. Repassivation potential measurements for Alloy 22 (cont'd)**

<b>Material</b>	<b>Chloride Concentration, M</b>	<b>Temperature, °C</b>	<b>pH</b>	<b>Repassivation Potential, mV<sub>SCE</sub></b>
8 hr @ 870 °C	0.01	95	6	54
12 hr @ 870 °C	0.01	95	6	202
24 hr @ 870 °C	4.0	95	6	-259
240 hr @ 870 °C	0.01	95	6	69

**Table A-2. Anodic current density for Alloy 22 measured under potentiostatic conditions after 48 hours**

Condition	[Cl <sup>-</sup> ] (M)	T (°C)	pH	E <sub>Applied</sub> (V <sub>SCE</sub> )	i <sub>steady state</sub> (A/cm <sup>2</sup> )
Wrought	0.028	20	8.0	200	2.5 × 10 <sup>-9</sup>
Wrought	0.028	20	8.0	200	1.5 × 10 <sup>-9</sup>
Wrought	0.028	95	8.0	200	3.0 × 10 <sup>-8</sup>
Wrought	0.028	95	8.0	400	1.4 × 10 <sup>-7</sup>
Wrought	0.028	95	8.0	600	2.6 × 10 <sup>-7</sup>
Wrought	0.028	95	8.0	800	4.7 × 10 <sup>-4</sup>
Wrought	0.13	95	0.7	200	6.9 × 10 <sup>-8</sup>
Wrought	0.13	95	0.7	400	7.5 × 10 <sup>-8</sup>
Wrought	0.13	95	0.7	600	9.8 × 10 <sup>-8</sup>
Wrought	0.13	95	0.7	800	6.5 × 10 <sup>-5</sup>
Wrought	0.5	20	8.0	200	9.8 × 10 <sup>-9</sup>
Wrought	0.5	20	8.0	400	3.9 × 10 <sup>-8</sup>
Wrought	0.5	20	8.0	600	4.7 × 10 <sup>-8</sup>
Wrought	0.5	20	8.0	800	1.1 × 10 <sup>-4</sup>
Wrought	0.5	95	8.0	0	1.3 × 10 <sup>-8</sup>
Wrought	0.5	95	8.0	200	1.9 × 10 <sup>-8</sup>
Wrought	0.5	95	8.0	400	1.8 × 10 <sup>-8</sup>
Wrought	0.5	95	8.0	600	4.3 × 10 <sup>-5</sup>
Wrought	1.0	95	8.0	200	9.4 × 10 <sup>-9</sup>
Wrought	1.0	95	8.0	800	8.2 × 10 <sup>-4</sup>
Wrought	4.0	20	8.0	200	8.5 × 10 <sup>-9</sup>
Wrought	4.0	20	8.0	800	7.2 × 10 <sup>-5</sup>
Wrought	4.0	95	8.0	-200	9.9 × 10 <sup>-9</sup>
Wrought	4.0	95	8.0	-200	1.0 × 10 <sup>-8</sup>

**Table A-2. Anodic current density for Alloy 22 measured under potentiostatic conditions after 48 hours (cont'd)**

Condition	[Cl <sup>-</sup> ] (M)	T (°C)	pH	E <sub>Applied</sub> (V <sub>SCE</sub> )	i <sub>steady state</sub> (A/cm <sup>2</sup> )
Wrought	4.0	95	8.0	0	6.6 × 10 <sup>-9</sup>
Wrought	4.0	95	8.0	200	2.6 × 10 <sup>-8</sup>
Wrought	4.0	95	8.0	400	3.9 × 10 <sup>-8</sup>
Wrought	4.0	95	8.0	600	7.4 × 10 <sup>-8</sup>
Wrought	4.0	95	8.0	800	7.3 × 10 <sup>-4</sup>
Wrought	4.0	95	2.7	200	6.2 × 10 <sup>-9</sup>
Wrought	4.0	95	2.7	400	2.5 × 10 <sup>-8</sup>
Wrought	4.0	95	2.7	600	3.2 × 10 <sup>-5</sup>
Wrought	4.0	95	2.7	800	6.4 × 10 <sup>-4</sup>
Welded	4.0	95	8	0	2.8 × 10 <sup>-8</sup>
Welded	4.0	95	8.0	200	2.3 × 10 <sup>-8</sup>
Welded	4.0	95	8.0	400	2.3 × 10 <sup>-8</sup>
Welded	4.0	95	8.0	600	4.3 × 10 <sup>-8</sup>
Welded	4.0	95	8.0	800	2.0 × 10 <sup>-4</sup>
Welded	4.0	95	2.7	-400	4.8 × 10 <sup>-9</sup>
Welded	4.0	95	2.7	-200	2.2 × 10 <sup>-8</sup>
Welded	4.0	95	2.7	0	2.9 × 10 <sup>-8</sup>
Welded	4.0	95	2.7	400	5.0 × 10 <sup>-8</sup>
Welded	4.0	95	2.7	600	4.2 × 10 <sup>-5</sup>
Welded	4.0	95	2.7	800	4.2 × 10 <sup>-4</sup>
Welded	4.0	95	11.0	-200	2.6 × 10 <sup>-8</sup>
Welded	4.0	95	11.0	0	2.1 × 10 <sup>-8</sup>
Welded	4.0	95	11.0	200	2.0 × 10 <sup>-8</sup>
Welded	4.0	95	11.0	400	2.4 × 10 <sup>-8</sup>
Welded	4.0	95	11.0	600	1.8 × 10 <sup>-6</sup>

**Table A-2. Anodic current density for Alloy 22 measured under potentiostatic conditions after 48 hours (cont'd)**

<b>Condition</b>	<b>[Cl<sup>-</sup>] (M)</b>	<b>T (°C)</b>	<b>pH</b>	<b>E<sub>Applied</sub> (V<sub>SCE</sub>)</b>	<b>i<sub>steady state</sub> (A/cm<sup>2</sup>)</b>
Welded	4.0	95	11.0	800	$6.7 \times 10^{-4}$
4 hours @ 800 °C	2.0	95	8.0	-200	$2.6 \times 10^{-9}$
4 hours @ 800 °C	4.0	95	8.0	-200	$2.3 \times 10^{-9}$
4 hours @ 800 °C	4.0	95	8.0	0	$2.3 \times 10^{-9}$
4 hours @ 800 °C	4.0	95	8.0	200	$1.1 \times 10^{-4}$
4 hours @ 800 °C	4.0	95	8.0	200	$7.5 \times 10^{-5}$
24 hours @ 800 °C	4.0	95	8.0	-200	$2.3 \times 10^{-9}$
24 hours @ 800 °C	4.0	95	8.0	0	$1.0 \times 10^{-7}$
24 hours @ 800 °C	4.0	95	8.0	0	$3.4 \times 10^{-8}$
24 hours @ 800 °C	4.0	95	8.0	200	$3.2 \times 10^{-8}$
24 hours @ 800 °C	4.0	95	8.0	200	$1.8 \times 10^{-8}$
24 hours @ 800 °C	4.0	95	8.0	400	$2.1 \times 10^{-2}$

**Table A-3. Localized corrosion testing results for Ti Grade 7**

Condition	[Cl <sup>-</sup> ] (M)	T (°C)	pH	E <sub>bd</sub> (V <sub>SCE</sub> )	E <sub>tp</sub> (V <sub>SCE</sub> )
Wrought	0.1	95	5.8	9.71	6.65
Wrought	0.1	95	5.7	10.48	6.13
Wrought	0.5	95	6.2	8.54	5.92
Wrought	0.5	95	5.8	8.12	6.27
Wrought	1.0	95	6.5	7.28	5.96
Wrought	1.0	95	5.9	6.65	5.33
Wrought	5.0	95	6.2	5.61	5.68
Wrought	5.0	95	5.9	6.43	5.07
Welded	0.1	95	5.9	9.63	5.98
Welded	0.1	95	6.4	9.12	6.47
Welded	0.5	95	6.6	7.81	5.94
Welded	0.5	95	6.1	8.18	5.59
Welded	1.0	95	6.5	6.85	5.62
Welded	1.0	95	6.2	6.22	5.04
Welded	5.0	95	5.4	5.44	5.36
Welded	5.0	95	5.6	6.29	4.74
Wrought	1.0	95*	6.9	5.67	3.96
Wrought	1.0	120	6.8	5.08	3.68
Wrought	1.0	140	6.7	4.06	2.03
Wrought	1.0	165	6.7	1.75	1.35
Welded	1.0	95*	6.5	5.50	3.86
Welded	1.0	125	6.9	4.42	3.33
Welded	1.0	127	6.8	4.30	3.22
Welded	1.0	133	6.6	4.17	2.37
Welded	1.0	140	6.7	4.02	1.60

**Table A-3. Localized corrosion testing results for Ti Grade 7 (cont'd)**

<b>Condition</b>	<b>[Cl<sup>-</sup>] (M)</b>	<b>T (°C)</b>	<b>pH</b>	<b>E<sub>bd</sub> (V<sub>SCE</sub>)</b>	<b>E<sub>rp</sub> (V<sub>SCE</sub>)</b>
Welded	1.0	152	6.4	1.55	1.45
Welded	1.0	165	6.5	1.33	1.25

**Table A-4. Anodic current density measurements for Ti Grade 7 at 95°C using potentiostatic polarization testing**

$E_{\text{Applied}} \text{ (V}_{\text{SCE}})$	$[\text{Cl}^-] \text{ (M)}$	$[\text{F}^-] \text{ (M)}$	pH	Time at Steady State (h)	$i_{\text{steady state}} \text{ (A/cm}^2)$
-0.25	0.1	0	6.5	24	$1.9 \times 10^{-6}$
-0.25	1.0	0	6.5	24	$1.4 \times 10^{-5}$
-0.25	1.06	0	2.2	24	$1.0 \times 10^{-5}$
-0.25	1.0	0	10.1	24	$5.8 \times 10^{-6}$
0.0	0.1	0	6.4	24	$3.7 \times 10^{-6}$
0.0	1.0	0	6.6	24	$2.2 \times 10^{-5}$
0.0	1.0	0	2.1	24	$1.3 \times 10^{-6}$
0.0	1.0	0	10.3	24	$5.4 \times 10^{-6}$
0.25	0.1	0	6.6	24	$4.2 \times 10^{-6}$
0.25	1.0	0	6.3	24	$9.6 \times 10^{-6}$
0.25	1.0	0	2.2	24	$2.4 \times 10^{-6}$
0.25	1.0	0	10.2	24	$3.1 \times 10^{-6}$
0.5	0.1	0	6.5	24	$3.9 \times 10^{-6}$
0.0	1.0	0	6.2	1,161	$8.2 \times 10^{-8}$
0.0	1.0	0	6.6	453	$7.4 \times 10^{-9}$
0.0	1.0	0.0001	6.9	453	$1.2 \times 10^{-8}$
0.0	1.0	0.0005	6.8	453	$3.2 \times 10^{-7}$
0.0	1.0	0.001	5.9	453	$5.3 \times 10^{-6}$
0.0	1.0	0.01	6.6	453	$4.2 \times 10^{-5}$
0.0	1.0	0.1	6.8	453	$6.0 \times 10^{-5}$
0.0	1.0*	0.1	7.9	220	$9.9 \times 10^{-5}$
0.0	3.84 <sup>†</sup>	0.07	6.8	220	$1.7 \times 10^{-4}$

\*Also contained 0.55 M  $\text{NO}_3^-$  and 0.92 M  $\text{SO}_4^{2-}$ .  
<sup>†</sup>Also contained 2.32 M  $\text{NO}_3^-$  and 0.15 M  $\text{SO}_4^{2-}$ .